Title

Perturbing the Edge of Consciousness: Examining signatures of criticality in the conscious and unconscious brain

Author

Dallavecchia, Alessandra

Publication Date

2023

Peer reviewed|Thesis/dissertation

UNIVERSITY OF CALIFORNIA

Los Angeles

Perturbing the Edge of Consciousness

Examining signatures of criticality in the conscious and unconscious brain

A dissertation submitted in partial satisfaction of the requirements for the degree of Doctor of Philosophy in Psychology

by

Alessandra DallaVecchia

2023

ABSTRACT OF THE DISSERTATION

Perturbing the Edge of Consciousness

Examining signatures of criticality in the conscious and unconscious brain

by

Alessandra DallaVecchia

Doctor of Philosophy in Psychology

University of California, Los Angeles, 2023

Professor Martin M. Monti, Chair

The waking brain demonstrates remarkable coordination across multiple scales and exhibits coherent global dynamics. However, in the transition to unconsciousness, the brain's cognitive processing capabilities diminish, accompanied by a reduction in the spatiotemporal complexity of global dynamics. The Critical Brain hypothesis is introduced as an explanatory framework, aiming to elucidate how the brain supports complex computations during wakefulness and the subsequent decline of these abilities in unconscious states. Neuroscientific evidence suggests that the brain operates slightly away from a critical point between percolating and non-percolating phases within the Mean Field Directed Percolation (MFDP) class while recent work suggests another critical point, the edge of chaos, may support the waking state. Experimental measures of proximity to the edge of chaos are difficult to find, but a new measure using concurrent transcranial magnetic stimulation and electroencephalography (TMS-EEG) has emerged as a potential proxy. Moreover, TMS-evoked responses can be leveraged to test MFDP-associated phenomena, allowing for the examination of proximity to either critical point within a single dataset. It remains unclear whether MFDP or the edge of chaos critical point sustains the wakeful conscious state or is associated with other cognitive functions. In the present dissertation, I first provide a general background on criticality and how TMS-EEG can be used to measure the proximity of the brain to MFDP or the edge of chaos. In the second chapter, I present work that confirms the hypothesis that a new measure using TMS-evoked responses can serve as an experimental indicator of proximity to the critical point at the edge of

chaos . In the third chapter, experimental measures of the edge of chaos and MFDP are applied to TMS-evoked responses and compared across stimulation site and conscious states (wake and NREM sleep). In the fourth chapter, I investigate if these two experimental measures of criticality can be dissociated during wakefulness, using neuromodulation. Across the three presented experiments, complexity of the TMS-evoked response is more closely associated with changes in conscious state than MFDP-associated phenomena, providing further evidence to support the association between the edge of chaos critical point and consciousness.

The dissertation of Alessandra DallaVecchia is approved by

Marco Iacoboni

Nanthia A. Suthana

Barbara Knowlton

Martin M. Monti, Committee Chair

University of California, Los Angeles

2023

DEDICATION

To my wonderful fiancé, who had to put up with a brain-dead partner who at times could not meaningfully contribute to discussions and plans with anything other than a No *or* I don't know.

To my amazing friends, who helped me laugh-off the lows and enjoy the highs.

And to my parents, thank you for your never ending support in spite of my stubborn determination to stay in school for ten years.

Contents

List of Figures

List of Tables

ACKNOWLEDGEMENTS

I would like to extend my heartfelt gratitude to several individuals and organizations whose support and contributions have been instrumental in the completion of this dissertation. First and foremost, I am deeply indebted to my advisor, Martin Monti, for his unwavering guidance, mentorship, and support throughout my dissertation journey. His expertise and dedication have been invaluable in shaping my research and helping me navigate the complex terrain of consciousness research. Without his sage advice and encouragement, this dissertation would not have been possible. To the members of the MontiLab, both past and present, I offer my sincere thanks. Your support, collaboration, and camaraderie throughout the years have been of immeasurable worth. Your contributions, both academically and personally, have enriched my research journey and made it all the more fulfilling. I would also like to express my sincere appreciation to my diligent research assistants–Tasha Bierling, Liberty Kolodny, Gina Spagarino, Maziyah Mayet & Autumn Haikal–who played a crucial role in the success of the projects presented in this work.

Daniel Toker played a critical role in designing and fine-tuning the computational model described in Chapter 2, ensuring its accuracy and reliability. His meticulous work in calibrating the parameters for both wakefulness and anesthesia states has been instrumental in simulating and analyzing the effect of cortical dynamics on TMS-evoked responses. Furthermore, I extend my heartfelt appreciation to Silvia Casarotto and Mario Rosanova, who generously provided access to the NREM sleep datasets used in Chapter 3. Their trust, collaboration, and commitment to advancing our understanding of brain dynamics and complexity during NREM sleep have been truly instrumental.

Lastly, I'd like to acknowledge the support of the American Psychological Association (APA), whose financial assistance supported data collection for the work presented in Chapter 4, through their COGDOP scholarship.

To everyone mentioned above and to those who have supported me in various ways, I offer my heartfelt thanks. Your contributions have left an indelible mark on this dissertation, my academic journey, and my life.

Chapter 2 is a version of the following article:

DallaVecchia, A., Toker, D., & Monti, M.M. (*In preparation*). *In silico* loss of consciousness: Does evoked neural complexity reflect proximity to edge-of-chaos criticality?

Alessandra DallaVecchia

adallave@ucla.com Google Scholar Orchid ID

Education

University of California, Los Angeles Expected Dec 2023

Doctorate of Philosophy, Psychology *GPA: 3.91/4.0*

University of California, Los Angeles Dec 2019

Masters of Arts, Psychology *GPA: 3.91/4.0*

Villanova University Dec 2015

Bachelor of Arts, Magna Cum Laude,Psychology *GPA: 3.76/4.0*

Publications

DallaVecchia, A., Toker, D., & Monti, M.M. (*In preparation*). Scale in the Brain: How concurrent TMS and EEG can be used to investigate information transmission in the brain.

DallaVecchia, A., Toker, D., & Monti, M.M. (*In preparation*). *In silico* loss of consciousness: Does evoked neural complexity reflect proximity to edge-of-chaos criticality?

Frohlich, J., Bayne, T., Crone, J. S., **DallaVecchia, A.**, Kirkeby-Hinrup, A., Mediano, P. A. M., Moser, J., Talar, K., Gharabaghi, A., & Preissl, H. (2023). Not with a "zap" but with a "beep": measuring the origins of perinatal experience Origins of perinatal experience. *NeuroImage*, 120057. https://doi.org/10.1016/j.neuroimage.2023.120057.

Davis, K. S., Kennedy, S. A., **Dallavecchia, A.**, Skolasky, R. L., & Gordon, B. (2019). Psychoeducational Interventions for Adults With Level 3 Autism Spectrum Disorder: A 50-Year Systematic Review. *Cognitive and Behavioral Neurology*, 32(3), 139-163.

Escolar, M. L., West, T., **Dallavecchia, A.**, Poe, M. D., & LaPoint, K. (2016). Clinical management of Krabbe disease. *Journal of Neuroscience Research*, 94(11), 1118-1125. https://doi.org/10.1002/jnr.23891.

Posters

DallaVecchia, A., Bierling, T., Hopkins, A., Kolodny, L., Iacoboni, M. & Monti, M.M. (2023, July). Theta burst stimulation to the left superior parietal lobule induces changes in single pulse TMS-induced oscillations and scale-free brain dynamics. Poster presented at the Organization for Human Brain Mapping conference, Montreal, Quebec, Canada.

DallaVecchia, A., Rosanova, M., Casarotto, S., & Monti M.M. (2023, June). Describing different critical points in conscious and unconscious states using TMS-EEG. Poster presented at the Association for the Scientific Study of Consciousness conference, New York City, NY.

DallaVecchia, A., Micheli, F., Frohlich, J., Toker, D., & Monti, M.M. (2021, November). Quantifying changes in complexity of the event related response to sensory stimuli in different states of arousal. Poster presented at the Society for Neuroscience 2021 Global Connectome virtual meeting.

Awards and Fellowships

COGDOP Graduate Research Scholarship	2022
American Psychological Foundation	*$2,000*
Trainee Professional Development Award (TDPA)	2021
Society for Neuroscience	
Graduate Research Mentorship Program (GRM)	2019
University of California, Los Angeles	*$36,848*
Psychology Graduate Summer Mentorship Program (PGSRM)	2018
University of California, Los Angeles	*$6,000*

Teaching Experience

Behavioral Neuroscience Laboratory	Fall 2023
Teaching Assistant	*UCLA*
Human Neuropsychology Laboratory	Spring 2023
Teaching Assistant	*UCLA*
Human Neuropsychology Laboratory	Winter 2023
Teaching Assistant	*UCLA*
Behavioral Neuroscience Laboratory	Fall 2021
Teaching Assistant	*UCLA*
Laboratory in Functional Neuroimaging	Fall 2020
Teaching Assistant	*UCLA*
Intro to MATLAB	Winter 2020
Teaching Assistant	*UCLA*
Intro to Psychology	Spring 2019
Teaching Assistant	*UCLA*

Chapter 1

General Introduction

A fundamental aspect of the human mind is the subjective feeling of experience, the "what it is like" or qualia, that accompanies certain mental processes. Yet, little is known about how subjective experience arises from our brain's processing of external and internal information. This explanatory gap has been termed the "hard problem" [1] and it contrasts with the "easy problem," which refers to the investigation of neural and computational mechanisms supporting different aspects of consciousness (e.g., attention, volitional control, and the differences between a conscious and unconscious state). This dissertation narrows its scope to address a particular facet of the "easy problem" by investigating the Critical Brain hypothesis as a potential mechanism supporting maximum computational capacity during wakefulness.

1.1 The easy problem of consciousness and brain dynamics

Within the broad umbrella of the term consciousness, one branch of scientific inquiry focuses on the neuroscience of intransitive consciousness [2], in contrast to transitive consciousness where awareness is focused on particular objects or individuals. This study of intransitive consciousness focuses on the neural mechanisms that underlie a state of consciousness (defined as state in which there is something "it is like" to be in, also known as wakefulness [3]), typically in comparison to states of unconsciousness (defined as states in which there is an absence of any subjective experience, such as general anesthesia and dreamless sleep).

One feature that has been associated with wakefulness is high dynamic complexity – defined as the simultaneous presence, within a biological system, of high functional differentiation and high functional integration [4]. In wakefulness, this complexity is identified by the presence of a large variety of brain states, or repertoires, as compared to NREM sleep [5], anesthesia [6, 7, 8, 9], and loss of consciousness due to traumatic brain injury [10]. In conditions of dimin-

ished consciousness, the brain appears to transverse fewer and less complex functional brain states. Indeed, a growing body of evidence leveraging both healthy volunteers and clinical populations consistently highlights the positive association between observed network complexity and level of consciousness, to the point that some measures of complexity appear capable of uncovering with high accuracy the presence of conscious awareness [11, 12]. The mechanisms through which the brain maintains its characteristic high complexity during states of awareness, however, remains unclear. With these insights in mind, it is essential to uncover the ways in which the brain navigates the fine line between exploitation and exploration while awake, and how this equilibrium is disrupted in the loss of consciousness. In what follows, I will describe why the Critical Brain hypothesis appears particularly suited as a mechanism of conscious state, a current issue with this hypothesis, and possible experimental methods that can aid in our investigation of this hypothesis within the study of consciousness.

1.2 A possible mechanism: Critical Brain Hypothesis

The Critical Brain hypothesis proposes that the brain operates at and self-organizes towards a critical point [13, 14, 15, 16]. Criticality refers to the phenomena that appear when a system is at a phase transition (at the critical point) and coincides with a breaking of some symmetry. This phase transition can be of the physical state, such as from liquid to ice water, where water's translational and rotational symmetries are broken, or from paramagnetism to ferromagnetism, where the rotational symmetry of magnetic spins is broken. Described originally in equilibrium systems, self-organized criticality describes how dissipative dynamical systems, common systems in nature and biology, naturally evolve towards a stable, robust critical state [17, 18]. Many phenomena that arise when a system is at a critical point are observed in the brain (e.g., the presence of 1/f noise) and are associated with peak computational abilities. This "inverted-U" of computation associated with criticality mirrors the peak dynamic complexity that we see in conscious vs unconscious states.

The first experimental evidence of critical phenomena in the brain was the observation of neural "avalanches" (a type of cascading activity) that showed power-law statistics in *in vitro* local field potential (LFP) recordings from rat somatosensory cortex [19, 20]. The presence of power-laws is indicative of criticality because it suggests the presence of scale invariance: a feature of a system whereby the structure and/or dynamical properties of a system have no

characteristic scale (for an in-depth review see [21]). This property is beneficial to a system as it allows for information to be integrated collectively across different scales. Experimental work with electroencephalography (EEG), magnetoencephalography (MEG), and local field potentials (LFPs) have also reported finding scale invariant neural avalanches, e.g., [22, 23, 24], supporting the presence of criticality in the brain.

It is not enough, however, to say the brain shows signs of criticality – identifying the critical point is important as different critical points can be associated with different phenomena, information processing benefits (e.g., dynamic range and communication), and "universality classes." Part of what makes the critical brain hypothesis appealing is the possibility to identify the universality class that may best describe brain dynamics. A universality class describes a group of systems that have similar macroscopic qualities, irrespective of their microscopic properties, and are identified by a specific critical point. They are useful classifications as the simpler systems of the class can be used to test hypotheses and theories about larger, more complex ones even if the two share no common underlying microscopic mechanisms. The scale invariant fluctuations seen in the seminal work of [19, 20] were suggestive of a critical branching process which led to the current hypothesis that the waking brain is poised near the mean field directed percolation (MFDP) critical point [25]. However, while the current literature focuses on the MFDP critical point, the original hypothesis proposed that the brain operated near a different critical point—between a stable, periodic phase and an unstable, chaotic phase because of the computational benefits in information processing found for systems at or near this "edge of chaos" [26, 27].

1.3 Two possible critical points: MFDP and edge-of-chaos

Directed percolation (DP) describes a class of models that exhibit phase transitions from a permeable (percolating) state to an impermeable (non-percolating) state, so these models mimic how fluids are filtered through porous materials along a given direction [28, 29]. DP is considered one of the simplest universality classes of transitions out of thermal equilibrium and is used widely to provide insights into collective behavior on large scales as the model can be scaled by varying the microscopic connectivity of the "pores." MFDP refers to the application of the mean field approximation to directed percolation models, meaning that the behavior of the system can be described by mean field equations where interactions between elements are

assumed to be uniform and independent [30]. The use of the mean field approximation differentiates this class from others as the approximation assumes that each elements interacts with the average behavior of the system, thus it does not have a well-defined spatial dimension. This neglect of the spatial dimension is in contrast to other models such as the Ising model [31] which has been used previously to model brain connectivity (e.g., [32]).

The concept of the "edge of chaos" encapsulates a transitional state that exists between stable and chaotic dynamics within a system and, unlike MFDP, it is not a universality class. Establishing its presence is still helpful, however, because it allows us to identify a number of simpler systems that can be used to simulate a variety of possible collective neural behavior (e.g., an Ising model or cellular automata), much like a universality class does. The connection between the edge of chaos and computation arose as a response to the idea that for a network to attain the utmost computational capacity, it must possess both flexibility and reliability, enabling it to adeptly respond to a diverse range of inputs while ensuring consistent reactions to those inputs. Critical systems, with their distinct attributes, seem to furnish a suitable environment for the cultivation of this equilibrium between flexibility and reliability. Here, the notion of "computation" is grounded in information theory, focusing on the system's capacity to store, modify, and transmit information. This connection was initially introduced concerning a system poised at the transition between stable and chaotic dynamics [33, 34, 35]. Although the criticality associated with the edge of chaos shares notable computational traits with MFDP and other instances of "avalanche criticality," it also presents unique attributes. These include heightened susceptibility to perturbations and the ability to integrate multiple inputs over varying timescales [36, 37, 38, 39] (Fig 1.1). Some evidence has suggested that the brain resides on the stable side of the edge of chaos critical point [40]. However, research conducted within our laboratory suggests that dynamics during wakefulness reside just beyond the edge of chaos, on the chaotic side, with states of unconsciousness coinciding with either supercritical, chaotic phase (i.e., general anesthesia) or the subcritical, stable phase (i.e., generalized

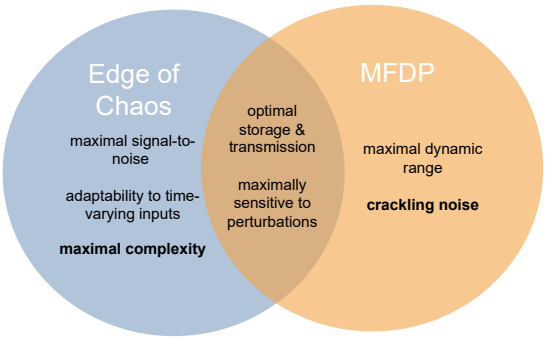

Figure 1.1: While some computational benefits have been seen in for both of these critical points, there are others that are unique to each. For this reason, it is best to use a variety of measures looking at different phenomena to ensure proper identification of the critical point.

seizures) [41].

Traditionally, researchers have tended to isolate specific facets of criticality for examination. Yet, a captivating avenue of investigation emerges when contemplating whether diverse critical points may be present simultaneously and support different aspects of consciousness, potentially encompassing various cognitive states (e.g., attention). Likewise, the presence of both critical and non-critical units may help better optimize performance by allowing for the individual modulation of different units' proximity to criticality [42]. For consciousness, the waking state may be supported by one of these critical points or a specific combination of critical points. But to determine whether one or more critical points correlate with shifts in conscious states, and not just cognitive states, we need measurements that can both distinguish between different critical points *and* are reliable in unconscious states.

1.4 Testing criticality in conscious states

One of the most common neuroimaging methods to study intransitive consciousness, compares and contrasts the spontaneous brain dynamics occurring under the different states and at the transitions from one state to another as recorded with functional magnetic resonance imaging (fMRI) or electroencephalography (EEG) (e.g., during full consciousness, drowsiness, loss-of-consciousness during general anesthesia; [43, 44, 45]). In this type of methodology, often referred to as passive or resting state paradigm [46], the similarities and differences between brain dynamics observed during conscious and unconscious states are then used to make inferences about what brain structures or activity are necessary to support consciousness. In general, passive paradigms in the transition from consciousness to unconsciousness show brain dynamics shifting from a state of high spatiotemporal variability in functional states or repertoires to one that has fewer repertoires [47, 10, 7, 48, 49, 5].

On the one hand, passive approaches have been very fruitful. In the clinical context, for example, these techniques hold the promise of allowing to disambiguate whether someone is conscious or not on the sole basis of brain activity. This is a very appealing prospect in circumstances where more traditional approaches to determining whether someone is conscious (which are typically based on whether someone can demonstrate the presence of behavior that appears to be voluntarily mediated, as opposed to reflexive) can be ineffective due to the presence of sensory or motor impairments [50]. On the other hand, passive approaches only offer

circumstantial evidence for what features of brain function are necessary for a state of consciousness and, by extension, only offer circumstantial evidence as to whether someone is conscious [51].

A different method for approaching the study of intransitive consciousness is that of so-called perturbational techniques. Rather than assessing spontaneous brain activity at different levels of consciousness, this approach focuses on characterizing evoked brain activity in response to a stimulus and, in particular, its temporal evolution. For example, one might analyze the brain's response to a sensory stimulation – referred to as an event related potential (ERP). Much like passive approaches, perturbational techniques circumvent the problem of requiring someone to be capable of expressing motor behavior in order to demonstrate a state of consciousness, but unlike passive paradigms, perturbational paradigms allow researchers to study the timeline of specific cortical properties or states that a stimulus follows during consciousness vs unconsciousness. So, while passive paradigms give a general idea as to how the brain is processing its environment, perturbational paradigms allow researchers to examine the specific, temporal processing associated with that stimulus in a particular conscious state. Thus, ERPs and other perturbational methods offer a great middle road between full behavioral assessments of consciousness that require full subject participation and the passive paradigms that require none.

Conventionally, ERP paradigms employ sensory input (e.g., auditory and somatosensory) as a form of perturbation. For example, auditory evoked potentials have been found to provide some evidence of consciousness in patients as the presence of late components (e.g., P300) are associated with conscious processing of stimuli and, therefore, a state of consciousness [52, 53, 54, 55]. Similarly, somatosensory stimulation has been employed to distinguish conscious from unconscious states, particularly in the clinical context (e.g., [56]). However, this type of stimulation relies on a relatively intact sensory system, and for those studies that use language-based stimuli [57, 58, 59], on a certain degree of language comprehension, both which may not be necessary prerequisites for consciousness.

A different approach that may bridge this last gap of sensory-based perturbation methods is the use of *concurrent transcranial magnetic stimulation and electroencephalography* (TMS-EEG). In this methodology, the need for intact sensory and peripheral pathways is bypassed by the direct stimulation of cortex using single pulses of TMS. The difference between TMS-EEG responses (TMS evoked potentials [TEPs]) in conscious vs unconscious brains mirrors

the evidence from passive rest paradigms and sensory paradigms, but with a high degree of specificity and sensitivity [60, 11, 61, 12]. During wakefulness, the brain response to TMS is highly variable over both spatial and temporal scales with multiple components peaking over different brain regions. Whereas in NREM sleep (and other states of unconsciousness), the response is characterized by large amplitude responses restricted in time, lasting only about 100 ms, and highly localized to the stimulated cortex [62].

1.5 Why use TMS-EEG?

TMS, originally developed by Barker and colleagues in 1985 [63], offers an important non-invasive, neurostimulatory therapeutic and experimental alternative. It offers a unique way to interact with ongoing neural activity, and, unlike other sensory stimulation approaches, it gives researchers more flexibility and control to directly perturb and evaluate the relevance of activity to a given neural event or activity in general. TMS works through the principle of electromagnetic induction and Faraday's Law wherein electrical currents are induced by a conductor placed in a changing, "time-varying", magnetic pulses. Rapidly changing magnetic fields are induced by running a short, strong electrical current through the TMS coil. When placed near the scalp, these magnetic fields can penetrate the scalp and skull to reach the cortical surface, where they can induce secondary ionic currents (eddy currents), resulting in action potentials or post-synaptic potentials. The reach of the coil-induced magnetic field is short, so it is typically assumed that cortical or subcortical white matter is being stimulated [64, 65, 66, 67]. Although its principal mechanism of action is relatively simple, understanding just how these eddy currents affect individual neurons and cortex is another matter.

TMS has been used since its invention to study brain-behavior relations under the assumption that the introduction of the eddy current results in some disruption of local processing that then can be used to make assumptions about the importance of certain cortical regions' contributions to the behavior of interest. In essence, TMS was described as forming a sort of 'virtual lesion' [68], and although the mechanisms were not understood, research could take advantage of said disruption, treating it as if it were an injection of random noise—ideal for making and testing claims of causality. The "disruption" caused by TMS can be useful not only by looking at its effects on other brain networks or cognition, but by pairing it with EEG, it can be used to investigate the stability of brain dynamics.

In 1997, Ilmoniemi and colleagues developed a specialized electroencephalography (EEG) amplifier using a sample-and-hold circuit which allowed for the concurrent collection of EEG data during TMS (TMS-EEG) [69]. The introduction of concurrent electrical recording has significantly enhanced the temporal precision of TMS studies, marking a significant advancement in experimental testing of the brain's spatiotemporal dynamics in response to TMS. Notably, the application of TMS-EEG has revealed a fascinating phenomenon: a TMS pulse triggers a distinctive "phase reset" that ripples from the stimulated region to cover the entire scalp. This unique response not only offers insights into the inherent oscillatory traits of various cortical regions but also unveils the intricate functional interplay between these regions. Central to this phenomenon are the dynamic properties of the system that affect these interactions. Consequently, the TMS pulse should not be thought of as a mere infusion of random "noise" or a virtual lesion [68], as repetitive rTMS has been previously described, but, instead, it embodies a targeted response, that momentarily impairs neuronal activity and results in a reaction that sparks an array of dynamic neural responses across neighboring and functionally connected regions. These cascading responses, in turn, allow researchers a way to deduce the dynamic characteristics of the brain precisely at the moment of stimulation.

A parallel thread of inquiry frames the TEP response as a representation of the brain's transition across diverse states—spanning from the baseline period state to either a response or non-response state [70, 71]. Mutanen et al. [72] hypothesized that TMS not only redirects the brain into an alternate subspace but also steers it towards a higher-energy subspace. Echoing this sentiment, other authors propose that TMS shifts the system away from its attractor, either entirely (with rTMS) or towards a distinct basin within the same attractor (with a single pulse or short pulse trains) [73]. Consequently, TMS-EEG emerges as a potent avenue to scrutinize the impact of dynamics, initial state characteristics, and structural attributes, including recurrence, on the brain's response to a single TMS pulse. As such, TMS-EEG and TEPs are uniquely placed to offer improvements in measurements of criticality and applying them to populations that have been traditionally difficult in which to assess consciousness.

1.6 Dissertation Outline

The overarching question of this dissertation is whether either critical point (edge of chaos or MFDP) is related more closely to *intransitive consciousness*, or conscious state. This question

is further broken down into the following three:

1. Does a previous measure using TMS-EEG that has been found to have high specificity and sensitivity to conscious state track a system's proximity to the edge-of-chaos critical point?

2. Do avalanche measures done on TEPs mirror the findings of complexity in different conscious states (wakefulness and deep sleep) and across different stimulation regions (premotor and parietal stimulation sites)?

3. Can we dissociate between different critical points and conscious state by manipulating proximity to either critical point during wakefulness with neuromodulation?

In chapter 2, we address the first question utilizing a modeling approach by simulating the TEP in a cortical patch and studying how the simulated response changes when the dynamics are shifted towards and away from the edge of chaos. This study serves to confirm the intuition that the complexity of a TEP response can be used to experimentally measure the proximity of the current brain state to the edge of chaos critical point. In chapter 3, we apply complexity and the neural avalanche analyses to previously acquired TEPs in wakefulness and NREM sleep to investigate how the two measures change with level of consciousness and across different stimulation sites. As anticipated, the complexity of the TEP response is lower in NREM sleep compared to wake, but, surprisingly, while we do see changes in neural avalanches, they do not completely align with previous findings. In chapter 4, we conclude by using a patterned TMS protocol to modulate cortical dynamics during resting eyes-open in healthy subjects. Here, we find that while complexity of the TEP response does not change before and after neuromodulation, we see a change in scale invariance. This change, however, does not appear to be induced by neuromodulation, but is probably due to changes in arousal.

Chapter 2

In silico loss of consciousness: Does evoked neural complexity reflect proximity to edge-of-chaos criticality?

2.1 Introduction

Over the last 25 years, the notion that human consciousness is characterized by a state of high dynamic complexity – defined as the the simultaneous presence, within a biological system, of high functional differentiation and high functional integration [74] – has gained increasing interest [75, 76]. Indeed, a growing body of evidence leveraging both healthy volunteers and clinical populations consistently highlights the positive association between observed network complexity and level of consciousness, to the point that some measures of complexity appear capable of uncovering with high accuracy the presence of conscious awareness [12, 11].

The mechanisms through which the brain maintains its characteristic high complexity during states of wakeful awareness, however, remains unclear. Numerous MRI studies have indicated that the number and complexity of functional states that the brain traverses over time changes across different conscious states. Wakefulness, in particular, is distinguished by a greater diversity of brain states, or repertoires, as compared to sleep [5], anesthesia [6, 9, 7, 8], and disorders of consciousness (DOC) [10]. In conditions of diminished consciousness, the brain appears to traverse fewer and less complex functional brain states. Given these observations, it is crucial to elucidate how the brain maintains a delicate balance between exploitation and exploration of its dynamics during wakefulness and how this balance is changed by loss of consciousness. This dynamic equilibrium, sometimes referred to as metastability, is often associated with criticality [77]. Criticality refers to a state in which a system exists at the threshold between two distinct phases of matter or temporal dynamics, accompanied by the breaking of some symmetry.

In the context of brain function, theoretical and neurophysiological work suggests that the

brain operates in a regime close to criticality, with so-called avalanche and edge-of-chaos criticality being the two most prominent types of phase transitions associated with brain function [26]. Indeed, our own prior work in a biologically realistic neural model shows that proximity to the edge-of-chaos critical point can support the information-richness of neural activity and the effective information communication typical of waking cortical electrodynamics [41, 78]. Moreover, the presence of weak chaos, in the proximity of the edge-of-chaos critical point, offers important advantages in terms of a system's response to perturbations, providing a unique balance of flexibility and stability. In this regime, despite the dynamic variability enabled by chaoticity, activity can still be stabilized, or provide predictable outputs, in response to perturbations [79, 27]. However, transitioning into the regime of strong chaos, or extreme sensitivity to inputs, disrupts this delicate balance between flexibility and control, impeding a system's ability to stabilize its response [80, 81]. This heightened flexibility or increased sensitivity to input leads to a notable decrease in information communication and processing efficiency as compared to the critical boundary [36, 33]. Consequently, the introduction of new information or perturbations supersedes and displaces old information derived from previous perturbations, resulting in the loss of valuable historical information. While these phenomena are fairly well-characterized in simulated systems, the determination of chaoticity and the assessment of proximity to the edge-of-chaos pose significant challenges when dealing with noisy, experimental neurophysiological data, which can be difficult to experimentally distinguish from noise [82, 83]. Therefore, determining how a range of experimental markers acts at and around the edge-of-chaos critical point, is essential to *in vivo* validation of simulation findings.

We propose exploring the relationship between the edge-of-chaos criticality, inter-trial variability and the complexity of the brain's response to transcranial magnetic stimulation (TMS) evoked responses (TEPs), called the perturbational complexity index (PCI) [60]. Indeed, the complexity of unperturbed or "resting state" neural electrodynamics has been shown to track level of consciousness, possibly because of deviations toward or away from the edge-of-chaos critical point in conscious versus unconscious brain states [41, 78]. But such "resting state" measures of complexity may be less reliable than PCI, owing to their lower signal-to-noise ratio, and so it is imperative to determine whether there may be a relationship between edge-of-chaos criticality and the brain's perturbational complexity, which is a more robust experimental measure of consciousness.

Inter-trial variability, once relegated to the category of intrinsic ”noise” in evoked brain responses, has gained increasing importance as it is now recognized to be intricately connected with two critical factors. These include 1) intrinsic noise stemming from random neural events, such as stochastic synaptic release, [84] and 2) alterations in network state [85]. In this study, we delve into the intricate interplay between changes in chaotic brain dynamics and their impact on the association between trial-to-trial variability and baseline oscillatory phase—an established metric of baseline state that has been previously linked to variability [86, 87].If the brain is near the edge-of-chaos critical point, then chaotic dynamics would result in amplification of small changes [88], leading to seemingly minor variations in the evoked response across trials with little to no apparent connection to the baseline oscillatory phase. The relationship between chaos and inter-trial variability is likely complex, as it has previously been found that networks with chaotic dynamics can exhibit stable responses by switching to locally stable dynamic attractors in response to perturbations [89, 90]. Therefore, inter-trial variability in response to perturbations (such as TMS) is a valuable supplement to measures of the chaoticity of neural systems, and is experimentally easier to quantify than resting-state variability, owing to the same signal-to-noise ratio issues discussed above.

In what follows, we leverage an *in silico* approach, using a neural field model (NFM), to assess the relationship between critical brain dynamics, the complexity of the brain’s response to a TMS pulse, and the inter-trial variability of the brain’s response to a TMS pulse. NFMs offer computationally tractable ways to simulate the response and interactions of populations of different types of neurons and by employing such models, it is possible to compare and evaluate the underlying characteristics against a “ground truth.” In our case, we can directly measure and manipulate the chaoticity of our model.

Neural mass models (NMMs), a class of mean field models like NFMs, have been previously used to study aspects of PCI [91]. Nonetheless, a comprehensive exploration of the relationship between response complexity and the underlying dynamics of conscious and unconscious states remains unaddressed. Moreover, while neural field and neural mass models have been employed to investigate the inter-trial variability of neural activity, they are predominantly focused on exploring the neurobiological underpinnings rather than specifically examining the cortical and cortico-thalamic dynamics that give rise to this canonical variability [92].

2.2 Results

We utilized a mean-field model developed in previous work to simulate the electrodynamics of the brain in both awake and anesthetized states [78]. To investigate the relationship between TEPs and chaos, we started with a wake parameter configuration identified in the previous study and employed a genetic algorithm to obtain a parameter set that could reproduce TMS-like evoked responses. The fitness function used in the algorithm evaluated the number of components in the response period and the amplitude of the first component relative to the baseline peaks. The resulting parameter set for the waking TEP response, along with the anesthesia parameters determined in our previous work, were then utilized to examine the effects of underlying dynamics on the simulated TEPs.

2.2.1 TEPs at the edge-of-chaos show a balance between high variability and stability

In our analysis of the wake parameters of our mean-field model, we uncovered noteworthy characteristics resembling experimental TEPs (Fig 2.1). Firstly, the initial components of the TEP response within the first 100 time-steps displayed magnitudes significantly larger than the baseline oscillations. Notably, the peak-to-trough amplitude was six times higher than the pre-stimulation peak-to-trough amplitude. Secondly, we observed a distinct pattern in the response. While the third component stood out as the largest, the overall response initiated with a significant amplitude, gradually decreased over time, and eventually returned to baseline. This pattern of response with components starting larger then diminishing with time is a distinct feature of empirical TEPs (Fig. 1.1, right) compared to sensory-evoked potentials. Thirdly, the response duration lasted approximately 200 ms before returning to baseline, consistent with typical wake TEPs that last between 200 and 300 ms. Lastly, we detected an intriguing interplay between inter-trial variability and response stability: manipulating the initial firing rates, even slightly, caused marked variability in the response amplitude, resembling the inter-trial variability observed in empirical studies (Fig 2.2). Remarkably, these salient features were not incorporated into the error function of our genetic optimization, and underwent notable changes when the system transitioned into a supercritical regime (Fig 2.3).

The presence of amplitude variability presents an intriguing opportunity to explore the factors associated with specific response characteristics in a near-critical regime. One potential

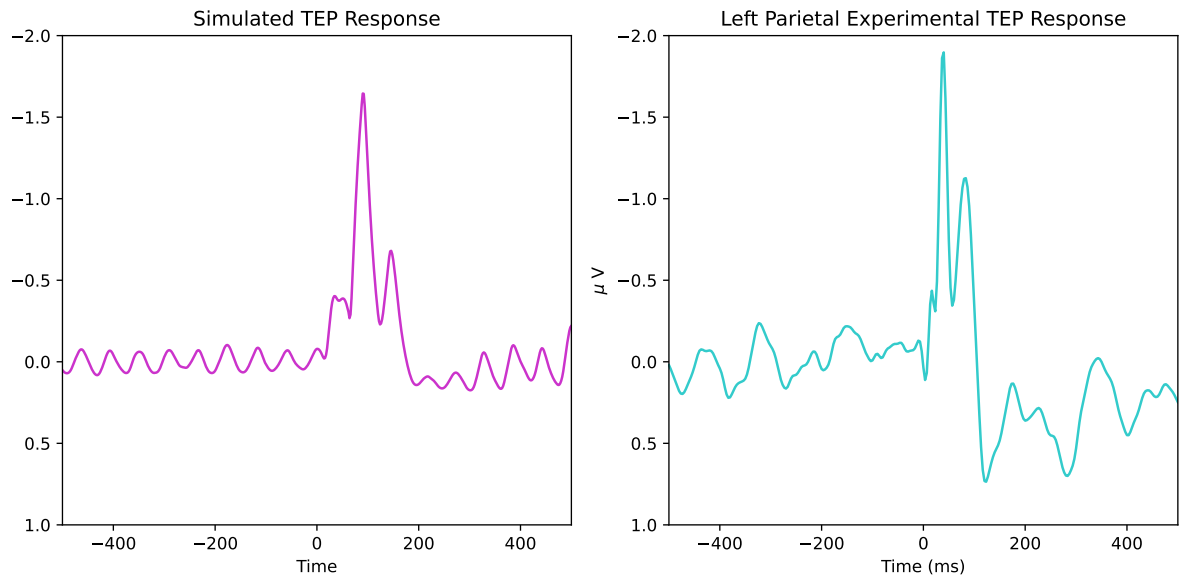

Figure 2.1: This figure depicts the response of our simulation across 20 runs with different initial firing rates for our wake parameter set compared to an experimental grand average response (N = 19) from a channel below the stimulator (CP3).

factor contributing to this variability is the pre-stimulus phase of the baseline oscillations. The impact of pre-stimulus phase on the amplitude of TMS- and motor evoked potentials (MEPs) has not been clearly determined. Some experiments find a connection [93, 94] while others find pre-stimulus power, rather than phase, to be more relevant [95, 96]. To investigate the potential influence of pre-stimulus phase on TMS-evoked responses in our model, we conducted simulations using 100 randomly generated initial firing rates and then employed three clustering methods to analyze the responses.

The first method, which we refer to as our "manual" approach, involved categorizing each run based on whether stimulation occurred at a peak, trough, or midpoint. This determination was based on the proximity of the time-step just before stimulation to the peak or trough of an oscillation (Fig 2.2).

Next, we applied an unsupervised learning technique, K-means clustering, to cluster the responses. This clustering was based on both the pre-stimulus baseline amplitude at the time-step just before stimulation and the responses themselves. The elbow method was employed to determine the optimal number of clusters. Using the baseline amplitudes, we partitioned the runs into three clusters, as determined by the elbow method, which corresponded well with our manual classifications of peaks, troughs, and midpoints (Fig 2.2). Cluster 1 appeared to include stimulation that occurred at a midpoint, Cluster 2 consisted of runs in which stimulation occurred at the peak of the baseline oscillation, and Cluster 3 consisted of runs in which

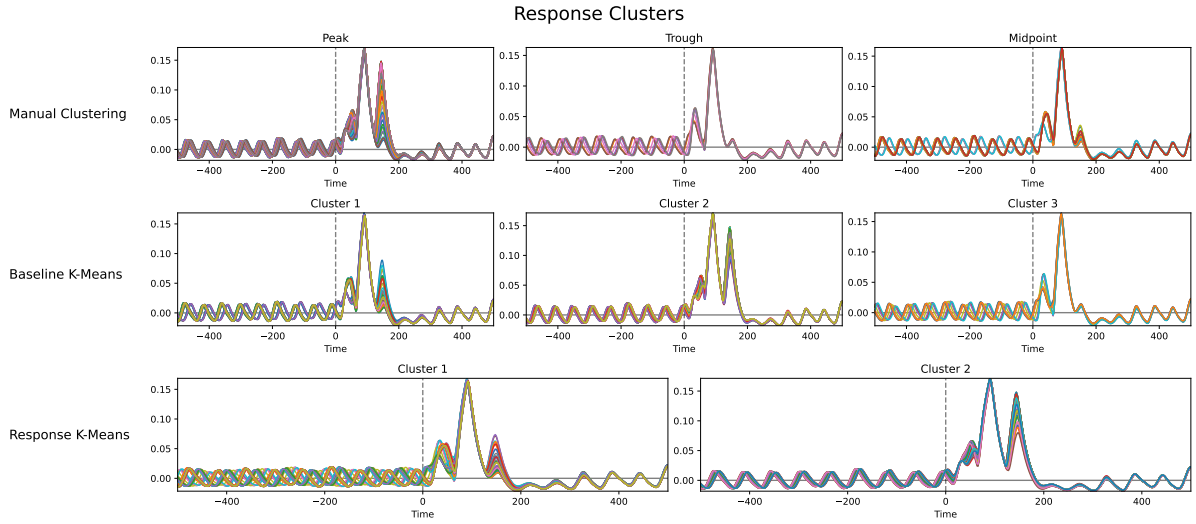

Figure 2.2: The results from the three outlined clustering methods: manual clustering, baseline-seeded k-means clustering, and response-seeded k-means clustering are shown. The clustering was performed on 100 runs of the wake parameter set with varying initial firing rates. The clusters suggested by K-means clustering are similar to the manually selected clusters at the trough, peak, and midpoint.

stimulation occurred at the trough of the baseline oscillation. The main difference was that our manual technique picked out more pre-stimulus peaks than the baseline K-means, which clustered more runs at what appears to be a "midpoint." Based on this clustering technique, the variability of the response appears to increase when stimulation hits the midpoint of a baseline oscillation relative to stimulation hitting at a peak or trough. Furthermore, the peak stimulations of Cluster 2 have a much larger third positive component than either Cluster 1 or Cluster 3.

In our third method, we investigated whether the baseline phases aligned when clustering was based on the response window (Fig 2.2). Here, the elbow method indicated two clusters that were appropriate for our data. The clusters born from this method, which is based only on the response, seem to separate trials in which stimulation occurred at peaks on the one hand, from trials in which stimulation occurred at troughs and midpoints on the other. The simulated TEP responses in Cluster 2 all occur after stimulation during the peak of the baseline oscillation. In addition, they result in less variability in the first two components, and the last positive component is much larger compared to Cluster 1. In Cluster 1, the first two components appear highly variable in amplitude and latency. The initial components in the other two clustering techniques do not show this latency variability, which implies that the midpoint and trough distinction is likely important to the latency of the first component.

The clustering analyses conducted using the three methods revealed interesting insights re-

garding the relationship between pre-stimulus phase and TEPs. All three methods identified a distinct cluster corresponding to the responses after stimulation at the peak of a baseline oscillation. Interestingly, the most distinctive feature of these responses is the increased magnitude of the final component before the return to baseline. These results imply a clearer association between pre-stimulus phase and amplitude variability in later components than earlier ones. The variability of these early components in our model does not appear to be fully associable to the pre-stimulus phase. The last observation is that the second positive TEP component exhibited the greatest robustness to changes in firing rate and baseline oscillation, regardless of the clustering method employed. This result implies that the mid-latency component may be the least associable to neural excitability.

These findings highlight the complexity of the relationship between pre-stimulus phase and TMS-evoked responses, suggesting that additional factors may contribute to the observed variability. Further investigations are warranted to gain a deeper understanding of the underlying mechanisms driving these dynamics and to explore potential interactions between pre-stimulus phase and other parameters influencing TEPs.

2.2.2 Increasing anesthetic dose slows and simplifies the simulated TEP response

With an established wake parameter set, we then used the anesthesia parameter set from our previous study [78] while keeping fixed the parameters related to the TMS stimulation (stimulation amplitude, couplings, and dendrites between the pulse and excitatory and inhibitory populations). First, we examined the response and neural dynamics under a 50% anesthesia dosage, representing an intermediate stage between the wake parameters discussed above and the previously established anesthesia parameter set (Fig 2.3). Notably, despite being still near the edge-of-chaos, the baseline oscillations became larger and slower, and the response amplitude dramatically increased while retaining the same number of positive components as the wake parameter set. The response duration remained around 200 ms.

We then explored the effects of full sedation and supercritical dynamics on the stimulation evoked response. In this parameter set, the response amplitude was several times larger than the response amplitude produced by our waking-state simulation, emulating a key observation of experimental TEPs after propofol anesthesia [12]. However, unlike experimental TEPs during anesthesia from GABAergic drugs such as propofol, our stimulation response results

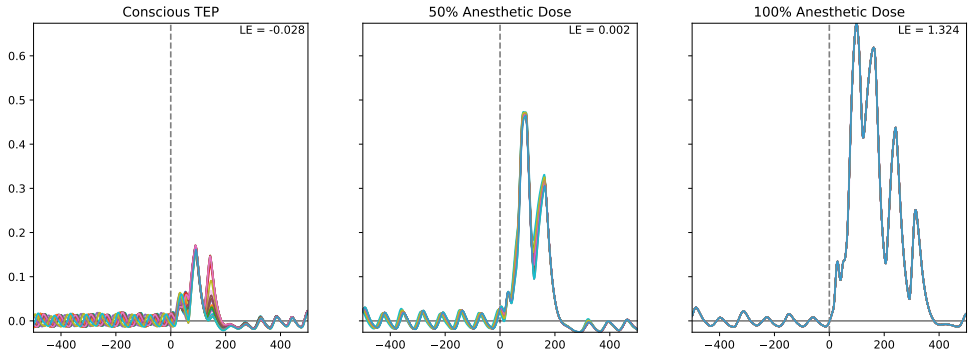

Figure 2.3: The simulated TEP responses from each parameter set (wake, 50% anesthetic dose, & 100% anesthetic dose) are plotted along with the calculated largest Lyapunov exponent (LE). The response to a simulated TMS pulse is shown for each dosage over 20 runs with different initial starting parameters. This figure showcases the large degree of variability in the simulated response for the wake parameter sets compared to either anesthetic dose.

in a substantially longer evoked response, lasting roughly double the duration compared to the critical sets. This response profile is more similar to the experimental TEPs during Xenon anesthesia [12], the pharmacology of which differs markedly from that of GABAergic anesthetics.

To investigate the influence of pre-stimulus phase in our simulation of the anesthesia TEP response, we manually adjusted the stimulation time to coincide with peak, trough, and midpoint of the baseline oscillation. In the 50% dosage, the response closely resembled the wake parameter set, with peak and trough stimulations resulting in nearly identical responses to our wake parameter sets (Fig 2.4). However, these responses were still much larger than those in the wake set and did not show the same variability between peak and trough. This result implies that the transition towards anesthesia diminishes the effect of pre-stimulus phase on response variability.

In contrast, while the 100% anesthesia dosage did exhibit some amplitude variability, in general the responses were similar no matter if stimulation occurred at a peak, trough or midpoint, despite the increased sensitivity to initial conditions (i.e. chaoticity) of the anesthesia simulation, as indexed by its largest Lyapunov exponent (Fig 2.4). Interestingly, the amplitude of the late-latency components (100-200 time-steps) differed only for midpoint stimulation, while peak and trough stimulations yielded similar responses, akin to the 50% dosage. As the 50% dosage represents a transitional state between wakefulness and anesthesia, it likely has elements of response variability observed in both parameter sets. Previous simulation work has shown a similar pattern where the relationship between pre-stimulus phase and phase-locking to a stimulus disappeared in sub and super-critical phases of a model at the edge-of-

synchrony [97].

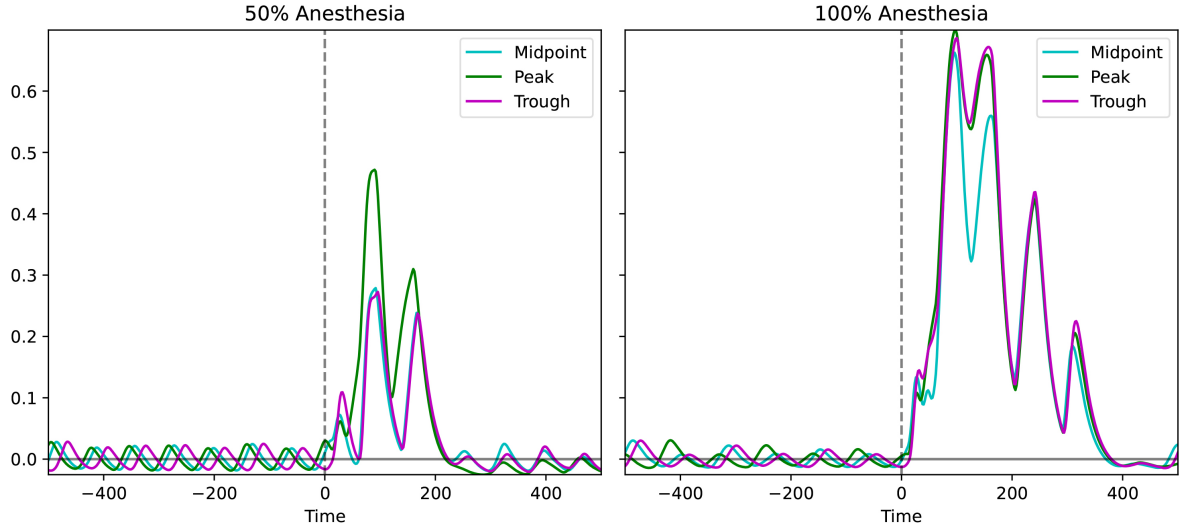

Figure 2.4: The response for the 50% and 100% anesthesia parameter sets are shown when the stimulation is delivered at the peak, trough, or midpoint of the baseline oscillation. For both doses, the main difference between the response when stimulation is delivered at the trough, midpoint, and peak is the magnitude of all components.

2.2.3 Complexity of the response tracks the underlying system dynamics

Finally, we assessed response complexity to our simulated TMS pulses and its relationship with underlying dynamics and pre-stimulus phase. The complexity of the stimulation-induced response was found to be similar between the two edge-of-chaos parameter sets: the wake parameter set (LZc = 0.47) and the 50% anesthesia dosage (LZc = 0.50). In contrast, complexity significantly decreased for the full anesthesia dosage (LZc = 0.15).

Regarding the clustering analysis, the wake parameter set exhibited consistent complexity levels across different pre-stimulus phases, whether at a peak, trough, or midpoint (mean LZc = 0.44 for all three). This pattern was also observed for both the baseline K-means cluster (mean LZc = 0.44) and the response K-means cluster (mean LZc = 0.44).

However, in the case of the 50% anesthesia dosage, the complexity varied depending on pre-stimulus phase. The midpoint and trough responses displayed higher complexity (LZc = 0.57 and 0.50, respectively) than the peak response (LZc = 0.38). In the 100% anesthesia dosage, the complexities of the peak and trough responses were similar (LZc = 0.15 for both), with a slightly higher complexity observed for the trough response (LZc = 0.20). Notably, pre-stimulus phase only seemed to affect complexity primarily in the 50% anesthesia dosage parameter set.

2.3 Discussion

We here present a model of a TEP response during wakefulness and show how the complexity of the model's response reflects its proximity to the edge-of-chaos critical point. Our findings suggest that the experimental measure of PCI [60] may indeed reflect the proximity of the brain's dynamics to criticality. Furthermore, we show that while different characteristics of the simulated response change prior to simulated anesthetic loss of consciousness, complexity remains high and lowers significantly only at the full anesthetic dose. In the original paper presenting PCI [60], Casali and colleagues report that PCI remains within the values associated with wakefulness and just barely dips towards value associated with unconscious states for intermediate stages of anesthesia (level 2 - 3 MOAA/S). In another anesthesia TMS-EEG study, Ferrarelli et al. [98] described TEPs from one subject during intermediate midazolam sedation (level 3 OAA/S) who exhibited features of both wake and anesthesia states, with a gradual emergence of the large positive-negative wave associated with deep sedation at the single trial level. Consistent with these findings, our model demonstrates similar behavior in response variability related to pre-stimulus phase. Specifically, stimulation at a midpoint elicits a larger, more sedation-like response compared to stimulation at a peak or trough. These findings suggest that the evolution towards larger and simpler responses in the supercritical phase becomes noticeable in the system's response to stimulation prior to its transition away from the critical point, and that this evolution is reflected in the relationship between pre-stimulus phase and the response. Based on these experimental reports, our 50% anesthetic dose likely represents a very early stage of anesthesia (e.g., stage 1 of Guedel's Classification or the induction stage [99] or levels 6 - 4 MOAA/S) where consciousness is reduced but the individual is still able to respond to commands.

Our second finding explores the intricate relationship between response variability, complexity, and dynamic phase in the context of TEPs. We show that pre-stimulus phase is related to the early and late latency components of the response but only for the wake TEP response. These findings align with previous experimental evidence highlighting the association between mu-rhythm phase and early and late latency TEP responses to stimulation of the supplementary motor area and motor cortex [100, 94, 93, 101]. Our results also provide novel hypotheses about the relationship between complexity and pre-stimulus phase for the transitional period between wakefulness and full sedation. In our model, as we progress toward the administra-

tion of 100% anesthetic dose, the relationship between pre-stimulus phase and TEP weakens and the response profile stabilizes across different phases. Nevertheless, complexity reduces slightly in the 50% dose model when stimulation occurs at a midpoint, yet it remains higher than the complexity observed during full sedation. This intriguing finding implies two important hypotheses: firstly, during the transition from wakefulness to full sedation, the TEP response exhibits characteristics of both states, depending on the pre-stimulus phase; and secondly, complexity can capture these transient responses while still remaining higher than the complexity observed during full sedation.

Notably, our model specifically captures the relationship between pre-stimulus phase and a single stimulation-induced response. It has been proposed that the variations in findings regarding MEPs could be attributed to differences in inter-stimulus intervals (ISIs), with the possibility that shorter ISIs (> 0.2 Hz) could promote heightened neural entrainment and consequently intensify the correlation between baseline phase and the entrained response [96]. Our findings present a contrast to this interpretation, as we observe a certain degree of phase-based modulation even with a single pulse. It is plausible that this relationship may be attenuated due to measurement error in experimental settings employing longer ISIs, but becomes more apparent when shorter ISIs are employed, facilitating greater neural entrainment and increasing signal-to-noise ratio. Furthermore, these conflicting studies aforementioned primarily looked at MEP amplitude rather than TEPs, suggesting the possibility that phase-based modulation of corticospinal excitability may require cortical-level entrainment. Future investigations should extend the current model to incorporate multiple pulses at different intervals, enabling a more comprehensive exploration of how phase-based modulation at the cortical level is influenced by entrainment and neural plasticity.

It is important to acknowledge two limitations of our study. Firstly, our model represents a single cortical patch beneath the stimulator, allowing us to assess only the temporal complexity of the simulated TMS response, whereas PCI captures the spatio-temporal complexity of TEPs. Moreover, the absence of intracortical connections and feedback mechanisms in our model may limit its ability to fully capture the effects of recurrent processing, which could potentially alter the response dynamics and contribute to increased complexity. However, previous research utilizing NMMs with different underlying dynamics and without thalamic or globus pallidus (GP) populations has demonstrated region-specific characterization of TEP responses, primarily relying on internal parameters for each region-specific NMM [102]. Thus, a model of a dis-

connected cortical patch may suffice to model region-specific responses. Nevertheless, future investigations should address these limitations by incorporating multiple patches and including appropriate neural connections.

Secondly, there is a discrepancy between the stimulation-induced response observed in full sedation in our model and the experimental findings. In the literature, while the complexity of the TEP remains low across different anesthetics (Xenon, propofol, midazolam, and ketamine) [12], the response profiles themselves vary slightly. For GABAergic anesthetics (propofol), the TEP results in a large positive component, followed by a large negative component and the response lasts in total around 100 ms, while for Xenon anesthesia, the TEP response is noticeably larger and longer lasting compared to wakefulness [12]. Our model's response to full sedation resembles the latter scenario, despite being designed to simulate GABAergic anesthesia. This difference will be interesting to investigate further in future work. Pharmacological studies have found that changes in GABAb affect mid-latency components (N100) of the M1-TEP response [103, 104]. Future work should address both of these issues by adding a fast, inhibitory cortical population and performing the same parameter search done previously [78] with this new wake parameter set.

2.3.1 Conclusion

In summary, we present a model of TEPs during wakefulness, and use this model to explore the relationship between response complexity, pre-stimulus phase, and anesthetic dosage. Crucially, our findings indicate that the complexity of the model's response reflects its proximity to the critical point between stability and chaos. We also demonstrate that different response characteristics change prior to simulated loss of consciousness (LOC), but with complexity significantly decreasing only at full anesthetic dose. Notably, our model exhibits similarities to experimental findings where TEPs recorded under intermediate sedation gradually transition to larger, simpler responses. We also investigate the impact of pre-stimulus phase on response variability and latency components, offering novel hypotheses regarding the relationship between complexity and pre-stimulus phase during the wakefulness-to-sedation transition. However, it is crucial to acknowledge that our model represents a single cortical patch, and further investigations involving multiple regions and the inclusion of intracortical connections are warranted. Additionally, the discrepancy between our full sedation response and experimental findings highlights the need for future studies to explore the complex dynamics of TEPs un-

der different anesthetics and consider the inclusion of additional neural populations in future studies.

2.4 Materials and methods

2.4.1 Mean-field model of the electrodynamics of the basal-ganglia-thalamocortical system

The basal-ganglia-thalamocortical mean-field model developed by van Albada and colleagues [105, 106] was used to simulate TEPs and study the relationship between TEPs and chaos. The model simulates the average response of a population of neurons by dividing the population's max firing rate by the mean membrane potential of those neurons above the reversal potential. The population firing rate (Q_a^{max}) at point r and time t is modeled with a sigmoidal function of the number of cells whose potential (V_a) is above the mean threshold (θ) of that population:

$$Q_a(r,t) = \frac{Q_a^{max}}{1 + \exp\left[-(V_a(t) - \theta_a/\sigma'\right]} \tag{2.1}$$

where σ' is the standard deviation of the firing thresholds. The change in mean cell-body potential (V_a) for a type a neuron is modeled as

$$D_{\alpha\beta}(t)V_a(t) = \sum_b v_{ab}\phi_b(t - \tau_a b) \tag{2.2}$$

where $\phi(t-\tau)$ is the incoming pulse rate, tau is the axonal time delay between type b to type a neurons, and v_{ab} is the change in mean cell-body potential due to afferent activity from type b neurons. $D_{\alpha\beta}$ is a differential operator that represents dendritic and synaptic integration of incoming signals:

$$D_{\alpha\beta}(t) = \frac{1}{\alpha\beta}\frac{d^2}{dt^2} + (\frac{1}{\alpha} + \frac{1}{\beta})\frac{d}{dt} + 1 \tag{2.3}$$

Where α and β are the decay and rise rates of the cell membrane potential. We made the following modification to the original Robinson mean-field [106]. While in the original, both the duration and peak η of synaptic responses is scaled by α and β:

$$\eta(\alpha,\beta) = \frac{\alpha\beta}{\beta - \alpha}\left[\exp\left(-\alpha\frac{ln(\beta/\alpha)}{\beta-\alpha}\right) - \exp\left(-\beta\frac{ln(\beta/\alpha)}{\beta-\alpha}\right)\right] \tag{2.4}$$

We modified the synaptic response h such that its duration and not its peak is modulated by α and β:

$$h(t) = \frac{H}{\eta\left(\alpha, \beta\right)}\overline{h}(t) \tag{2.5}$$

Where $\overline{h}(t)$ is the original synaptic response and $H = 31.5\ s^{-1}$ [107]. This modification was done in accordance with prior anesthesia modeling studies as an effect of GABAergic anesthesia is to prolong the duration of postsynaptic inhibition without altering the peak of the postsynaptic chloride current[107, 108]. Lastly, a damped-wave equation was used to model the propagation of mean electric field ϕ_{ab} from population b to population a:

$$D_{ab}\phi_{ab}(r,t) = Q_b(r,t) \tag{2.6}$$

$$D_{ab} = \left[\frac{1}{\gamma_{ab}^2}\frac{\partial^2}{\partial t^2} + \frac{2}{\gamma_{ab}}\frac{\partial}{\partial t} + 1 - r_{ab}^2\nabla^2\right] \tag{2.7}$$

where r_{ab} is the spatial axonal range and ∇^2 is the Laplacian operator, and γ_{ab} is the temporal damping coefficient:

$$\gamma_{ab} = \frac{v_{ab}}{r_{ab}} \tag{2.8}$$

Finally, we introduced several populations and connections not in the original van Albaba and Robinson model: the globus pallidus (both internal and external capsules) and D1 and D2 striatal populations. We added inhibitory connections from GPe to cortical inhibitory neurons [109, 110], the thalamic reticular nucleus [111], and both D1 and D2 populations [112, 113, 114]. The TMS pulse was modeled as a biphasic external driving stimulation to the cortical excitatory and inhibitory populations. The strength of the stimulation was modified by altering the coupling (γ_{ex} and γ_{ix}) between the stimulation population (x) and the excitatory (e) and inhibitory (i) populations. In sum, the model contained 192 free parameters.

Determining a new wake parameter set

We previously identified a parameter configuration for waking brain states [78] that resulted in low-amplitude and weakly chaotic oscillations of local field potentials (LFPs), simulated by taking the sum of synaptic currents [115]. To identify a parameter set that resulted in a TMS-like evoked response, we used a genetic algorithm to modify the wake parameter set we previously identified.

In our first step, our fitness function error increased if 1) there were more or less than 3

components in the response period (around 300 time-steps post stimulation), and as 2) the first component got smaller and more like the average amplitude of the baseline . As the model was oscillating prior to stimulation, the second error was included to increase the error of parameter sets where the stimulation was not strong enough to elicit an oscillatory response larger than the average baseline oscillation. The component error was calculated with a double inverse symmetric logistic function:

$$E(x) = L - \left(\frac{L}{1 + e^{-k(x-c1)}} - \frac{L}{1 + e^{-k(x-c2)}} \right) \tag{2.9}$$

Where L is the maximum error, $c1$ is 0.5 times the lowest acceptable bound, $c2$ is 1.5 times the highest acceptable bound, and k is the rate at which the error increased as the given value moved below $c1$ or above $c2$. The baseline error was calculated as the reciprocal of the amplitude of the first response component and the mean amplitude of baseline peaks with a maximal bound of 0.2.

From that initial wake parameter set, an addition 19 'mutations' were created where the chance that any given parameter would be mutated will be 10% and parameters would 'mutate' by multiplying their original number by a random number uniformly sampled between 0.5 and 1.5. After which, for each new generation, 20 pairs of randomly selected parameter configurations were selected for 'cross-over,' yielding 40 new parameter configurations, and another 20 will be created through mutation. Then, from those 50 parameters sets, 10 will be selected that yield the lowest error (as calculated above) to cross over and mutate in the next generation. The genetic algorithm ran for 100 generations for 10 parallel runs. After the 10 runs, the parameter set with the lowest error was chosen. Once the wake TEP parameter set had been identified, the system's largest Lyapunov exponent and the average response were assessed by adding and or subtracting 0.0 – 0.1 to the initial firing rates to modify the initial state of the system 20 times. The average largest Lyapunov exponent from these twenty runs was used as the final measure of chaoticity for the parameter set while the average of the propagator responses was taken as the final evoked response.

In our second step, we ran a final genetic algorithm with the parameters obtained from the above to bring the baseline oscillations to an amplitude similar to the original wake parameters while keeping the fixed indices from the original wake parameters. The fitness function in this step included the same component error as the first step, but replaced the baseline error with

a max baseline peak error where the absolute difference was taken between the max peak amplitude in the first five seconds before stimulation and the max peak height from our original wake parameters. This difference was then multiplied by some constant k to keep the model from converging too quickly.

Once we identified a set of parameters for the waking TEP response, we used our previously identified anesthesia parameters [78] to test how underlying dynamics affect the simulated TEP. Our anesthesia parameters result in strongly chaotic LFPs dominated by large-amplitude delta (< 4 Hz) oscillations in the baseline period prior to stimulation. We then used the following equation to produce a parameter set (P) at 50% and 100% doses D of the simulated anesthetic:

$$P = P_0 \left(\frac{P_1}{P_0} \right)^D \tag{2.10}$$

where P_0 and P_1 are our wake and anesthesia parameter sets, respectively. As D increases, the model moves from its awake state ($D = 0$) towards its anesthetized state ($D = 1$).

2.4.2 Calculating the Lyapunov Exponents

We calculated the stochastic Lyapunov exponent of the mean-field model's excitatory firing rate in the period before stimulation to measure the chaoticity of the model. A positive large exponent indicates chaos while a negative large exponent indicates periodicity. The edge-of-chaos is at the transition between these two states and therefore occurs when the Lyapunov exponent is at zero with near-zero exponents indicating near-critical dynamics. To calculate the Lyapunov exponent, a simulation with initial starting parameters was run for 20 seconds, then rerun but with the additional of random noise perturbation to all neural populations at 9.999 seconds. The rate of divergence between the two simulation runs was calculated over the final 10 seconds. The divergence $e(t)$ was estimated by the summed squared difference between the first $Qe^{(1)}$ and second $Qe^{(2)}$ simulation run, divided by the maximum possible difference:

$$\epsilon(t) = \frac{(Qe^{(1)}(t) - Qe^{(2)}(t))^2}{\epsilon^{max}} \tag{2.11}$$

$$\epsilon^{max} = (max(Qe^{(1)}) - max(Qe^{(2)}))^2 \tag{2.12}$$

The largest Lyapunov exponents is then calculated by estimating the rate of divergence:

$$\epsilon(t) = \epsilon(0) \exp(\Lambda t) \tag{2.13}$$

Where $\epsilon(0)$ is the initial distance between the two simulations at t = 0. The slope of the $\ln \epsilon(t)$ versus time gives the estimate of the largest Lyapunov exponent, and, because both simulation runs had the same noise inputs, this slope gives the estimate of the stochastic Lyapunov exponent for the model.

2.4.3 Calculating Lempel-Ziv complexity of the simulated TEP response

To calculate the Lempel-Ziv complexity (LZc) of the simulated TEP response, we made the following modification to the traditional methodology; the binarization threshold for the response period was calculated based on the mean of the absolute Hilbert of the 500 timestep period prior to stimulation. The LZc algorithm was then applied to the binarized response period and normalized by dividing by the LZc of 15 Fourier-transformed surrogates [116].

Chapter 3

TMS-evoked complexity & avalanches in wakefulness & NREM sleep

3.1 Introduction

Sleep is a temporary and reversible state of reduced consciousness experienced by most animals on a daily basis. At a broad level, sleep is divided into two different categories of states: non-rapid-eye-movement sleep (NREM) and REM sleep. Physiologically, the two conditions differ dramatically between each other. REM is identified by the emergence of wake-like EEG activity but absent muscle activity and the presence of the eponymous rapid eye movements while NREM sleep can be identified by an increased density of slow oscillations and, depending on the stage, the presence of K-complexes and sleep spindles. Phenomenologically, the main difference between NREM and REM is that while REM is associated with conscious-like experiences, while during NREM people report either a complete the absence of experience, much like general anesthesia, or very vague abstract experiences [117, 118].

NREM sleep is of particular interest in consciousness because it is endogenously generated, unlike general anesthesia, and reversible. In both NREM and anesthesia, the brain remains structurally intact and functionally active, but unable to sustain long-range communication [62, 12]. There is, however, increasing evidence that the brain in NREM can still process sensory input to some extent [119]. Cortical activity switches to a bistable regime where cortical neurons alternate between periods of increased, wake-like activity (UP states) followed by periods of suppressed firing (DOWN states) [120]. The appearance of these DOWN states has been hypothesized to be the mechanism that interrupts long range correlations [121, 122] and suppresses effective communication between different brain regions triggered in response to incoming signals (e.g., a TMS pulse) [123, 124]. Thus, there is a well-established cortical mechanism for the loss of effective communication and information integration in NREM sleep.

3.1.1 Criticality and NREM sleep

If criticality supports conscious experience and therefore wakefulness, then measures of criticality should indicate that during NREM, the brain deviates away from criticality towards either the sub- or supercritical regime. As mentioned in the general introduction (1.2), scale invariant fluctuations are typically used to study criticality in the brain. These scale invariant fluctuations are otherwise known as neural avalanches—a separate mode of neural activity different from oscillations, synchrony, and waves [19]. This type of activity is defined by the presence of increased bursts of neural activity that occur continuously in time across a variety of sources (Fig. 3.1). Avalanches are different from waves or other modes of activity in that although activity is propagating out from the starting neural population, it does not need to propagate in a spatially contiguous way (it need be only temporally contiguous). Avalanches and the distributions of their sizes and durations are used to identify the critical point of interest, the proximity of the system to this critical point, and to confirm that the power-laws represent "crackling noise."

The term "crackling noise" refers to high-amplitude scale invariant fluctuations with long autocorrelations [125]—take for example a piece of paper being crumpled and the sound it produces [126]. It is the presence of both a *critical slowing down* (increase in long-range temporal correlations [LRTCs]) and *scale invariant fluctuations* that are indicative of a critical phase transition. Critical points associated with this "crackling noise" are referred to as avalanche criticality (for a review see [13, 26]). However, evidence for criticality in the brain relies generally on evidence for one of the two (power-laws or LRTCs) even though scale invariant avalanches have been seen in non-critical systems [127, 128, 129, 130] and have been observed in regions surrounding the critical phase transition [131, 132]. Crackling noise can be recognized by a specific scaling relation (outlined further in the methods section 3.2.4) that has not been observed for other non-critical systems [128, 130, 129].

Evidence of criticality that incorporates this scaling relation suggests that the waking brain operates not at criticality, but in a slightly subcritical regime or in a 'quasi-critical' regime [133, 132, 16]. There has also been an argument for an "extended" critical phase where a system shows critical phenomena over an extended parameter space (Griffiths phase) [134, 135, 136]. The idea of a quasi-critical regime or an extended critical phase has gained traction as it seems highly unlikely that a complex system like the brain would be able to maintain precise tuning to a specific point in parameter space.

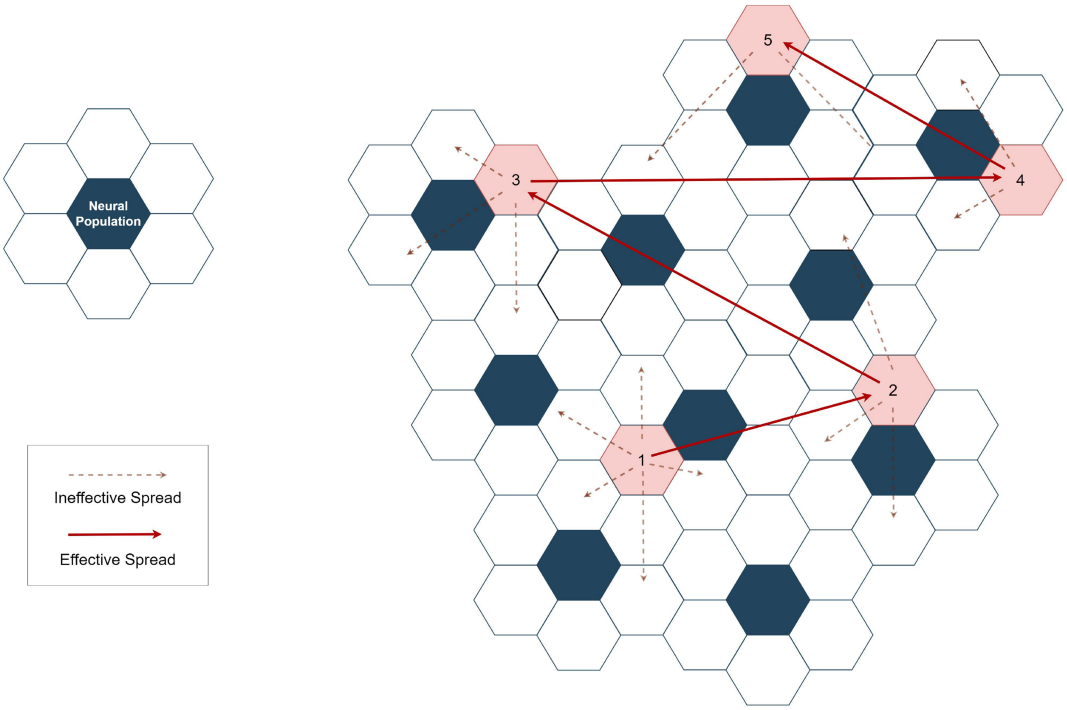

Figure 3.1: A depiction of how information may be communicated in a patch of cortex through scale invariant fluctuations. The patch of cortex is represented by a 2D lattice structure of hexagonal neural populations. The pink hexagons reflect information transmission through a change in the neural system's phase (e.g., if it is a system of oscillators, the pink could represent synchronization between the specific populations) in the spatial domain. The numbers on the pink hexagons represent the order in which the information is transmitted from node to node in the temporal domain. The first change in phase in pink hexagon 1 leads to the change in pink hexagon 2 and so on until the last pink hexagon fails to elicit a change in another neural population, resulting in an avalanche of specific size (# of pink hexagons whose phase was changed) and duration. A probability density function (PDF) can be created based on the size and duration of all the avalanches in the system. If this distribution of size and duration are most similar to a power-law function as compared to other distributions like a lognormal or exponential distribution, then the avalanches are scale-invariant.

Despite the experimental support for the idea that a state of wakefulness correlates with critical or near critical dynamics, there is some ambiguity in the evidence that NREM sleep results in a deviation away from criticality. On one hand, there is clear evidence in support of changes in scale-free connectivity, structure, and loss of LRTCs in sleep [121, 137, 122] (cf. [138]) with decreased LRTC and increased synchronization indicative of supercritical dynamics. On the other hand, evidence from neural avalanches appears to indicate that scale invariance is preserved in NREM sleep with the main difference between wake/REM and NREM being an increase in tails of the distribution in NREM [121, 139]. This increase in the tails of a power law distribution indicates that there is a tendency to see either larger or longer events. In the supercritical phase, this increase becomes a "bump" near the end of the distribution [140, 141]. Evidence of flattened power laws (and a lack of a bump) suggests that NREM dynamics are closer to criticality

than wake [140, 139]. Interestingly, drowsiness and sleep deprivation are also associated with similar changes in LRTC and neural avalanches [140, 141]. Taken together, it would appear that NREM sleep pushes critical dynamics towards the supercritical phase, but as the waking resting state operates in a subcritical regime, it effectively pushes the system closer to criticality. In comparison, anesthesia is associated with similar results for LRTCs [142] and persevered scale invariance [143, 140], but more studies in anesthesia have found a loss of scale invariant fluctuations during anesthetic loss of consciousness [144, 145, 146, 147, 148].

Unfortunately, not much work has been done to investigate how the edge of chaos critical point and NREM sleep. Experimentally, complexity is reduced in NREM sleep like it is in anesthesia and other unconscious states [149, 150, 151, 60]. There is some modelling work that has suggested that the slow oscillations during NREM sleep are chaotic (largest Lyapunov exponent > 0) [152]. These results are consistent with our previous study outlined in the preceding chapter, where brain dynamics during GABAergic anesthesia deviate from the edge of chaos critical point towards the supercritical phase [153]. Thus, there is also evidence that cortical dynamics during NREM sleep also transition towards the supercritical, chaotic phase. Therefore, based on the evidence presented above, neural avalanches calculated on TMS-evoked potentials during N2/N3 sleep will still show signs of near critical behavior (scale invariant fluctuations) while the complexity of a TEP will decrease significantly.

3.1.2 TMS-EEG & Avalanches

Applying avalanche statistics to evoked TEPs during NREM sleep allows for the comparison of two criticality measures within the same dataset and under the same brain state (stimulation during rest as compared to traditional spontaneous rest recordings). Moreover, this investigation affords us the opportunity to assess whether a TMS-evoked paradigm yields consistent outcomes with those obtained through resting-state paradigms or if it shows distinct and complementary findings, akin to the distinctions found for complexity in previous studies [154, 155]. Prior research has often relied on intracranial recordings, which are not always logistically feasible in various conditions of consciousness loss, such as those encountered in clinical settings. EEG, although more adaptable, grapples with a limitation known as the coarse-graining problem [156], according to which measurement overlap obscures the true underlying dynamics as it introduces spurious correlations between neural populations. However, I posit that TMS-EEG holds the potential to circumvent many of these challenges, including those related to

coarse-graining and signal-to-noise ratio issues.

Avalanches can be obfuscated in EEG via volume conduction, noise, and merging. Some previous evidence for avalanches in EEG uses channel-space which means that the data are more susceptible to the effects of volume conduction (e.g., [157, 158]). A spread of the signal due to volume conduction would create larger avalanches as more channels appear to be participating in the avalanche [159, 160]. Source localization can help attenuate this effect and other studies have applied avalanche measures on it (e.g., [22, 161]). The first way TMS-EEG helps is by attenuating the effect of experimental noise where peaks may appear due to measurement error or other physiological signals. For example, if a subject has a lot of muscle activation, even with filtering and ICA, not all of that activation may be removed resulting in some signal reaching the applied threshold for avalanches when it should not. Averaging trials, as is done for evoked data, can help further diminish the effect of transients or other physiological noise that is not related to the avalanche. Additionally, we use online monitoring to further eliminate muscle and other event-related noise associated with the TMS pulse. The second way is related to avalanche measurement itself and not to the EEG. In resting state, avalanches are spontaneously evoked from different regions and different times. As such, the data represents many different avalanches from different precipitating events. During measurement of avalanches, as if all instances of significant signal are taken from across the scalp, the presence of multiple avalanches at different trajectories (time-points) would lead to their merging in the analysis– which has been shown can lead to the incorrect identification of the critical point [162]. By using TMS-evoked activity we can address this concern by focusing on avalanches associated with a specific start time and place. Thus, TMS occupies a unique position in surmounting the challenges associated with measuring avalanches when employing a coarse-grained method like EEG. Finally, given the versatility of TMS in its applicability across various cortical regions, it is imperative to ascertain that the stimulation site does not influence the overall power-law behavior. *The primary objectives of this study are, consequently, to assess 1) how two measures of criticality change when using TMS-evoked potentials, and 2) for potential variations in the scale invariance due to the site of stimulation.*

3.2 Methods

3.2.1 Single Pulse TMS procedure & Healthy control data

TMS-EEG data was recorded from subjects with no history of major medical/neurological disorders (n = 20, female = 10, age = 25 ± 6) while they were awake with eyes open. The neural responses to TMS stimulation and the resting state EEG were recorded with a 60-channel TMS-compatible amplifier (BrainAmp; Brain Products GmbH, Germany), referenced to the forehead, and 2 extra sensors were used to record the electrooculogram. Single pulse TMS was delivered to the left or right Brodmann areas 6 (premotor cortex and the supplementary motor area) and 7 (superior parietal lobule) with a focal biphasic figure-of-eight coil driven by a mobile stimulator unit (Nexstim Ltd., Finland). A neuronavigation software using the obtained participant structural MRIs was used to provide improved targeting both within and across TMS stimulations. During the single pulse TMS stimulations, participants wore earphones that continuously played an individualized masking noise to avoid eliciting auditory evoked potentials [163]. To record TEP responses, 200 single TMS pulses were delivered at an ITI of 2.1 – 2.3 seconds (0.53 – 0.58 Hz). Single pulse intensity was set at the % MSO needed to elicit high quality TEPs with 5-10 mV peak-to-peak between the first two components, monitored online [164].

3.2.2 NREM Sleep Data

We used a subset (N = 9, female = 3, age = 29 ± 5) of TMS-EEG data that has been previously reported during N2 and N3 sleep [60, 62, 165]. The setups and equipment were similar between the sleep and our healthy control data apart from the use of a different 60-channel TMS-compatible amplifier (eXemia; Nexstim Ltd., Finland).

3.2.3 Data Preprocessing

EEG preprocessing and analysis was done with in Python with custom scripts and MNE [166, 167]. While delivering TMS pulses, the brief current flow in the coil, lasting for a few hundred microseconds and peaking at several kiloamperes [168], generates a significant voltage in the EEG leads. To remove the TMS artefact, a section from 5 ms after the stimulation was removed, then replaced by mirroring the previous 5ms piece of baseline prior to the cut

section and smoothed with a moving average window. This section -5:5ms around the stimulation was ignored for all subsequent analyses. After the pulse artefact was removed, TMS-EEG data were manually cleaned for bad channels or trials, bandpass filtered from 0.1 – 45 Hz with a bandstop at 60 Hz (zero-phase shift Butterworth, 3rd order), segmented from -600:800 ms around the stimulation, rereferenced to the average, down-sampled to 1000 Hz, and baseline corrected. Independent component analysis (ICA; picard function [169]) was used to remove ocular, muscular, and magnetic artefacts.

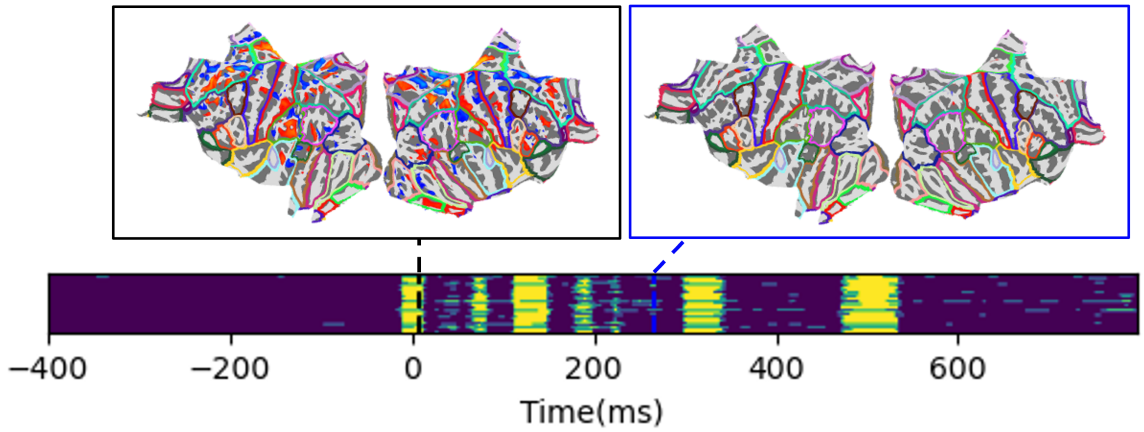

Figure 3.2: Here an example of a binarized 20-trial epoch from one subject during left parietal stimulation is shown on the bottom. On the top, the spatial layout of avalanches at two time-points (8 ms and 268 ms post stimulation) are shown. The first time-point reflects the spatial activations (in red and blue) of the initial evoked avalanche while the second shows the spatial activations of a small later avalanche.

3.2.4 TMS-evoked avalanches

To measure scale-free dynamics, the distribution of size, duration, and size-by-duration of neural avalanches were analyzed for proximity to a scale-free distribution using a maximum likelihood-based analysis and Kolmogorov-Smirnov (KS) goodness-of-fit. For TEPs, the data was down-sampled again to 300 Hz, then neural avalanches were calculated for each subject by dividing the cleaned single-pulse trials into 20 1200ms epoch subsets and running a source reconstruction using sLORETA (standardized low-resolution brain electromagnetic tomography; [170]) on the 20-epoch averaged response. For the wake participants, source reconstruction was done with individual T1 MRIs and digitized positions. For the NREM subjects, as neither individual T1s nor electrode positions were available, source reconstruction was done on a template MRI. Non-parametric statistics were then used to create a binary matrix of significant sources to identify periods of increased activation (Fig. 3.2). The discretized time series of the

response period only (800 ms) was then divided into bins of duration Δt with avalanche size defined as the total number of unique activations of sources within the cascade and its time as the length of time spanned until hitting a time-bin with no significant events. Five time-bins were used starting from the Δt min (the inverse of the sampling rate) and increasing by 1 ms. This allowed us to see how stable the calculated power-law was over different timescales. A maximum likelihood-based analysis and KS goodness-of-fit was used to fit the avalanche size and duration distributions to a truncated power-law, lognormal, and exponential distributions [171, 172] using the powerlaw package [173].

If all the resulting distributions were best fit by a power-law, they were tested against the "crackling noise" scaling relation [125]:

$$\frac{\alpha - 1}{\tau - 1} = \frac{1}{ovz} \tag{3.1}$$

where α and τ are the power-law exponents of the time and size avalanche distributions:

$$f(S) \sim S^{-\tau} \tag{3.2}$$

$$f(T) \sim T^{-\alpha} \tag{3.3}$$

and $\frac{1}{ovz}$ is the power-law exponent for the average size-by-time function:

$$< S > (T) \sim T^{\frac{1}{ovz}} \tag{3.4}$$

ovz are a set of critical exponents, but, in our case, determining the values of each are not central to determining the presence of crackling noise. For the MFDP critical point, we expect τ = 1.5, α = 2.0, and $\frac{1}{ovz}$ = 2.

3.2.5 PCI

The complexity of the TEP responses were calculated using PCI^{LZ} (Lempel-Ziv PCI; [60]). To calculate PCI^{LZ}, the data were down sampled to 325.5 Hz and resegmented to -400:400 ms around the TMS pulse. The data was then source modeled using dSPM (dynamic statistical parametric mapping; [174]) and the same nonparametric bootstrapping was used to binarize the data, creating a matrix of significant sources. Finally, the Lempel-Ziv compression algo-

rithm was calculated on the resulting matrix and normalized by its entropy.

3.2.6 Statistical Analysis

A random-intercept mixed-effects analysis was used to assess differences in PCI^{LZ} between the different conscious states (wakefulness and NREM) and area (BA6 and BA7), using the 'lme4' library [175] in R [176]. A mixed effects analysis was used as it accounts for the random effects of subjects. As for the TMS-evoked avalanches (TEAs), the results will be described qualitatively as our analysis technique resulted in limited data pool. Determining whether a distribution fits a power law requires a very large amount of data, which we are able only to achieve with TMS-EEG data by collapsing across individuals, leaving us with only one set of scaling exponent for each time-bin.

3.3 Results

3.3.1 PCI

There was a significant main effect of conscious state on PCI^{LZ} ($F(1,27)=56.58$, $p < 0.001$) where complexity of the TEP was higher during wakefulness than NREM sleep (Fig 3.3). A likelihood ratio test (LRT) conducted to compare the fit of the full and a null model with no predictors and an intercept term only, found a significant difference in fit (likelihood ratio=19.66, $p<0.001$). The significantly lower AIC and BIC values for the full model (-67.96 and -57.98, respectively) compared to the null model (-54.30 and -49.09, respectively) provide further evidence that the full model is a better fit for the data.

3.3.2 Wake TEAs

For wakefulness and sleep, individual subjects showed PDFs with similar power-law distributions, but due to the low number of avalanche samples, the fit scaling exponents were not reliable enough to compare. This same issue was apparent even when separating individuals by stimulation side (left parietal vs right parietal). For this reason, we collapsed across individuals and stimulation side, but not area, and report scaling exponents from these group distributions (Fig 3.4).

Across all five time bins and collapsing across subjects and for both premotor and parietal sites, avalanche sizes and duration were best fit by a truncated power law. Premotor stimulation

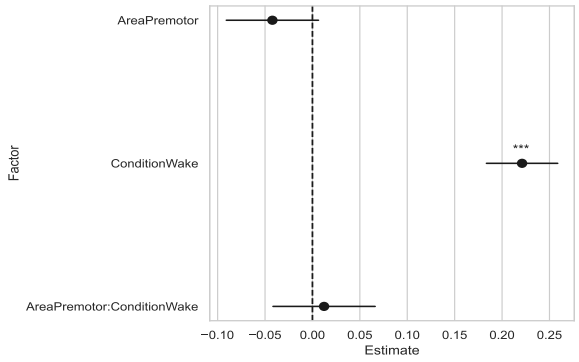

(a) Fixed Effects

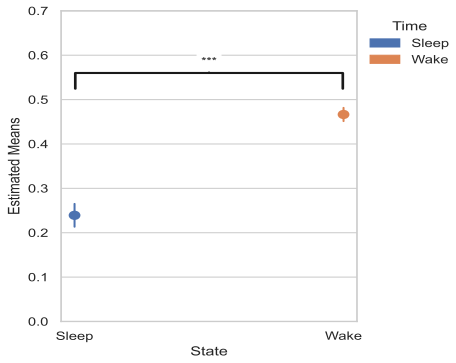

(b) Estimated Marginal Means of Sleep & Wake

Figure 3.3: The fixed effects point plot (a) illustrates the relationship between conscious state (wake and NREM sleep) and area (premotor and parietal) of the mixed-effects model. Each point represents the estimated fixed effect for a specific condition, with error bars indicating standard errors. Asterisks (* p<0.05, ** p <0.01, *** p <0.001) indicate statistically significant differences. The plot suggests that on average PCI increased in the wake condition compared to NREM sleep by 0.25 per 1-unit increase in the predictor. The estimated marginal means graph (b) further illustrates the effect of conscious state on PCI^{LZ} . Error bars represent 95% confidence intervals around the estimated marginal means.

resulted in a mean τ of 1.64 across the five time bins while for parietal stimulation most time bins had a mean scaling exponent of 1.39. In general, the scaling exponents associated with premotor stimulation were marginally higher than for parietal stimulation.

The smallest time-bin (3ms) for both stimulation sites and the 4ms time-bin for premotor showed the least reliable power law fits for avalanche durations— most likely due to missing data in the tails of the distribution or to a breaking up of the avalanches due, so we report on the results from the three remaining time bins. Both sites showed an α that was either 1.00 or 2.3 and fitted $\frac{1}{ovz}$ around 1.06 (premotor) and 1.02 (parietal). In no time-bin did the fitted $\frac{1}{ovz}$ fit the predicted $\frac{1}{ovz}$ in equation 3.1 (for a summary see Table 3.1.

	τ	α	Fitted $1/ovz$	Predicted $1/ovz$
Premotor	1.62	2.06	1.05	1.71
Parietal	1.09	2.13	1.02	12.56

Table 3.1: Table 1 shows the size, duration, and estimated and fitted $\frac{1}{ovz}$ for one exemplary time bin (6.33ms).

3.3.3 NREM Sleep Avalanches

Evoked avalanche size during NREM sleep were both fit best by a power-law over the majority of time-bins across both areas (Fig 3.5) . Compared to wakefulness, the avalanche size scaling exponents were slightly *steeper* (premotor mean = 1.96, parietal mean = 2.05). Similarly to

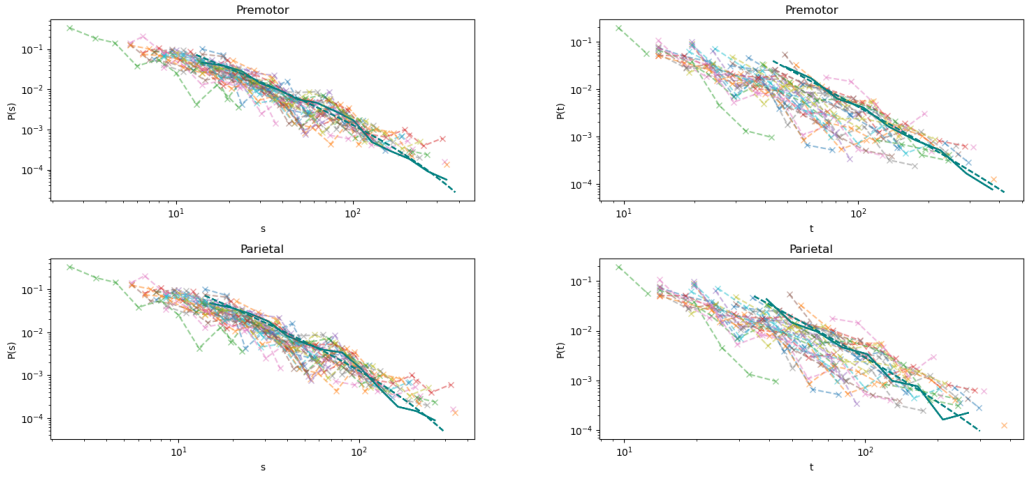

(a) Wake Size PDF (b) Wake Duration PDF

Figure 3.4: Avalanche size and duration PDFs are shown for one time-bin (4ms) from all awake subjects for both premotor and parietal regions. The distributions begin and end near the same values and have a similar linear look in log-log scale. This linearity and overall similarity are important because a superimposition of many exponential processes will look like a power law.

wakefulness, the avalanche durations did not show as reliable fitting as avalanche sizes, but most time bins were found to be best fit by a truncated power law. Interestingly, while both α exponents for premotor and parietal stimulation were flatter compared to wakefulness, the parietal α decreased less than premotor (premotor mean = 1.26, parietal mean = 1.89). For those time bins with reliably fit exponents, the fitted (premotor = 1.07 parietal mean = 1.18) still did not fit the predicted $\frac{1}{\sigma\nu z}$, but for parietal stimulation it did increase compared to wake.

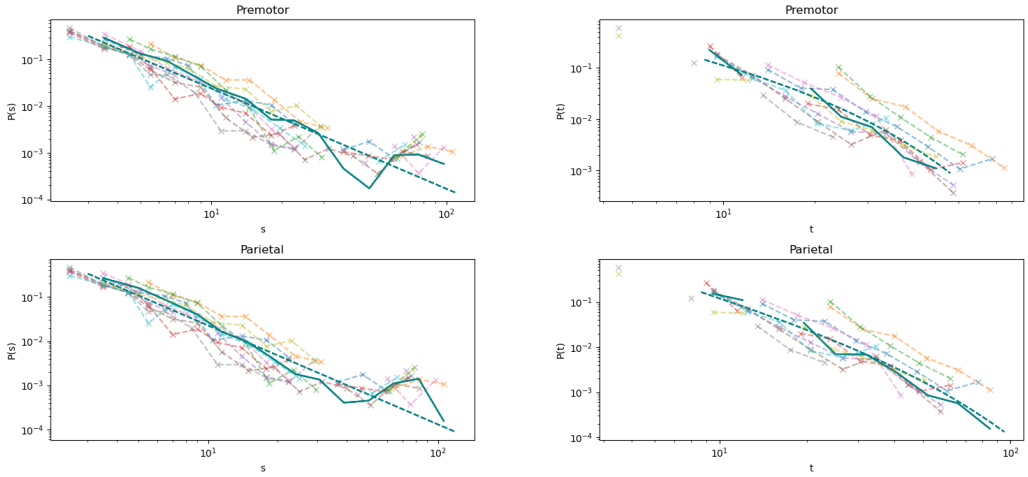

(a) NREM Size PDF (b) NREM Duration PDF

Figure 3.5: Avalanche size PDFs are shown for one time-bin (4ms) from all NREM sleep subjects for both premotor and parietal regions. A "bump" near the tail of the size distribution is seen in all subjects, indicating an increase in the presence of larger avalanches for both sites. This same "bump" is not present in the avalanche duration distributions.

3.4 Discussion

Our results indicate that while TEAs during wakefulness show scaling exponents for size and duration in line with MFDP, they do not follow the scaling relationship (Eq 3.1). Thus, we do not find evidence to fully support MFDP criticality as the generative mechanism for scale invariance, but our results do align with previous work suggesting that the brain may be subcritical. We also show that scale invariant fluctuations are present even during states of unconsciousness (NREM sleep), indicating that unlike PCI^{LZ}, the presence of scale invariant avalanches is not a correlate of consciousness. However, we do see changes in the scaling behavior of these fluctuations in NREM sleep that indicates that there is some change in the underlying scaling laws.

3.4.1 Wake TEAs do not fully support the presence of crackling noise

The scaling exponents for avalanche size and duration are close to those associated with MFDP (τ = 1.5, α = 2) [177, 178], but fail to follow the crackling noise relation. In fact, the scaling relation is near unity (1), which has been associated with a driven time-varying stochastic process [128]. It may be argued that our negative findings for a critical branching process or other avalanche criticality are due to a TMS-induced change in brain dynamics. Although we describe the brain state during TEPs to be resting, we recognize that the TMS stimulation itself may be inducing a change in the underlying brain state by pushing the dynamics away from the subcritical regime that has been previously been found in resting state [146, 140, 160]. Indeed, studies have found that brain dynamics look more subcritical during focused attention and other tasks [179, 180, 181], so it could be argued that the single pulse paradigm is more akin to these evoked and event related paradigms and therefore the deviation of the scaling function further away from crackling noise should be expected. This interpretation would align with previous interpretations where the distance between the fitted to the predicted is taken as a measure of the proximity of the system to the MFDP critical point (e.g., [182]).

An alternative intriguing avenue could be that these avalanches are related to a different critical point—the edge of synchrony (a critical point between asynchronous and synchronous phases). The edge of synchrony critical point has also shown scale invariant avalanche size and duration with similar scaling exponents (1.5 and 2) and a non-critical scaling relation ($\simeq$1.24) [183]. There is also other evidence that at the edge of synchrony, an evoked response becomes

less variable and can co-occur with chaotic dynamics [89]. In fact, it was previously found in our dataset that phase-locking (a proxy for inter-trial variability) is decreased in TEPs during NREM sleep compared to wakefulness [165]. Our fitted $\frac{1}{\sigma\nu z}$ is closer to unity compared to the edge of synchrony relation, but our avalanche duration scaling exponents do not show highly consistent scaling exponents across the five chosen time bins so it is possible that we do not have good estimate of avalanche duration to reliably estimate α. Furthermore, our epoch window is restricted ($\simeq$800 ms) so we likely are missing samples from the tails of the distribution which would greatly influence the fitting of heavy-tailed distributions, such as power laws.

3.4.2 NREM TEAs suggest a possible supercritical shift

Our NREM sleep data may help elucidate possible other generative mechanisms behind the scale invariance. The TEP changes extensively in N2/N3 sleep compared to wakefulness, identifiable by its very large and long-lasting components (Fig 3.7). This change appears to be well tracked by PCI^{LZ} [60]. We, here, endeavored to see how evoked avalanches changed in sleep compared to wake and found that there tended to be a higher incidence of *smaller* avalanches (Fig 3.6). Typically, a steepening of the scaling exponent is indicative of a subcritical shift. As for the avalanche duration distribution, we saw a region-specific change in scaling exponents where premotor stimulation led to a much flatter exponent while parietal stimulation only showed a slight flattening compared to wakefulness. When a power law exponent becomes less steep, then we see a greater incidence of *longer* avalanches, associated with a supercritical deviation.

On their face, these changes are counter to previous evidence of avalanches in NREM [121, 139]and also how we generally think of sleep. NREM is associated with increased broadband synchronization [184, 185] and the presence of a large, low frequency wave that covers the whole scalp (sleep slow oscillation: SSO [186]). This SSO is likely why in resting state avalanches we see a bump in the tail, indicating the increased tendency to see larger, longer avalanches. We see a similar pattern in our data with a distinct "bump" in the probability of larger avalanches (Fig 3.5), but unlike resting state, our size scaling exponent is *steeper* for the TMS evoked avalanches. These findings would reflect the one characteristic of NREM TMS evoked responses where fewer sources are found to be activated by a TMS pulse. A similar bump was found with whisker stimulation by Mariani et al [187] and "heaps" found in edge of synchrony simulation work [188]. These bumps or heaps are associated with increased occurrences of large highly synchronous events, which would be consistent with cortical behavior in N2/N3

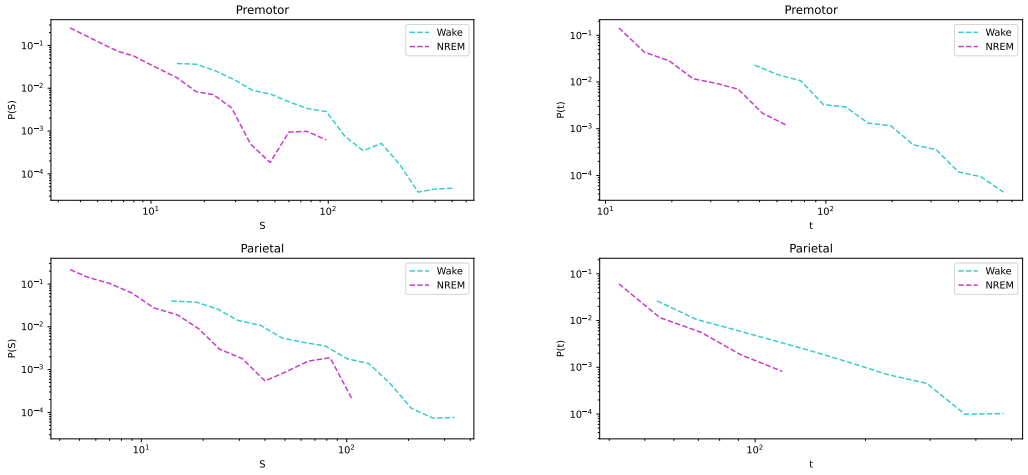

(a) Comparison Size PDF

(b) Comparison Duration PDF

Figure 3.6: In this figure, avalanche sizes and durations between the wake and NREM sleep groups are compared. The NREM avalanches size PDFs have a steeper slope than the wake group that typically indicates that larger avalanches are less likely to occur during sleep than wake. However, the 'heaps' seen in the NREM sleep group indicates that there is a large probability of seeing very large avalanches. The NREM durations are highly similar between wake and NREM sleep, but appear to be missing the tails of the distribution.

sleep. The bump, here, indicates that for some sets of trials, the TMS pulse results in a response with a large number of sources. These bumps represent the presence of "infinite" avalanches that take over the whole system typical of the supercritical regime. The findings for avalanche durations are also consistent with a supercritical regime. The avalanche durations flattened, as would be expected for sleep, but without the presence of the bump near the tails . The absence of a bump in the duration distributions indicates that the TMS-evoked synchronous waves were not scale invariant events, meaning they remained concentrated in certain time bins. Furthermore, while the change in size is consistent across premotor and parietal sites, for duration, the premotor sites show a much larger change in exponent than parietal sites.

The contrasting changes in scaling exponents are perplexing for two primary reasons. Firstly, while the PDF of avalanche size displays bumps near the tails, typical of a supercritical phase, instead of the anticipated decrease, we see an increase in τ. This unexpected direction of change is likely due to issues with estimation of the slope. For the NREM dataset, we have both fewer overall subjects, and therefore samples, and the source localization is done on a template MRI which could lead to poor estimation of activations compared to the wake cohort. The limited sample size may also have been a factor in the disparity in the amount of flattening of α between premotor and parietal stimulation (only three subjects compared to seven). Therefore, although the changes in τ and α appear contradictory, ultimately, the presence of "bumps" in

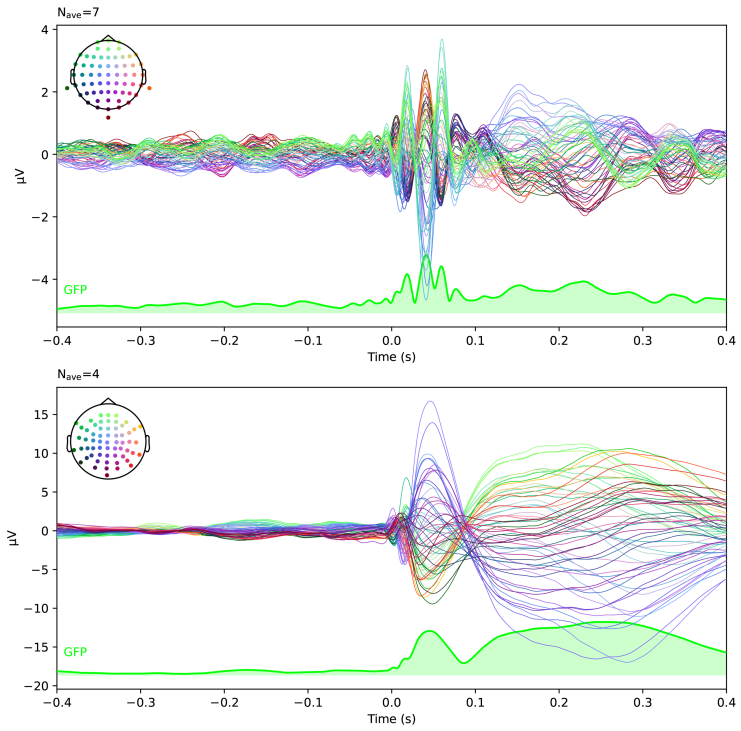

Figure 3.7: Comparison of the grand average brain response to stimulation over left premotor (BA6). As can be seen, the wake (top) response is highly variable over time while the response in NREM sleep (bottom) results in fewer components.

the size PDFs and the flattening of avalanche duration PDFs together suggest a deviation towards the supercritical regime during NREM sleep.

3.4.3 Possible alternative ways that lead to changes in scaling exponents

However, it is important to note that changes in scaling exponents may be due not just to deviation from the critical point, but also by changes in the critical exponent or critical state, such as those caused by changes in topography [189]. Our data would suggest a deviation towards the supercritical regime in N2/N3, but while the estimated scaling relation does change for parietal stimulations in NREM sleep compared to wake, there is also evidence of changes in topography that could also explain these changes. It has been shown that avalanche scaling exponents can increase when the network in a critical system changes from next neighbor to random connectivity [189]. In NREM sleep, there is evidence of large-scale changes in connectivity where the degree distribution changes into a short-range topology [121] and the modularity of brain networks increase [190, 191, 192]. The change in our scaling exponents could also be explained by changes in functional connectivity during NREM sleep that are then emphasized by the TMS stimulation. Follow-up work needs to be done to investigate whether this change may be due to

topography (and therefore represents a different critical state) or shows a true deviation from criticality.

3.4.4 Limitations and Conclusion

While this study has provided valuable insights into evoked avalanches and changes in scale invariance between NREM sleep and wake, it is essential to acknowledge certain limitations that have shaped the scope of our findings. The decision to pool avalanches across subjects was done to maximize the samples for the determination of the distributions. Power laws are best identified by the tails of their distributions, so it is vital to have a large enough sample of larger avalanches to best approximate the distribution. But, pooling across subjects may result in a power law if the samples are pulled from multiple exponential processes [128]. In our case, subjects appeared to have similar individual distributions (Fig 3.4) and all were found to fit a power law prior to pooling. However, we do compare across subject pools for wake and NREM sleep. It is possible that the NREM sleep group shows different scaling exponents during wakefulness which might affect the conclusions of the current study. Furthermore, the source localization differed between the two conditions which could affect avalanche size as the localization would not be as accurate for the NREM sleep group. However, as neuronal avalanches are a generalized measure of the spread of activity, the reliability of the source localization should not have an out-sized effect on its determination.

In conclusion, we do not find evidence of critical slowing down in wakefulness but do find evidence of scale invariance that persists even in NREM sleep. The lack of critical slowing down does not necessarily indicate that criticality is not present because the scaling exponents during wake could be indicative of a subcritical regime. Although the estimated τ and α change in opposing directions in NREM sleep, the distributions of size and duration are suggestive of a supercritical shift, but these changes could be due to the large-scale changes in connectivity seen concurrently. Overall, both PCI^{LZ} and TEAs show changes between wake and NREM sleep, but the changes in PCI^{LZ} have cleaner interpretations than TEAs. As for stimulation site, there is some evidence that premotor and parietal stimulation may result in small differences in scaling exponents between sites both in wakefulness and sleep, but more work is needed to determine the reliability of these effects.

Chapter 4

Neuromodulation of cortex leads to changes in avalanches statistics but not complexity

4.1 Introduction

While I've previously focused on the presence of criticality and its potential correlation with conscious states, a fundamental question arises: Does criticality truly underpin conscious states, or is it more closely associated with other brain states during wakefulness? In this regard, I aim to examine whether criticality is primarily linked to the maintenance of brain states unrelated to conscious awareness.

4.1.1 Critical phenomena are affected by brain state and disease

In the past decade, there has been increasing evidence that the brain operates not exactly at a critical point, but instead the resting state brain wanders within a near-critical region [157, 193, 140, 182, 160, 194]. This evidence is mostly supported by changes in neural avalanche statistics and long-range temporal correlations (LRTC) during task and in atypical brains. There is some evidence that during different brain states this distance is modulated further. The relationship between cognitive load and criticality remains equivocal, with studies reporting both positive associations [195] and negative associations [196, 197] between task performance and criticality. While, there is clearer evidence for deviation from criticality during focused tasks [179, 180, 181]. The distance from the critical point may be dynamically adapted to help optimize for different computational tasks that require more stable responses [42, 198, 199, 200]. Even outside of the criticality literature, task brain dynamics have been shown to stabilize and are less complex than resting state dynamics [201].

Evidence from atypical brains, such as from individuals suffering from psychiatric disorders, shows signs of deviation from the critical regime as well. Patients with MDD show an

increase LRTC in the theta band as compared to healthy controls over the entire scalp, indicative of more persistent correlations and more stable dynamics [202, 203]. Interestingly, this deviation is not always a global phenomenon. For example, some studies suggest that the frontal cortex in individuals with schizophrenia may exhibit reduced or lost power-law scaling [204, 205], while other investigations indicate decreased LRTC in posterior regions [206, 207].

The notion of attractors can provide a valuable framework for understanding these task-related and disease-related changes in dynamics. Attractors are specific subspaces within the larger state space where the system tends to converge over time. They derive their name from their ability to attract and capture the trajectories of the system's dynamics. Within the state space, attractors serve as distinct regions that characterize different types of behaviors and patterns exhibited by the system. These behaviors can range from stable and repetitive oscillations, known as limit cycles, to more complex and intricate patterns observed in strange attractors with fractal structure [208]. Each type of attractor offers a unique representation of the system's dynamics and its characteristic behaviors.

Task-related brain activity can be considered as a temporary deviation from the resting-state "attractor" [209, 210]. The description of resting state, however, is more complicated. There is some evidence that a multistable model may best describe resting state EEG where the brain jumps erratically between a limit cycle and fixed-point attractor [211, 212, 213, 214]. But there is also evidence that supports metastability during resting state [215, 216, 217, 218], where the *absence* of attractors renders the system unstable, causing it to wander across phase space. Critical systems share similarities with metastable systems but possess weak stability. The brain during wakefulness may possess a critical attractor that allows it to visit specific subspaces, some of which are subcritical. When focusing on specific tasks, the brain may appear subcritical as it traverses through that particular state space before returning to the critical regime during resting state.

4.1.2 Directed changes in brain dynamics using TMS

While task- and disease-related changes are very useful in better understanding critical dynamics in the brain, they are indirect ways to modify system dynamics. A more direct, causal experimental method would be valuable as it allows greater control or knowledge of the underlying neural changes that may be inducing the shift in dynamics. Fortunately, TMS can also be used to modulate cortical dynamics by using either a patterned (theta burst stimulation; TBS)

or repetitive (rTMS) stimulation protocol to induce changes in cortical excitability and behavior [219, 220, 221].

The effects of rTMS and TBS on behavior and cortical excitability can also be explored from a dynamic theory perspective. For example, rTMS and TBS have been explored as alternative treatments for medication resistant MDD, providing an alternative option to electro-convulsive therapy (ECT) and have demonstrated modest remission rates [222, 223]. Typically, TMS is applied to the right and or left dorsolateral prefrontal cortex (DLPFC) based on evidence of reduced cortical excitability in the frontal cortices of individuals with MDD [224, 225, 226, 227]. While the therapeutic effect of TMS can be perceived as simple facilitation of a specific region (DLPFC), we may also consider its impact on the overall system in light of the pathological attractor model and criticality. The pathological attractor model posits that a patient's pathology can be understood as their brain remaining in a specific abnormal attractor state [228, 229]. In the context of criticality, a pathological attractor may steer the global dynamics of the brain away from a critical state, essentially self-organizing away from the critical point. The evidence pertaining to major depressive disorder (MDD) and criticality would appear to support this perspective. Applying this interpretation to neurostimulatory interventions, TBS's therapeutic effect may derive from helping global dynamics shift back towards the "normal" subcritical state by modulating a poorly performing sub-region.

A similar interpretation can be applied to behavioral changes induced by TBS during task. For instance, continuous TBS (cTBS) reliably decreases task performance on attention-related behaviors [230, 231]. If the brain should be pushed away from criticality during focused or attention-based tasks, as previously reviewed, it is plausible that cTBS affects the system's movement or transition away from the critical point or through a subcritical subspace. Specifically, cTBS has been shown to impair attention-dependent regulation of somatosensory event-related potentials (ERPs) [232]. Interpreting these findings within the criticality framework suggests that cTBS impedes the system's transition into this subcritical subspace, consequently impairing the attentional switch between attended and unattended stimuli in the study. Therefore, while TMS exerts a direct influence on individual regions, its potential to re- or mis-align specific subunits within the system highlights its potential to significantly impact global critical dynamics.

In regard to edge of chaos criticality, higher LZc values have been associated with better performance [233, 234], but Mediano et. al. [233] demonstrated that LZc was lower during task

engagement compared to the resting state, indicating that increased cognitive demand reduces complexity. This finding aligns with the avalanche criticality studies outlined above, which found that critical dynamics were shifted towards a subcritical regime (e.g., [179]). It is conceivable that the authors' results reflect a similar deviation towards a slightly subcritical regime, where task performance improves as the dynamics approach the critical point. However, in the context of TMS-evoked responses, an alternative measure of response complexity known as the perturbational complexity index (PCI) has shown greater sensitivity and specificity in assessing arousal compared to resting state LZc [154, 155]. Yet, it remains unknown whether the response complexity of TMS-evoked responses exhibits similar changes as event-related response complexity during different tasks or following neuromodulation interventions.

4.1.3 Applying avalanches to TMS and TBS

Collectively, the evidence suggests that avalanche criticality may play a role in supporting specific cognitive states rather than the general conscious state while the evidence is unclear for edge of chaos criticality. One thing that the literature is missing is an experiment testing whether a non-pathological, waking brain is pushed away from criticality using extrinsic (neuromodulation) instead of intrinsic (task vs rest) stimulation. Although previous work has used complexity to investigate differences between responders and non-responders to rTMS therapy in MDD [235], there has been no work that directly applies different measures of criticality pre- and post-neuromodulation in a healthy population.

In this study, our aim is to investigate the impact of TBS on the resting state dynamics and measures of criticality, specifically avalanche criticality and edge of chaos criticality. By modulating the underlying brain state through TBS, we can examine whether changes in critical dynamics are induced and explore their potential relationship with conscious state. Previous evidence on TBS, cognitive task performance, therapeutic applications, and avalanche behavior leads us to hypothesize that TBS has the capacity to alter avalanche behavior, given its ability to modify brain dynamics during wakefulness. This second study also functions as a way to test our evoked avalanche measure developed in Study 1 against traditional resting state measures.

If both measures of criticality, namely response complexity and avalanche criticality, can be modulated during wakefulness as observed in resting state and event-related responses, it would suggest that criticality may not be exclusively supportive of conscious state. On the other hand, if criticality and conscious state are indeed linked, any deviation from the critical point

should correspond to a concurrent change in consciousness. In this current study, we are only able to address this first point and not the second as TBS-induced changes in brain dynamics do not significantly alter global conscious state (unless a seizure is triggered).

To ensure a focused investigation on critical dynamics and cortical excitability, we have designed the study without a behavioral component. Including a behavioral task could potentially induce a shift to a subcritical unit that may not be directly involved in the dynamic processes necessary to support consciousness. Additionally, we are aware that TBS applied to the dorsolateral prefrontal cortex (DLPFC) can induce changes in transcranial evoked potentials (TEPs) and subsequent dynamics in healthy controls [236, 237]. TBS has also been applied over the left parietal cortex and found that it affected language comprehension [238]. Therefore, we have chosen to target a less commonly studied region, the superior parietal lobule (SPL), for TBS application. This decision is supported by previous work demonstrating the reliability of TEPs and PCI in the SPL [239]. Also, by selecting the SPL as the stimulation site, we can minimize potential confounding factors such as somatosensory feedback, which may arise from TBS applied to the motor area [240].

4.2 Methods

The neural responses to TMS stimulation (TEPs) and the resting state EEG was collected from a cohort of 22 subjects (female = 14; age = 22.5 ± 5.2) and recorded with a 60-channel TMS-compatible amplifier (BrainAmp; Brain Products GmbH, Germany), referenced to the forehead, and 2 extra sensors were used to record the electrooculogram. Participants attended two sessions of TMS stimulation, spaced at least 72 hours apart. A T1-weighted MRI was obtained for neuronavigation and source localization purposes for every participant. In each session, participants underwent a baseline TEP and resting state EEG recording followed by a dose of either cTBS or iTBS. Participants then underwent a second TEP acquisition (at five minutes post TBS), a five minute long eyes-open resting state EEG recording (at 15 minutes post), and a final TEP acquisition at 20 minutes post TBS (Fig 4.1). Participants received one dose of TBS (either iTBS or cTBS), with the order counterbalanced across subjects. Participants were given a questionnaire asking for demographic data (age, sex, ethnicity, race, handedness, height, weight, and level of education), and after each single pulse stimulation were asked about any perceived 1) pain, 2) annoyance, and 3) how audible the TMS click was.

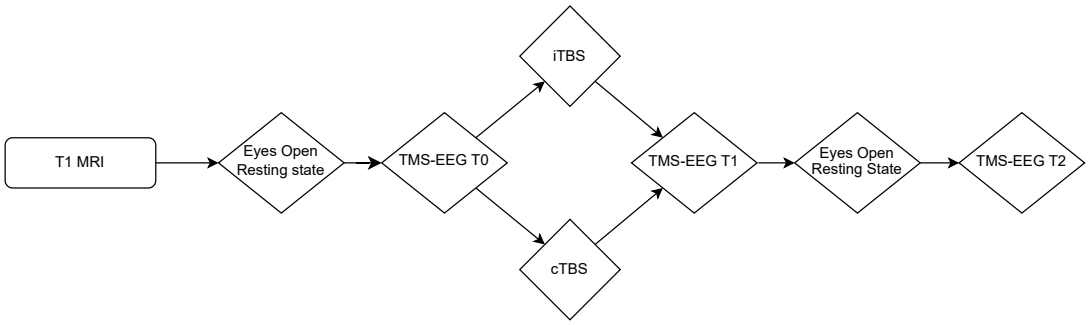

Figure 4.1: The experimental procedure is depicted here, showing the general flow for both stimulation sessions, except for the MR acquisition which occurs only in the first session.

4.2.1 Single-Pulse TMS procedure

Both single-pulse and TBS protocols were delivered to the left superior parietal lobule (BA7) (Fig 4.2a) with a focal biphasic figure-of-eight coil driven by a mobile stimulator unit (Nexstim, Helsinki, Finland). A neuronavigation software using the obtained participant structural MRIs was used to provide improved anatomical targeting both within and across TMS stimulations. During the single pulse TMS stimulations, participants wore earphones that continuously played an individualized masking noise [163]. To record TEP responses, 200 single TMS pulses were delivered at an ITI of 2.1 – 2.3 seconds (0.53 – 0.58 Hz). Single pulse intensity was set at the % MSO needed to elicit high quality TEPs with 5-10 mV peak-to-peak between the first two components, monitored online [164].

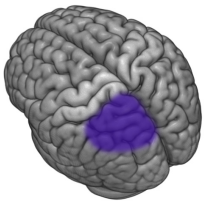

(a) All subjects were stimulated over left SPL, but the exact locations differ based on the optimal XYZ coordinates and coil rotation that resulted in the TEP response with the least amount of induced artefacts & largest response.

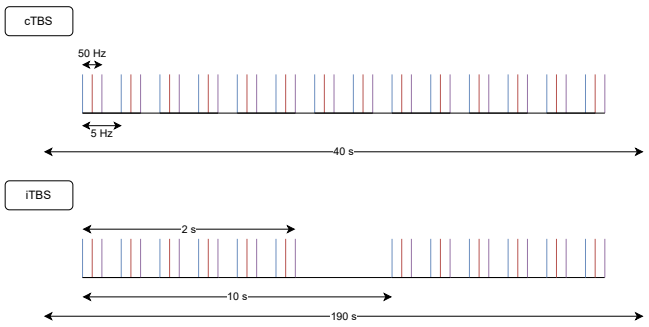

(b) A graphical representation of the difference between the iTBS & cTBS protocols is shown. Each triplet is indicated by a trio of colors (blue, red, and purple). The main distinction between cTBS & iTBS is the inclusion of time between 2s long bursts of TBS.

Figure 4.2

4.2.2 TBS

cTBS was delivered in an uninterrupted train for a total of 600 pulses (about 40 s total) while iTBS was delivered for 2 seconds every 10 seconds for a total of 600 pulses (about 190 s total) (Fig 4.2b). Intensity of stimulation was set at 80% active motor threshold for both protocols except for cases where 80% aMT exceeded limitations set by the machine in which case the intensity of stimulation was set at the maximum allowed (45% MSO). The active motor threshold (aMT) was determined for the right first dorsal interosseus (FDI) muscle while the subject contracted the muscle. To facilitate iterative adjustment of the TMS intensity after each pulse after determining whether an MEP was observed, the program Adaptive PEST [241, 242] was used.

4.2.3 Data Preprocessing

EEG preprocessing and analysis was done with in Python with custom scripts and MNE [167, 166] with the same procedure as the study described in Chapter 3. In brief, the TMS artefact was removed in a ten second window around the pulse (-5:5ms), bandpass filtered from 0.1 - 45 Hz with a bandstop at 60 Hz (zero-phase shift Butterworth, 3rd order), manually cleaned for bad channels and trials, segmented from -600:800 ms around the stimulation, rereferenced to the average, down-sampled to 1000 Hz, and baseline corrected. ICA (MNE picard function [169]) was used to remove ocular, muscular, and magnetic artefacts.

Resting state data was cleaned using a combination of artifact subspace reconstruction (ASR; [243]) with a cutoff of 20, manual cleaning, and ICA. It was bandpass filtered at 1 – 45 Hz with a bandstop at 60 Hz (zero-phase shift Butterworth, 3rd order), down-sampled to 300 Hz, and referenced to the average. Bad channels were interpolated using spherical splines for both TEP and resting state recordings.

4.2.4 TMS-evoked avalanches and PCI

The same procedures as described in methods section of the previous chapter (3.2.4 and 3.2.5) was used to analyze TEAs and PCI in this study. For resting state data, neural avalanches were detected from the EEG data using methodology from published MEG and EEG criticality studies [157, 158, 22, 24]. First, the current source density was calculated for the resting state EEG data, then nonparametric bootstrapping was used to extract a binary matrix of significant sources.

For both TEP and resting state data, the discretized time series was then divided into bins of duration Δt with its size defined as the total number of events within the cascade and its time as the length of time spanned until hitting a time-bin with no significant events. For resting state avalanches, three Δt were used (3 ms, 7 ms, and 12 ms) that have been previously used in the literature [157, 158, 22, 24] while for the evoked avalanches, three time-bins were used starting from the $\Delta t_{\text{min,}}$ the inverse of the sampling rate, and increasing by 1 ms. This allowed us to see how stable the calculated power-law was over different timescales.

A maximum likelihood-based analysis and KS goodness-of-fit were used to fit the avalanche size and duration distributions to a discrete power-law, lognormal, and exponential distributions [171, 172]. As a reminder, critical fluctuations, or crackling noise, follow the previously outlined scaling relation (Eq. 3.1) and, for MFDP, the expected scaling exponents are τ = 1.5, α = 2.0, and $\frac{1}{ovz}$ = 2.

4.2.5 Statistical Analysis

For PCI^{LZ} and resting state avalanches, we conducted random-intercept-only linear mixed models using the 'lme4' library [175] in R [176]. For PCI^{LZ} , we included PCI^{LZ} as our dependent variable, protocol (iTBS or cTBS) and time (pre, post 5, and post 20) as our fixed effects, and each subject as a random effect. The model specification is as follows:

$$PCI \sim Protocol + Time + Protocol * Time + (1|Subject) \tag{4.1}$$

For resting state avalanches, we conducted separate analyses for each scaling exponent and time-bin where we included the scaling exponent (τ, α, or $\frac{1}{ovz}$) as our dependent variable, protocol and time (pre and post 15) as our fixed effects, and each subject as a random effect:

$$\tau \sim Protocol + Time + Protocol * Time + (1|Subject) \tag{4.2}$$

$$\alpha \sim Protocol + Time + Protocol * Time + (1|Subject) \tag{4.3}$$

$$\frac{1}{ovz} \sim Protocol + Time + Protocol * Time + (1|Subject) \tag{4.4}$$

4.3 Results

No significant differences were found between the baseline and two post TBS time-points for PCI^{LZ} (cTBS = 0.43 ± 0.07, iTBS = 0.44 ± 0.09) for either cTBS or iTBS.

The following scaling exponents for the resting state data are reported across all baseline conditions (pre cTBS and iTBS):

Time bin	τ	α	$1/ovz$
3 ms	2.68 ± 0.51	2.68 ± 0.56	1.00 ± 0.0
7 ms	1.59 ± 0.22	2.39 ± 0.38	1.30 ± 0.03
12 ms	1.37 ± 0.22	2.11 ± 0.41	1.32 ± 0.06

Table 4.1: This table gives a summary of the mean ± standard deviations for the slopes of the fitted power-laws for size (tau), duration (alpha), and average size by duration (1/ovz).

The scaling exponents for the avalanche size and duration of the resting state data are similar to those expected for a mean-field branching process (MFDP) (tau = 1.5, alpha = 2.0), but the fitted size-by-duration does not. The smallest time bin was the only one to show extremely steep slopes that could not be well estimated (exponent > 2.5). This could be due to the window being too small, leading to break up of avalanches.

No significant differences were found between the baseline and post TBS and between the two baseline conditions (pre iTBS and cTBS) in the scaling exponents for the avalanche size, duration, and size-by-duration of the resting state data for two of three time-bins. However, a significant interaction effect of protocol and time ($F(1,49.81) = 4.33$, $p=0.04$) was found for the avalanche duration exponent in the 12 ms time bin. The comparison between the null model, which included only the intercept, and the full model was statistically significant ($\chi^2(3) = 9.20$, $p=0.03$), but the inclusion of predictors only resulted in a moderate improvement in model fit, as indicated by a decrease in the Akaike Information Criterion ($\Delta AIC = 3$) and Bayesian Information Criterion ($\Delta BIC = 3$). Post-hoc comparisons of the estimated difference in the marginal means using a Bonferroni correction showed there was a significant increase from the baseline in the post 15 minutes ($t(47.7) = -2.59$, $p=0.013$) only for the cTBS protocol (Fig 4.3).

The model included random intercepts for participants. The variance component estimates indicated that there was small variability in participants' baseline scaling exponents (sigma2_participant = 0.0048), suggesting that the duration scaling exponent is relatively con-

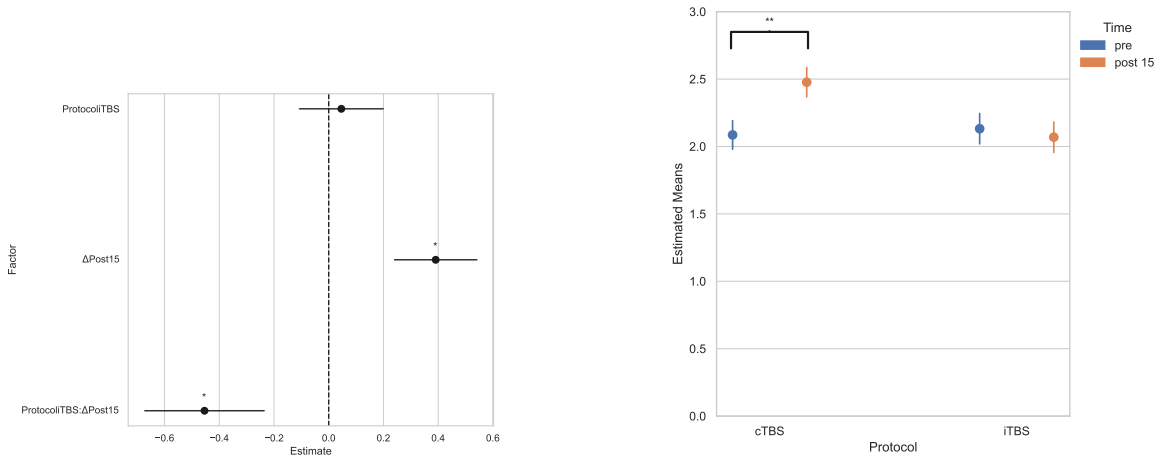

(a) (b)

Figure 4.3: Fixed effects point plot (a) illustrating the relationship between protocol, time, and α based on the results of a linear mixed-effects model. Each point represents the estimated fixed effect for a specific condition, with error bars indicating standard errors. The plot suggests that between baseline and 15-minutes after TBS on average, the avalanche duration scaling exponent increase by 0.4 per 1-unit increase in the predictor. Post-hoc comparisons of the estimated margin means (b) pre and post α show a significant increase only for the cTBS protocol. Error bars represent 95% confidence intervals around the estimated marginal means. Asterisks (* p<0.05, ** p <0.01, *** p <0.001) indicate statistically significant differences.

sistent across participants.

As for TMS-evoked avalanches, we find similar fits for avalanche size (τ = 1.5) and duration (α = 2.3) for our baseline TEP data in all five time bins (Fig 4.4). The main difference between resting state and our baseline TEP recordings is in the fitted $\frac{1}{\sigma\nu z}$ slope (mean = 1.05). TMS-evoked avalanches show slight differences in avalanche size from baseline to five minutes with size increasing slightly after cTBS and decreasing slightly after iTBS while size increases after both protocols twenty minutes post. Avalanche duration scaling exponents and fitted $\frac{1}{\sigma\nu z}$ remain similar across time.

4.4 Discussion

In this study, we examined how three distinct criticality signatures—namely, resting state avalanches, TEAs, and complexity – changed after TBS during eyes open rest in healthy, awake individuals. The scaling exponents corresponding to avalanche size and duration for both TEAs and resting state avalanches closely approximated those observed in MFDP exponents (τ = 1.5; α = 2.00), but neither followed the "crackling noise" scaling relationship (Eq. 3.1). The scaling relation exhibited by the resting state data was close to previously reported values (1.3) [157, 24] while the evoked avalanche showed a scaling relation ($\simeq$ 1.07) close to unity (1). We

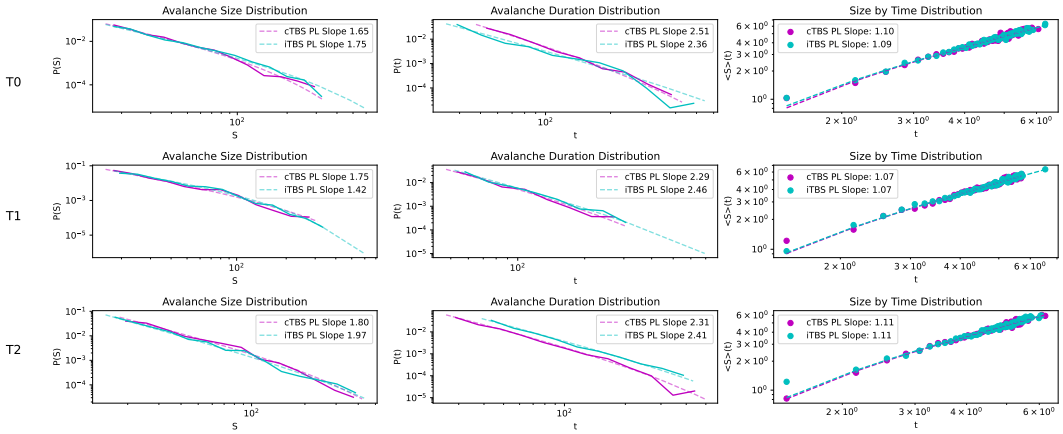

Figure 4.4: The PDFs for size, duration, and average size-by-duration are shown for the three time-points for one time-bin (4ms). The fitted power-law and scaling exponents are also reported. The difference in avalanche size τ between the cTBS and iTBS sessions can be seen here in the first column and second row where iTBS appears to slightly dip while cTBS goes up. This pattern of change is similar across all five time-bins. There are also slight differences in avalanche duration α between the three time-points, but these changes are not consistent across all time-bins.

also show that while the different TBS protocols affected the scaling of the duration of resting state avalanches, TMS-evoked avalanches appeared to fluctuate after stimulation with some indication of neuromodulation for size scaling exponents. Complexity, however, did not significantly differ after TBS.

4.4.1 Differences in scaling relations

The differences in the scaling relation could be interpreted as reflecting a difference in brain state between resting state and the single pulse TMS paradigm. As reviewed in the introduction of this chapter (4.1), brain dynamics stabilize during evoked or event-related paradigms compared to resting state. In our case, the single pulse protocol parameters may have induced increased stabilization and possible deviation from criticality as previously discussed in the previous chapter (3.4.1).

The phenomenon of neural entrainment within evoked paradigms entails synchronization between internal neural activity and the external environment, thereby enhancing processing capacity [244]. In these paradigms, the intervals between consecutive stimuli (Inter-Trial Intervals, ITI) and the inclusion of random temporal fluctuations (jitter) are integral components of the experimental design, governing the extent of neural entrainment to the applied stimulation. Conceptually, shorter ITIs with minimal or no jitter are expected to result in greater neural entrainment compared to longer ITIs or those with substantial jitters. Notably, the manipulation of ITIs finds practical application in TMS, where protocols involving rTMS utilize specified ITI

durations devoid of jitter to induce a certain degree of "entrainment" within the underlying cortical region. In our study, we capitalize on this entrainment using TBS. Conversely, TMS-MEP procedures incorporate longer ITIs (ranging from 8 to 12 seconds) to circumvent inadvertent entrainment within the motor pathway. In the context of TMS-EEG research, various research groups adopt diverse ITI and jitter patterns. For instance, certain groups employ shorter ITIs accompanied by jitter (e.g., 0.8 – 2 seconds ITI with 100 or 500 ms jitters [245, 246]), while others embrace longer ITIs either with or without jitter, akin to the TMS-MEP methodology (e.g., 3.3 – 8 seconds [247, 248]). Though the incorporation of jitter is essential to prevent neural entrainment, shorter ITIs are generally preferred as they substantially curtail data acquisition duration. It is plausible that the comparatively shorter ITI employed in our study could have led to a more stabilized brain state than the typical resting state, potentially contributing to the observed effects.

To test for entrainment, we looked at how the TEP response changed in the first vs second half of the stimulation period during the baseline periods (iTBS and cTBS) (Appendix 4.5.1). We found a significant difference between the first and second half of the TEP responses centered around 200 ms post stimulation, but no differences in induced oscillations. The differences in the time domain are indicative of some effect of entrainment or habituation and would support the hypothesis that TEPs in our study reflect a resting brain state with some stabilization. Previous authors have interpreted the distance between the fitted $\frac{1}{ovz}$ to the predicted $\frac{1}{ovz}$ as a measure of the proximity of the system to the MFDP critical point [182]. Our fitted $\frac{1}{ovz}$ could thus be interpreted as reflecting the shift away from baseline resting state by entrainment induced by the TMS-evoked paradigm.

4.4.2 The effect of attention and arousal on avalanches

There was a significant change in resting state avalanches in the largest time-bin (12 ms) fifteen minutes following cTBS where the duration scaling exponent increased, indicating a *steepening* of the power-law. The increase in the duration scaling exponent could be indicative of some scale-specific changes due to cTBS but given the marginal improvement in model fit observed in the full model and the significant findings in only 1 time-bin and scaling exponent, caution is warranted in drawing strong conclusions.

The changes could be alternatively be due to the single pulse stimulation used to assess TEPs. The ITI and jitter were chosen based on prior work and the necessity of obtaining a

high number of trials with good signal-to-noise ratio, but it is possible that the frequency of stimulation was not low enough or jittered enough to avoid possible neuromodulatory effects. However, if the single pulse was inducing changes, then it would be interacting with the TBS. We might then expect that subjects that then received fully inhibitory protocols (cTBS & single pulse) would show different changes than subjects that received a mix of excitatory and inhibitory protocols (iTBS & single pulse). In fact, cTBS does appear to cause steepening of the scaling exponent to occur faster than iTBS, but it is unclear if both are causing a modulation of cortical dynamics or just one. To provide further evidence of neuromodulation, we investigated whether cortical excitability changed after TBS using a linear mixed model (Appendix 4.5.2). We found that there was evidence of neuromodulation but only for cTBS. The lack of change in iTBS could be a result of interaction between the low-frequency single pulse (inhibitory effect) and the excitatory iTBS, resulting in a "nullification" of the excitation of iTBS. Alternatively, it is possible that iTBS did not have a % MSO high enough to affect cortical excitability and, in effect, acted as a sham in our study. In which case, our results would suggest that cTBS is having the modulating effect on τ, resulting in a quicker subcritical shift than iTBS. The *steepening* of the avalanche size in the twenty minutes post stimulation may be due to either arousal or our single pulse protocol. This change would be inline with previous findings on more task-based changes [179], but is difficult to interpret alongside the change after cTBS.

There is no work to date that looks at neural avalanches of resting state EEG before and after TBS *or* low frequency rTMS, so it is difficult to determine if we are seeing an interaction between our single pulse protocol and TBS. A comprehensive exploration into the potential influence of entrainment due to single pulse paradigms on cortical excitability and neural avalanches is warranted. To achieve this, subsequent studies could perform avalanche calculations and compare difference in peak-to-peak amplitudes on TEPs derived from diverse protocols with varying ITIs and jitters. This would provide a more holistic understanding of how entrainment factors into our findings.

4.4.3 What does this mean for TBS?

Aside from avalanches, our findings also shed light on the effect of TBS on non-motor regions specifically on the parietal cortex—a region that has not been previously explored using TBS and TEPs. Studies investigating TBS effects on TEP components from the motor cortex have yielded mixed findings [249]; although, there does appear to be a correlation between early TEP

components (N15 and P30) and MEPs [250]. On the other hand, a study done in dorsolateral prefrontal cortex identified significant changes in late TEP components (N150 and P200) following iTBS and cTBS and with TMS-evoked theta oscillations [237]. Our findings suggest that cTBS does have an inhibitory effect on cortical excitability when applied to SPL. Furthermore, we did not find evidence of a difference after iTBS, but this could be due to the low MSO (80% aMT), originally chosen to facilitate between protocol comparisons, or an interaction with our single pulse paradigm. Our work underscores the effectiveness of TEPs in evaluating TBS effects on non-motor regions, while highlighting potential interactions that may arise from the combined use of these paradigms.

4.4.4 Conclusion

Regardless of the differences between resting state and evoked avalanches, our data from both states do not support the idea of an MFDP critical point or the presence crackling noise. As further analyzed in the discussion of Chapter 3.4, the scaling relation for TEAs and resting state EEG fall between those found for a driven time-varying stochastic process (1.0) and edge of synchrony (1.3). While our data analysis lacks the granularity to examine subsampled spiking activity directly [156], and assuming that the scaling relation does represent the proximity to the MFDP critical, our findings suggest that during single pulse stimulation brain dynamics are further from the MFDP critical point compared to resting state, but are in a point in phase space where scale invariance can be maintained. Furthermore, we have shown here that avalanches, both evoked and spontaneous, suggest are sensitive to neuromodulatory effects than the complexity of a TMS-evoked response. Finally, although TBS did slight elicit changes in brain dynamics, evoked and spontaneous avalanches fluctuated during wakefulness while complexity remained constant.

4.5 Appendix

4.5.1 Supplementary Analyses of TMS entrainment in the time and spectral domains

To test the extent of neural entrainment induced by our single pulse TMS protocol, we split the recordings for the baseline (T0) time point for both iTBS and iTBS in half, then applied a spatiotemporal cluster permutation paired t-test (alpha = 0.01, permutations=10,000, two-tailed),

using built-in functions in MNE, in both the time and spectral domain. The initial phase involved grouping and computation of the test statistic based on clusters in the subsequent manner: For each individual data point, responses marked by high and low arousal were subjected to paired samples t-tests. Samples exhibiting t-values with a significance level of $p<0.05$ were selected and grouped based on their temporal adjacency. The summation of t-values within each cluster yielded cluster-level statistics. The most substantial of these cluster-level statistics was selected, and significance was assessed employing the Monte Carlo Method, tailored for within-subjects designs. This test would indicate if there were differences in the time domain between the responses in the first and second half of the stimulation period which would presumably be due to the continued application of single pulse.

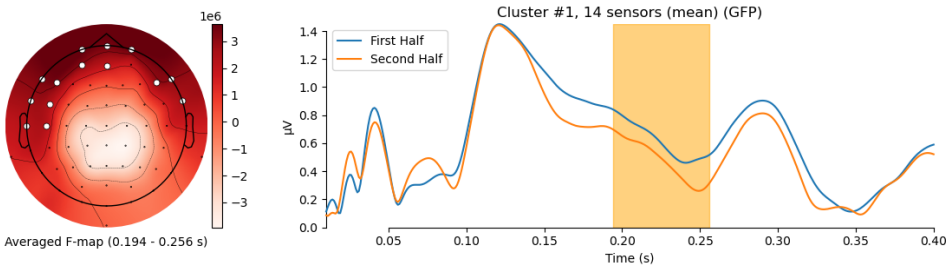

(a)

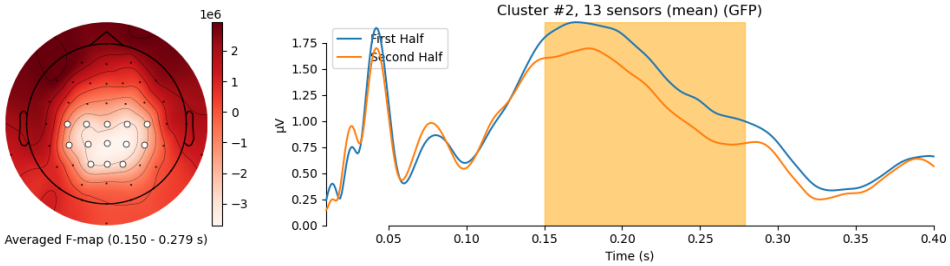

(b)

Figure 4.5: The results of the spatiotemporal cluster permutation tests are shown for cTBS. The orange shaded region indicates the temporal extent and the white dots on the topography refer to the electrodes associated with the cluster.

Cluster permutation analysis indicated a significant difference between the responses to the first and second half of trials for cTBS baseline, with differences around 200 ms post stimulation across the entire scalp (Fig 4.5). For iTBS, a significant difference was found centered around 200 ms post stimulation over central channels (Fig 4.6).

Time-frequency decomposition and power were calculated with complex Morlet waves using the built-in functions in MNE. The signal was decomposed in frequencies ranging from 6 to 35 Hz, increasing logarithmically and the number of cycles were increased as a function of frequency. After decomposition, power was calculated and converted into decibels. No significant

differences were indicated by cluster permutation analyses.

Taken together, these results would indicate that there are no signs of neural entrainment of oscillations, but in the time domain, there are what appear to be effects of habituation.

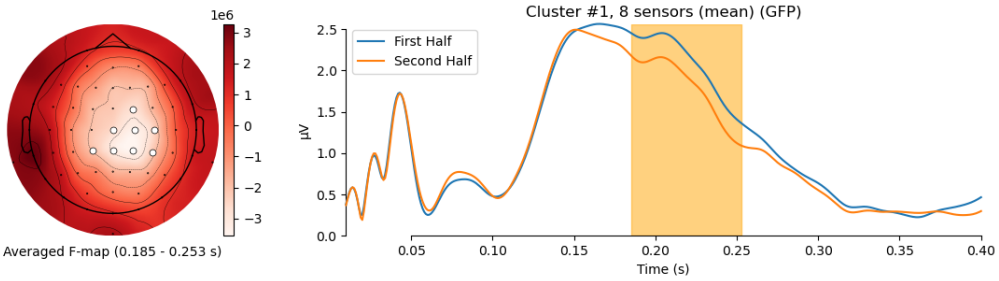

Figure 4.6: The results of the spatiotemporal cluster permutation tests are shown for iTBS. There is a general agreement between the analysis that differences between the first and second halves of the baseline recordings are centered in the very late components (>150ms) and across the scalp.

4.5.2 Analysis of changes in cortical excitability post TBS

Cortical excitability was operationalized as the peak-to-peak (P2P) amplitude of the first two components. To investigate changes in cortical excitability after TBS, the difference in P2P values was calculated between the pre-stimulation period and the two post-stimulation recordings. The electrode with the maximum P2P in the pre-stimulation period was chosen for each subject from a consistent subset of channels over the parietal cortex (Cz, C1, C3, CPz, CP1, CP3). The mean latency of the first component was 18.35ms $\pm$ 7.03 while the mean latency of the second component was 40.86 $\pm$ 16.99 across channels, subjects, and conditions.

We conducted a random-intercept-only linear mixed model analysis using the 'lme4' library (Bates) in R (REF). Due to the positively skewed nature of the raw data, a square root transformation was applied to achieve a more symmetric distribution before conducting the analysis. We included P2P as our dependent variable, protocol (iTBS or cTBS) and time (pre, post 5, and post 20) as our fixed effects, and each subject as a random effect. The model specification is as follows:

$$P2P \sim Protocol + Time + Protocol * Time + (1|Subject) \tag{4.5}$$

The comparison between the null model, which included only the intercept, and the full model was statistically significant ($\chi^2(5) = 91.604$, p<.001). The inclusion of predictors resulted in a substantial improvement in model fit, as indicated by a decrease in the Akaike Information Criterion (ΔAIC = 81.6) and Bayesian Information Criterion (ΔBIC = 59.5). These findings

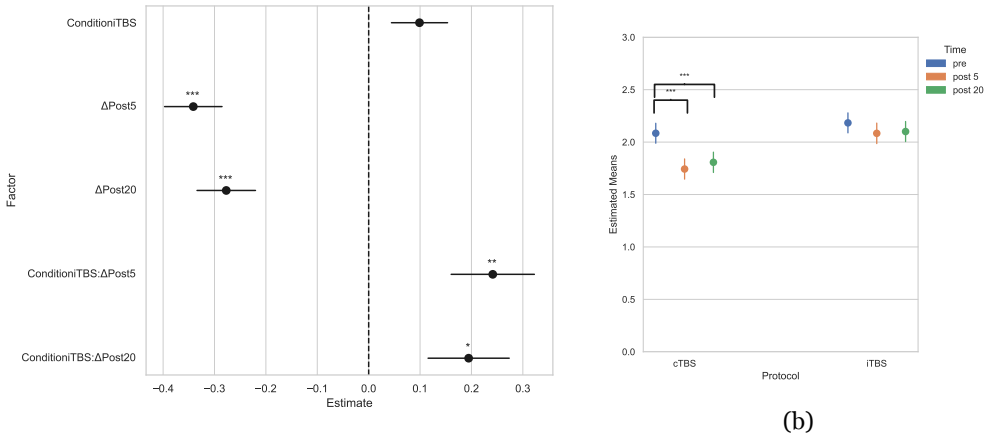

(a) (b)

Figure 4.7: Fixed effects point plot (a) illustrating the relationship between protocol, time, and cortical reactivity based on the results of a linear mixed-effects model. Each point represents the estimated fixed effect for a specific condition, with error bars indicating standard errors. The plot suggests that between baseline and 5 and 20-minutes after stimulation on average, the square root of P2P decreases by 0.3 - 0.35 for a 1-unit increase in the predictor. Post-hoc comparisons (b) reveal a significant decrease in the estimated marginal mean of P2P in both post time-points, but only for cTBS. The error bars for this plot represent 95% confidence intervals. Asterisks (* p<0.05, ** p <0.01, *** p <0.001) indicate statistically significant differences.

suggest that the full model provides a significantly better fit to the data compared to the null model, justifying the inclusion of the additional predictors. The model included random intercepts for participants, and the variance component estimates (σ^2 $_{\text{participant}}$ = 0.167) indicated small variability in participants' baseline scaling exponents.

There was a significant main effect of Time, F(2,591.46) = 17.46, p<.001, Protocol, F(1,597.98) = 50.95, p<0.001, and a significant interaction effect, F(2,591.28) = 5.20, p<0.01, suggesting that change in P2P over time varied based on the protocol. Post-hoc comparisons of the estimated difference in the marginal means using a Bonferroni correction showed there was a significant decrease from the baseline in the post 5 minutes (t(591) = 6.11, p<0.001) and post 20 minutes peak-to-peak amplitudes (t(592) = 4.87, p < 0.001) only for the cTBS protocol (Fig X).

Chapter 5

General Discussion

Identifying the mechanism supporting the complex dynamics that characterize a state of wakefulness and their loss in unconsciousness remains a challenge. This mechanism should ideally exhibit consistent behavior regardless of the method inducing unconsciousness (such as anesthesia or NREM sleep) and in states involving conscious experiences, such as REM sleep. The Critical Brain hypothesis, which proposes that the waking brain might operate at or near a critical point where specific phenomena that support a high degree of complex dynamics are present, emerges as a theoretical framework that could fulfill this criterion. Evidence suggests the brain operates in a slightly subcritical regime of the MFDP critical point, and that the proximity to this critical point is modulated during wakefulness by task or level of arousal [179, 158, 141, 122]. This modulation stands in opposition to the specificity of PCI^{LZ}, associated with the edge of chaos critical point, which remains high during wakefulness and has been found to fall only in different unconscious states [60, 154, 155]. Measures of MFDP have yet to be applied to TMS-evoked responses, but this methodology offers a potential avenue to explore the connection between MFDP and the edge of chaos critical points in relation to conscious states. This thesis aims to investigate this connection by comparing how two measures of phenomena associated with criticality vary across different conscious states (wakefulness, anesthesia, and sleep) and after neuromodulation during wakefulness using TMS-EEG.

5.1 Complexity of TEPs consistently tracks conscious state and is not modulated in wakefulness

In Chapter 3, we present simulation work that supports the intuition that the complexity of a TEP reflects the proximity of the electrodynamics to the edge of chaos critical point. Our experimental findings from Chapter 4 further corroborate previous work that finds that PCI^{LZ}

changes only with conscious state by showing that it does not change after neuromodulation even though there are changes in cortical reactivity. These findings are similar to how inter-trial variability, another characteristic of TEPs, was altered before the full anesthetic dose, but complexity only changed in the latter case in Chapter 3. This dissociation seems to be something unique to TMS-evoked response because the complexity of sensory evoked responses has been found to be modulated during wakefulness [233].

The specificity of TEP complexity to global conscious state as compared to other evoked responses may be due to a couple of the inherent properties of TEPs. The first is that TEPs are typically an order of magnitude larger than most sensory evoked responses, so even if there is some modulation in amplitude, these components are more likely to remain significant sources that are consistently above the threshold for complexity calculation. As long as the binarization of the response remains relatively consistent between two conditions, their compressibility remains similar. The second property is that TEPs can bypass the thalamus which consequently allows us to gather information about the thalamocortical circuit, even in cases where the peripheral and central nervous systems are compromised. Thus, the insights derived from TEPs differ slightly from sensory ERPs, as they track causal information transmission from *cortico*-thalamic connections. Thalamocortical communication is important to supporting information processing during wakefulness [251], while states of unconsciousness are consistently characterized by disrupted communication [252, 253, 254]. PCI^{LZ} would then be a measure of the complexity of the causal effects of cortical-thalamic information transfer. Future basic research that further investigates the differences between the causal evolution of TMS-evoked responses and sensory evoked responses and their effects on complexity would help illuminate possible explanations as to why the complexity of TEPs is more specific and sensitive to changes in conscious state than sensory perturbations.

5.2 TMS-evoked neural avalanches change in wakefulness and NREM sleep

As opposed to PCI^{LZ}, neural avalanches did show modulation both across conscious states (wakefulness vs NREM sleep) and during wakefulness (post TBS). The avalanche size scaling exponent (τ) changed in both studies while the duration scale exponent (α) was less reliable. Interestingly, τ was very similar between NREM sleep and 20-minutes post TBS, which would

appear to indicate that the two states had some similar dynamics in their responses to the single pulse TMS. If the change in the post TBS τ is due to changes in arousal, then it follows that the two states would change in similar directions. An increase in τ would suggest a subcritical shift, but this finding would be counter to what has been found in previous literature for arousal and sleep. For both sleep deprivation and NREM sleep, previous work has found a flattening of τ and α, indicating a shift towards the supercritical regime or back towards the critical point if waking is in the subcritical regime [121, 255, 139]. In our NREM sleep data, although τ is steepening, there is a 'heap' or 'bump' near the tail of the distribution which points to a deviation towards the supercritical regime and not a subcritical one so it may just be the result of poor estimation due to data quality and the between subject's design, that resulted in a steeper τ. This interpretation would align more closely with previous literature.

Unfortunately, the interpretation of why the size distribution post TBS is steepening is difficult to parse, especially after considering how the steepening of the NREM τ does not appear to be reliable in describing this state given the presence of supercritical 'bumps.' If the TBS results are interpreted strictly by both their distribution and their change in τ, then it would indicate that after five minutes, there is a steepening of τ (indicating a shift towards the supercritical regime, like NREM) after cTBS, then an opposite shift in arousal 20 minutes after TBS towards the subcritical regime. If the iTBS functioned as a 'control' due to lack of neuromodulation (no modulation of cortical reactivity), then our findings would indicate that the avalanche size scaling exponent was fluctuating over the course of the session. Deviations towards the subcritical regime have been reported during tasks and focused attention (e.g., [179]), so it is possible that these changes in τ follow changes in arousal during the session. Yet, the changes seen in our data would be relatively rapid compared to previous experiments that have indexed a change in exponents related to time spent awake (tens of minutes vs 9 hours in [158]). This relative sensitivity to brief changes in arousal is only true, however, for TEAs and not spontaneous avalanches where we see changes in duration after cTBS. More research is needed to better evaluate the difference in sensitivity to different magnitudes of arousal changes between TMS-evoked and spontaneous avalanches.

Overall, the PDF of τ in NREM sleep is suggestive of a shift towards the supercritical regime while the flattening and steepening of τ post TBS suggests a vacillation around the critical point which might be correlated with an interaction between slight changes in arousal, the single pulse protocol, and neuromodulation. In which case, the two studies show opposing effects on

avalanche size. This conclusion, however, assumes that scale invariance is generated due to the brain tuning dynamics towards or away from the MFDP or other critical point associated with avalanches, i.e., edge of synchrony. As previously mentioned, a change in the scaling exponent could be due to changes in structure and, furthermore, it is possible that the underlying mechanism for the changes post TBS and NREM sleep is different. In other words, the change in one case could be due to a shift away from the critical point while the other is due to a change in network topology. While there is evidence from NREM sleep of changes in functional connectivity that could drive changes in scaling behavior, the same cannot be said for TBS. Unfortunately, there has been limited research assessing changes in scale invariance and functional connectivity after rTMS or TBS to the parietal cortex without a specific task. Although rTMS has been shown to alter functional connectivity [256, 257], it does not necessarily impact scale invariance. Follow-up work should address if a) TBS did induce changes in functional connectivity and scale invariance and b) if these changes in structure are related to changes in TMS-evoked τ. Nevertheless, our results do show changes in the scaling laws behind neural avalanches that appear to follow slight changes in arousal while the changes in complexity of TEPs were specific to global conscious state.

5.3 Complexity vs Neural Avalanches: Why is one more specific than the other?

While potential explanations for why the complexity of TEPs more closely follow global conscious state compared to sensory evoked potentials, it is also important to discuss why complexity of TEPs outperforms neural avalanches also in this regard. One possible explanation could be that the TEP response gives us unique insight into both integration *and* differentiation in the brain while neural avalanches reflect mostly integration. PCI^{LZ} is theoretically based on the idea that a balance between integration and differentiation is needed for conscious experience [258, 259]. A highly complex TEP response should be marked by large deflections—integration—across many different sources—differentiation while a low complexity TEP should have either low integration, low differentiation, or both. Interestingly, a dissociation has been found between this complexity measure and complexity of spontaneous signals [154, 155]. It has been suggested that as PCI^{LZ} is computed on TMS-evoked responses more generally reflects the brain's ability to compute complex causal interactions which differentiates it from the

complexity of spontaneous EEG complexity, that reflects more signal diversity over time [154]. Thus, PCI^{LZ} gives us unique insight into the average richness of the information that is being spread across cortex.

Scale invariance is important for collective behavior as it aids with information integration across scales even in large, complex systems. So, the neural avalanches measurements used here reflect whether *integration* depends on one specific spatiotemporal scale. The results presented in this dissertation provide further evidence supporting the presence of scale invariance, and therefore the ability for the brain to integrate information irrespective of scale, even in unconscious states such as NREM sleep. Although the scaling laws behind such scale invariance does change in NREM sleep, so there is still some indication that integration is affected in the transition between wake and sleep. The amount of differentiation does not seem to affect scale invariance as is evident from the NREM sleep TEAs. Although the TEP visits fewer sources, we still see scale invariant fluctuations. While complexity is low in NREM sleep, it is low because there is low differentiation, but high integration—as evidenced by components with larger amplitude than during wakefulness. Even if changes in functional connectivity are behind the changes in τ, and therefore we see an effect of low differentiation, we still have high integration and thus scale invariance. If consciousness dynamics are marked by a loss of balance between the two, then complexity is a measure of the balance while neural avalanches show a combination of both on integration.

5.4 Limitations

While the primary objective of this study was to contrast the MFDP and the edge of chaos critical points, it is important to note that we have not dismissed the possibility that the edge of synchrony could serve as an alternative generative mechanism for neural avalanches. Although our interpretations of the neural avalanche findings are mainly discussed through the lens of MFDP, if we were to assume that the critical point of interest for avalanches were the edge of synchrony, our interpretation would not be significantly altered. However, it is also possible that neural avalanches are signs of proximity to the edge of chaos critical point. The co-occurrence of criticality exhibiting critical slowing down (like in MFDP) and the edge-of-chaos critical point has been observed in certain instances [260, 261, 34, 262], although this phenomenon is not universally consistent [263]. Previous modelling work has reported the presence of scale invariant

avalanches with similar scaling exponents to MFDP when the model was shifted more towards the supercritical phase of critical point defined by the maximization of complexity and information transfer [264]. In other words, both phenomena were present in the model but at different parameters of the system, indicating how the system can be dynamically tuned to better exploit these phenomena. In which case, our avalanche results would suggest that there is some type of vacillation around the edge of chaos critical point, but not strong enough for complexity to diminish.

Additionally, we have not ruled out the hypothesis that the relationship between these two critical points could underpin conscious experience during wakefulness. If scale invariant avalanches are not due to the edge of chaos critical point, then it may be that brain dynamics need to be slightly supercritical with respect to the edge of chaos critical point (as our lab has previously suggested; [41]) and slightly subcritical with respect to either MFDP or the edge of synchrony (as suggested by evidence from neural avalanches) [264]. A more fine-grained analysis of simulations is needed to better understand if this behavior can be explained by one critical point instead of the presence of two.

5.5 Final Conclusion

The overarching conclusion from the results presented in this work is 1) that PCI^{LZ} can track proximity to the edge of chaos critical point, and it consistently changes only with global changes in conscious state, and 2) changes in neural avalanches do not consistently change only with global changes in conscious state, but also to slight changes in dynamics. Furthermore, both resting and evoked avalanches show scaling exponents that have been associated with MFDP, but neither follow the crackling noise relationship. In fact, they are closer to values associated with a non-critical system or the edge of synchrony critical point. It is possible that the difference in sensitivity and specificity to conscious state between the two measures could be that neural avalanches measure only integration while PCI^{LZ} captures the balance between integration and differentiation. Regardless, the results from these three experiments suggest that the edge of chaos critical point correlates more closely to conscious state, and therefore, is more likely to be important in supporting a state of consciousness. Future work to further test this correlation should focus on cases in which complexity changes and the behavior of TMS-evoked neural avalanches is unknown, like in other states of unconsciousness (i.e., anesthesia,

coma, or vegetative state), altered states of consciousness where resting state complexity increases (i.e., psychedelic drugs), and lesions where proximity to the lesioned area dramatically changes TMS-evoked responses.

References

[1] Chalmers, D. The Hard Problem of Consciousness. In Schneider, S. & Velmans, M. (eds.) *The Blackwell Companion to Consciousness*, 32–42 (WILEY Blackwell, Hoboken, 2017), 2 edn.

[2] Rosenthal, D. M. State Consciousness and Transitive Consciousness. *Consciousness and Cognition* **2**, 355–363 (1993).

[3] Nagel, T. What Is It Like to Be a Bat? *The Philosophical Review* **83**, 435 (1974).

[4] Tononi, G., Sporns, O. & Edelman, G. M. A measure for brain complexity: relating functional segregation and integration in the nervous system. *Proceedings of the National Academy of Sciences* **91**, 5033–5037 (1994).

[5] Tagliazucchi, E., Crossley, N., Bullmore, E. T. & Laufs, H. Deep sleep divides the cortex into opposite modes of anatomical–functional coupling. *Brain Structure and Function* **221**, 4221–4234 (2016).

[6] Barttfeld, P. *et al.* Signature of consciousness in the dynamics of resting-state brain activity. *Proceedings of the National Academy of Sciences* **112**, 887–892 (2015).

[7] Hudetz, A. G., Liu, X. & Pillay, S. Dynamic Repertoire of Intrinsic Brain States Is Reduced in Propofol-Induced Unconsciousness. *Brain Connectivity* **5**, 10–22 (2015).

[8] Hutchison, R. M., Hutchison, M., Manning, K. Y., Menon, R. S. & Everling, S. Isoflurane induces dose-dependent alterations in the cortical connectivity profiles and dynamic properties of the brain's functional architecture. *Human Brain Mapping* **35**, 5754–5775 (2014).

[9] Varley, T. F., Denny, V., Sporns, O. & Patania, A. Topological analysis of differential effects of ketamine and propofol anaesthesia on brain dynamics. *Royal Society Open Science* **8**, 201971 (2021).

[10] Demertzi, A. *et al.* Human consciousness is supported by dynamic complex patterns of brain signal coordination. *Science Advances* **5** (2019).

[11] Casarotto, S. *et al.* Stratification of unresponsive patients by an independently validated index of brain complexity. *Annals of Neurology* **80**, 718–729 (2016).

[12] Sarasso, S. *et al.* Consciousness and Complexity during Unresponsiveness Induced by Propofol, Xenon, and Ketamine. *Current Biology* **25**, 3099–3105 (2015).

[13] Cocchi, L., Gollo, L. L., Zalesky, A. & Breakspear, M. Criticality in the brain: A synthesis of neurobiology, models and cognition. *Progress in Neurobiology* **158**, 132–152 (2017).

[14] Girardi-Schappo, M. Brain criticality beyond avalanches: open problems and how to approach them. *Journal of Physics: Complexity* (2021).

[15] Hesse, J. & Gross, T. Self-organized criticality as a fundamental property of neural systems. *Frontiers in Systems Neuroscience* **8**, 166 (2014).

[16] Wilting, J. & Priesemann, V. 25 years of criticality in neuroscience — established results, open controversies, novel concepts. *Current Opinion in Neurobiology* **58**, 105–111 (2019).

[17] Bak, P., Tang, C. & Wiesenfeld, K. Self-organized criticality. *Physical Review A* **38**, 364–374 (1988).

[18] Bak, P. *How Nature Works: the science of self-organized criticality* (Copernicus New York, NY, 1996), 1 edn.

[19] Beggs, J. M. & Plenz, D. Neuronal Avalanches in Neocortical Circuits. *Journal of Neuroscience* **23**, 11167–11177 (2003).

[20] Shew, W. L., Yang, H., Petermann, T., Roy, R. & Plenz, D. Neuronal Avalanches Imply Maximum Dynamic Range in Cortical Networks at Criticality. *The Journal of Neuroscience* **29**, 15595–15600 (2009).

[21] Khaluf, Y., Ferrante, E., Simoens, P. & Huepe, C. Scale invariance in natural and artificial collective systems: a review. *Journal of The Royal Society Interface* **14**, 20170662 (2017).

[22] Palva, J. M. *et al.* Neuronal long-range temporal correlations and avalanche dynamics are correlated with behavioral scaling laws. *Proceedings of the National Academy of Sciences* **110**, 3585–3590 (2013).

[23] Petermann, T. *et al.* Spontaneous cortical activity in awake monkeys composed of neuronal avalanches. *Proceedings of the National Academy of Sciences* **106**, 15921–15926 (2009).

[24] Shriki, O. *et al.* Neuronal Avalanches in the Resting MEG of the Human Brain. *The Journal of Neuroscience* **33**, 7079–7090 (2013).

[25] Plenz, D. & Niebur, E. (eds.) *Criticality in Neural Systems*. Reviews of Nonlinear Dynamics and Complexity (Wiley-VCH, Weinheim,Germany, 2014).

[26] O'Byrne, J. & Jerbi, K. How critical is brain criticality? *Trends in Neurosciences* (2022).

[27] Roli, A., Villani, M., Filisetti, A. & Serra, R. Dynamical Criticality: Overview and Open Questions. *Journal of Systems Science and Complexity* **31**, 647–663 (2018).

[28] Hinrichsen, H. Non-equilibrium critical phenomena and phase transitions into absorbing states. *Advances in Physics* **49**, 815–958 (2000).

[29] Hinrichsen, H. Non-equilibrium phase transitions. *Physica A: Statistical Mechanics and its Applications* **369**, 1–28 (2006).

[30] Messer, A. & Hinrichsen, H. Crossover from directed percolation to mean field behavior in the diffusive contact process. *Journal of Statistical Mechanics: Theory and Experiment* **2008**, P04024 (2008).

[31] Cho, S. & Fisher, M. P. A. Criticality in the two-dimensional random-bond Ising model. *Physical Review B* **55**, 1025–1031 (1997).

[32] Marinazzo, D. *et al.* Information Transfer and Criticality in the Ising Model on the Human Connectome. *PLoS ONE* **9**, e93616 (2014).

[33] Crutchfield, J. P. & Young, K. Computation at the Onset of Chaos. *Complexity, Entropy, and Physics of Information* (1989).

[34] Langton, C. G. Computation at the edge of chaos: Phase transitions and emergent computation. *Physica D: Nonlinear Phenomena* **42**, 12–37 (1990).

[35] Packard, N. H. Adaptation toward the edge of chaos. *Dynamic patterns in complex systems* **212**, 293–301 (1988).

[36] Bertschinger, N. & Natschlger, T. Real-Time Computation at the Edge of Chaos in Recurrent Neural Networks. *Neural computation* **16**, 1413–1436 (2004).

[37] Boedecker, J., Obst, O., Lizier, J. T., Mayer, N. M. & Asada, M. Information processing in echo state networks at the edge of chaos. *Theory in Biosciences* **131**, 205–213 (2012).

[38] Dahmen, D., Grün, S., Diesmann, M. & Helias, M. Second type of criticality in the brain uncovers rich multiple-neuron dynamics. *Proceedings of the National Academy of Sciences of the United States of America* **116**, 13051–13060 (2019).

[39] Legenstein, R. & Maass, W. Edge of chaos and prediction of computational performance for neural circuit models. *Neural Networks* **20**, 323–334 (2007).

[40] Ezaki, T., Reis, E. F. d., Watanabe, T., Sakaki, M. & Masuda, N. Closer to critical resting-state neural dynamics in individuals with higher fluid intelligence. *Communications Biology* **3**, 52 (2020).

[41] Toker, D. *et al.* Consciousness is supported by near-critical slow cortical electrodynamics. *Proceedings of the National Academy of Sciences* **119**, e2024455119 (2022).

[42] Gollo, L. L. Coexistence of critical sensitivity and subcritical specificity can yield optimal population coding. *Journal of The Royal Society Interface* **14**, 20170207 (2017).

[43] Crone, J. S., Lutkenhoff, E. S., Bio, B. J., Laureys, S. & Monti, M. M. Testing Proposed Neuronal Models of Effective Connectivity Within the Cortico-basal Ganglia-thalamocortical Loop During Loss of Consciousness. *Cerebral Cortex* bhw112 (2016).

[44] Monti, M. M. *et al.* Dynamic Change of Global and Local Information Processing in Propofol-Induced Loss and Recovery of Consciousness. *PLoS Computational Biology* **9**, e1003271 (2013).

[45] Schrouff, J. *et al.* Brain functional integration decreases during propofol-induced loss of consciousness. *NeuroImage* **57**, 198–205 (2011).

[46] Greicius, M. D., Krasnow, B., Reiss, A. L. & Menon, V. Functional connectivity in the resting brain: A network analysis of the default mode hypothesis. *Proceedings of the National Academy of Sciences* **100**, 253–258 (2003).

[47] Barttfeld, P. *et al.* Factoring the brain signatures of anesthesia concentration and level of arousal across individuals. *NeuroImage: Clinical* **9**, 385–391 (2015).

[48] Jobst, B. M. *et al.* Increased Stability and Breakdown of Brain Effective Connectivity During Slow-Wave Sleep: Mechanistic Insights from Whole-Brain Computational Modelling. *Scientific Reports* **7**, 4634 (2017).

[49] Lee, U. *et al.* Brain Networks Maintain a Scale-free Organization across Consciousness, Anesthesia, and Recovery. *Anesthesiology* **113**, 1081–1091 (2010).

[50] Monti, M. M., Coleman, M. R. & Owen, A. M. Neuroimaging and the Vegetative State. *Annals of the New York Academy of Sciences* **1157**, 81–89 (2009).

[51] Monti, M. M. & Schnakers, C. Flowchart for Implementing Advanced Imaging and Electrophysiology in Patients With Disorders of Consciousness: To fMRI or Not to fMRI? *Neurology* (2022).

[52] Fischer, C., Luaute, J. & Morlet, D. Event-related potentials (MMN and novelty P3) in permanent vegetative or minimally conscious states. *Clinical Neurophysiology* **121**, 1032–1042 (2010).

[53] Höller, Y. *et al.* Preserved oscillatory response but lack of mismatch negativity in patients with disorders of consciousness. *Clinical Neurophysiology* **122**, 1744–1754 (2011).

[54] Morlet, D. & Fischer, C. MMN and Novelty P3 in Coma and Other Altered States of Consciousness: A Review. *Brain Topography* **27**, 467–479 (2014).

[55] Rodriguez, R. A., Bussière, M., Froeschl, M. & Nathan, H. J. Auditory-evoked potentials during coma: Do they improve our prediction of awakening in comatose patients? *Journal of Critical Care* **29**, 93–100 (2014).

[56] Pruvost-Robieux, E., Marchi, A., Martinelli, I., Bouchereau, E. & Gavaret, M. Evoked and Event-Related Potentials as Biomarkers of Consciousness State and Recovery. *Journal of Clinical Neurophysiology* **39**, 22–31 (2022).

[57] Beukema, S. *et al.* A hierarchy of event-related potential markers of auditory processing in disorders of consciousness. *NeuroImage: Clinical* **12**, 359–371 (2016).

[58] Chennu, S. *et al.* Dissociable endogenous and exogenous attention in disorders of consciousness. *NeuroImage: Clinical* **3**, 450–461 (2013).

[59] Rohaut, B. *et al.* Probing ERP correlates of verbal semantic processing in patients with impaired consciousness. *Neuropsychologia* **66**, 279–292 (2015).

[60] Casali, A. G. *et al.* A theoretically based index of consciousness independent of sensory processing and behavior. *Science Translational Medicine* **5** (2013).

[61] Fecchio, M. *et al.* 4. Reliability of the perturbational complexity index in discriminating chronic patients with disorders of consciousness. *Clinical Neurophysiology* **126**, e1–e2 (2015).

[62] Massimini, M. *et al.* Breakdown of Cortical Effective Connectivity During Sleep. *Science* **309**, 2228–2232 (2005).

[63] Barker, A. T., Jalinous, R. & Freeston, I. L. Non-invasive Magnetic Stimulation of Human Motor Cortex. *The Lancet* **325**, 1106–1107 (1985).

[64] Basser, P. J. & Roth, B. J. New currents in electrical stimulation of excitable tissues. *Annual Review of Biomedical Engineering* **2**, 377–397 (2000).

[65] Roth, B. & Basser, P. A model of the stimulation of a nerve fiber by electromagnetic induction. *IEEE Transactions on Biomedical Engineering* **37**, 588–597 (1990).

[66] Rudin, D. O. & Eisenman, G. The action potential of spinal axons in vitro. *The Journal of General Physiology* **37**, 505–538 (1954).

[67] Rushton, W. A. H. The effect upon the threshold for nervous excitation of the length of nerve exposed, and the angle between current and nerve. *The Journal of Physiology* **63**, 357–377 (1927).

[68] Pascual-Leone, A., Bartres-Faz, D. & Keenan, J. P. Transcranial magnetic stimulation: studying the brain–behaviour relationship by induction of 'virtual lesions'. *Philosophical Transactions of the Royal Society of London. Series B: Biological Sciences* **354**, 1229–1238 (1999).

[69] Ilmoniemi, R. J. *et al.* Neuronal responses to magnetic stimulation reveal cortical reactivity and connectivity. *NeuroReport* **8**, 3537–3540 (1997).

[70] Chang, J.-Y. *et al.* Assessing Recurrent Interactions in Cortical Networks: Modeling EEG Response to Transcranial Magnetic Stimulation. *Journal of Neuroscience Methods* **312**, 93–104 (2019).

[71] Comolatti, R. *et al.* A fast and general method to empirically estimate the complexity of brain responses to transcranial and intracranial stimulations. *Brain Stimulation* (2019).

[72] Mutanen, T., Nieminen, J. O. & Ilmoniemi, R. J. TMS-evoked changes in brain-state dynamics quantified by using EEG data. *Frontiers in Human Neuroscience* **7**, 155 (2013).

[73] Chervyakov, A. V., Chernyavsky, A., Sinitsyn, D. O. & Piradov, M. A. Possible Mechanisms Underlying the Therapeutic Effects of Transcranial Magnetic Stimulation. *Frontiers in Human Neuroscience* **9**, 303 (2015).

[74] Tononi, G. & Edelman, G. M. Consciousness and complexity. *science* **282**, 1846–1851 (1998).

[75] Arsiwalla, X. D. & Verschure, P. Measuring the complexity of consciousness. *Frontiers in neuroscience* **12**, 424 (2018).

[76] Sarasso, S. *et al.* Consciousness and complexity: a consilience of evidence. *Neuroscience of Consciousness* (2021).

[77] Chialvo & Dante, R. Emergent complex neural dynamics. *Nature Physics* **6**, 744–750 (2010).

[78] Toker, D. *et al.* Criticality supports cross-frequency cortical-thalamic information transfer during conscious states. *bioRxiv* 2023.02.22.529544 (2023).

[79] Boccaletti, S., Grebogi, C., Lai, Y.-C., Mancini, H. & Maza, D. The control of chaos: theory and applications. *Physics Reports* **329**, 103–197 (2000).

[80] Oliver, N., Jüngling, T. & Fischer, I. Consistency Properties of a Chaotic Semiconductor Laser Driven by Optical Feedback. *Physical Review Letters* **114**, 123902 (2014).

[81] Jüngling, T., Lymburn, T. & Small, M. Consistency Hierarchy of Reservoir Computers. *IEEE Transactions on Neural Networks and Learning Systems* **33**, 2586–2595 (2022).

[82] Theiler, J. Spurious dimension from correlation algorithms applied to limited time-series data. *Physical Review A* **34**, 2427–2432 (1986).

[83] Osborne, A. & Provenzale, A. Finite correlation dimension for stochastic systems with power-law spectra. *Physica D: Nonlinear Phenomena* **35**, 357–381 (1989).

[84] Faisal, A. A., Selen, L. P. J. & Wolpert, D. M. Noise in the nervous system. *Nature Reviews Neuroscience* **9**, 292–303 (2008).

[85] Fontanini, A. & Katz, D. B. Behavioral States, Network States, and Sensory Response Variability. *Journal of Neurophysiology* **100**, 1160–1168 (2008).

[86] Daniel, E., Meindertsma, T., Arazi, A., Donner, T. H. & Dinstein, I. The Relationship between Trial-by-Trial Variability and Oscillations of Cortical Population Activity. *Scientific Reports* **9**, 16901 (2019).

[87] VanRullen, R., Busch, N. A., Drewes, J. & Dubois, J. Ongoing EEG Phase as a Trial-by-Trial Predictor of Perceptual and Attentional Variability. *Frontiers in Psychology* **2**, 60 (2011).

[88] London, M., Roth, A., Beeren, L., Häusser, M. & Latham, P. E. Sensitivity to perturbations in vivo implies high noise and suggests rate coding in cortex. *Nature* **466**, 123–127 (2010).

[89] Nolte, M., Reimann, M. W., King, J. G., Markram, H. & Muller, E. B. Cortical reliability amid noise and chaos. *Nature Communications* **10**, 3792 (2019).

[90] Laje, R. & Buonomano, D. V. Robust timing and motor patterns by taming chaos in recurrent neural networks. *Nature Neuroscience* **16**, 925–933 (2013).

[91] Bensaid, S., Modolo, J., Merlet, I., Wendling, F. & Benquet, P. COALIA: A Computational Model of Human EEG for Consciousness Research. *Frontiers in Systems Neuroscience* **13**, 59 (2019).

[92] Pinotsis, D. A. & Friston, K. J. Extracting novel information from neuroimaging data using neural fields. *EPJ Nonlinear Biomedical Physics* **2**, 1–12 (2014).

[93] Dugue, L., Marque, P. & VanRullen, R. The Phase of Ongoing Oscillations Mediates the Causal Relation between Brain Excitation and Visual Perception. *Journal of Neuroscience* **31**, 11889–11893 (2011).

[94] Kundu, B., Johnson, J. S. & Postle, B. R. Prestimulation phase predicts the TMS-evoked response. *Journal of Neurophysiology* **112**, 1885–1893 (2014).

[95] Poorganji, M. *et al.* Pre-Stimulus Power but Not Phase Predicts Prefrontal Cortical Excitability in TMS-EEG. *Biosensors* **13**, 220 (2023).

[96] Madsen, K. H. *et al.* No trace of phase: Corticomotor excitability is not tuned by phase of pericentral mu-rhythm. *Brain Stimulation* **12**, 1261–1270 (2019).

[97] Avramiea, A.-E. *et al.* Pre-stimulus phase and amplitude regulation of phase-locked responses are maximized in the critical state. *eLife* **9**, e53016 (2020).

[98] Ferrarelli, F. *et al.* Breakdown in cortical effective connectivity during midazolam-induced loss of consciousness. *Proceedings of the National Academy of Sciences* **107**, 2681–2686 (2010).

[99] Guedel & Arthur, E. Stages of Anesthesia and a Re-Classification of the Signs of Anesthesia. *Anesthesia & Analgesia* **6**, 157 (1927).

[100] Granö, I. *et al.* Local brain-state dependency of effective connectivity: evidence from TMS–EEG. *bioRxiv* 2021.10.01.462795 (2021).

[101] Fehér, K. D., Nakataki, M. & Morishima, Y. Phase-Dependent Modulation of Signal Transmission in Cortical Networks through tACS-Induced Neural Oscillations. *Frontiers in Human Neuroscience* **11**, 471 (2017).

[102] Cona, F., Zavaglia, M., Massimini, M., Rosanova, M. & Ursino, M. A neural mass model of interconnected regions simulates rhythm propagation observed via TMS-EEG. *NeuroImage* **57**, 1045–1058 (2011).

[103] Premoli, I. *et al.* Short-interval and long-interval intracortical inhibition of TMS-evoked EEG potentials. *Brain Stimulation* **11**, 818–827 (2018).

[104] Premoli, I. *et al.* Characterization of GABAB-receptor mediated neurotransmission in the human cortex by paired-pulse TMS-EEG. *NeuroImage* **103**, 152–162 (2014).

[105] Albada, S. v. & Robinson, P. Mean-field modeling of the basal ganglia-thalamocortical system. I Firing rates in healthy and parkinsonian states. *Journal of Theoretical Biology* **257**, 642–663 (2009).

[106] Robinson, P. A., Rennie, C. J. & Rowe, D. L. Dynamics of large-scale brain activity in normal arousal states and epileptic seizures. *Physical Review E* **65**, 041924 (2002).

[107] Hindriks, R. & Putten, M. J. v. Meanfield modeling of propofol-induced changes in spontaneous EEG rhythms. *NeuroImage* **60**, 2323–2334 (2012).

[108] Hutt, A. & Longtin, A. Effects of the anesthetic agent propofol on neural populations. *Cognitive Neurodynamics* **4**, 37–59 (2010).

[109] Zheng, Z. S. & Monti, M. M. Thalamic and extra-thalamic connections of the Globus Pallidus in the human brain: The ultradirect pathway. *bioRxiv* 688283 (2019).

[110] Saunders, A. *et al.* A direct GABAergic output from the basal ganglia to frontal cortex. *Nature* **521**, 85–89 (2015).

[111] Hazrati, L.-N. & Parent, A. Projection from the external pallidum to the reticular thalamic nucleus in the squirrel monkey. *Brain Research* **550**, 142–146 (1991).

[112] Kuo, H. & Chang, H. T. Ventral pallido□striatal pathway in the rat brain: A light and electron microscopic study. *Journal of Comparative Neurology* **321**, 626–636 (1992).

[113] Rajakumar, N., Elisevich, K. & Flumerfelt, B. The pallidostriatal projection in the rat: a recurrent inhibitory loop? *Brain Research* **651**, 332–336 (1994).

[114] Sato, F., Lavallée, P., Lévesque, M. & Parent, A. Single□axon tracing study of neurons of the external segment of the globus pallidus in primate. *Journal of Comparative Neurology* **417**, 17–31 (2000).

[115] Buzsáki, G., Anastassiou, C. A. & Koch, C. The origin of extracellular fields and currents — EEG, ECoG, LFP and spikes. *Nature Reviews Neuroscience* **13**, 407–420 (2012).

[116] Lancaster, G., Iatsenko, D., Pidde, A., Ticcinelli, V. & Stefanovska, A. Surrogate data for hypothesis testing of physical systems. *Physics Reports* **748**, 1–60 (2018).

[117] McNamara, P. *et al.* Rem And Nrem Sleep Mentation. *International Review of Neurobiology* **92**, 69–86 (2010).

[118] Stickgold, R., Malia, A., Fosse, R., Propper, R. & Hobson, J. A. Brain-Mind States: I. Longitudinal Field Study of Sleep/Wake Factors Influencing Mentation Report Length. *Sleep* **24**, 171–179 (2001).

[119] Bastuji, H., Perrin, F. & Garcia-Larrea, L. Semantic analysis of auditory input during sleep: studies with event related potentials. *International Journal of Psychophysiology* **46**, 243–255 (2002).

[120] Timofeev, I. & Chauvette, S. Chapter 1 Neuronal Activity During the Sleep-Wake Cycle. *Handbook of Behavioral Neuroscience* **30**, 3–17 (2019).

[121] Allegrini, P. *et al.* Sleep unconsciousness and breakdown of serial critical intermittency: New vistas on the global workspace. *Chaos, Solitons & Fractals* **55**, 32–43 (2013).

[122] Meisel, C., Klaus, A., Vyazovskiy, V. V. & Plenz, D. The Interplay between Long- and Short-Range Temporal Correlations Shapes Cortex Dynamics across Vigilance States. *The Journal of Neuroscience* **37**, 10114–10124 (2017).

[123] Nieminen, J. O. *et al.* Consciousness and cortical responsiveness: a within-state study during non-rapid eye movement sleep. *Scientific Reports* **6**, srep30932 (2016).

[124] Pigorini, A. *et al.* Bistability breaks-off deterministic responses to intracortical stimulation during non-REM sleep. *NeuroImage* **112**, 105–113 (2015).

[125] Sethna, J. P., Dahmen, K. A. & Myers, C. R. Crackling noise. *Nature* **410**, 242–250 (2001).

[126] Houle, P. A. & Sethna, J. P. Acoustic emission from crumpling paper. *Physical Review E* **54**, 278–283 (1996).

[127] Faqeeh, A., Osat, S., Radicchi, F. & Gleeson, J. P. Emergence of power laws in noncritical neuronal systems. *Physical Review E* **100**, 010401 (2019).

[128] Priesemann, V. & Shriki, O. Can a time varying external drive give rise to apparent criticality in neural systems? *PLoS Computational Biology* **14**, e1006081 (2018).

[129] Touboul, J. & Destexhe, A. Can Power-Law Scaling and Neuronal Avalanches Arise from Stochastic Dynamics? *PLoS ONE* **5**, e8982 (2010).

[130] Touboul, J. & Destexhe, A. Power-law statistics and universal scaling in the absence of criticality. *Physical Review E* **95**, 012413 (2017).

[131] Kinouchi, O. & Prado, C. P. C. Robustness of scale invariance in models with self-organized criticality. *Physical Review E* **59**, 4964–4969 (1999).

[132] Kinouchi, O., Pazzini, R. & Copelli, M. Mechanisms of Self-Organized Quasicriticality in Neuronal Network Models. *Frontiers in Physics* **8**, 583213 (2020).

[133] Fosque, L. J., Williams-García, R. V., Beggs, J. M. & Ortiz, G. Evidence for Quasicritical Brain Dynamics. *Physical Review Letters* **126**, 098101 (2021).

[134] Girardi-Schappo, M., Bortolotto, G. S., Gonsalves, J. J., Pinto, L. T. & Tragtenberg, M. H. R. Griffiths phase and long-range correlations in a biologically motivated visual cortex model. *Scientific Reports* **6**, 29561 (2016).

[135] Moretti, P. & Muñoz, M. A. Griffiths phases and the stretching of criticality in brain networks. *Nature Communications* **4**, 2521 (2013).

[136] Ódor, G., Dickman, R. & Ódor, G. Griffiths phases and localization in hierarchical modular networks. *Scientific Reports* **5**, 14451 (2015).

[137] Allegrini, P. *et al.* Self-organized dynamical complexity in human wakefulness and sleep: Different critical brain-activity feedback for conscious and unconscious states. *Physical Review E* **92**, 032808 (2015).

[138] Wang, J. W. J. L., Lombardi, F., Zhang, X., Anaclet, C. & Ivanov, P. C. Non-equilibrium critical dynamics of bursts in θ and δ rhythms as fundamental characteristic of sleep and wake micro-architecture. *PLoS Computational Biology* **15**, e1007268 (2019).

[139] Priesemann, V., Valderrama, M., Wibral, M. & Quyen, M. L. V. Neuronal Avalanches Differ from Wakefulness to Deep Sleep – Evidence from Intracranial Depth Recordings in Humans. *PLoS Computational Biology* **9**, e1002985 (2013).

[140] Hahn, G. *et al.* Spontaneous cortical activity is transiently poised close to criticality. *PLoS Computational Biology* **13**, e1005543 (2017).

[141] Meisel, C., Bailey, K., Achermann, P. & Plenz, D. Decline of long-range temporal correlations in the human brain during sustained wakefulness. *Scientific Reports* **7**, 11825 (2017).

[142] Krzemiński, D., Kamiński, M., Marchewka, A. & Bola, M. Breakdown of long-range temporal correlations in brain oscillations during general anesthesia. *NeuroImage* **159**, 146–158 (2017).

[143] Fontenele, A. J. *et al.* Criticality between Cortical States. *Physical Review Letters* **122**, 208101 (2019).

[144] Agrawal, V., Chakraborty, S., Knöpfel, T. & Shew, W. L. Scale-Change Symmetry in the Rules Governing Neural Systems. *iScience* **12**, 121–131 (2019).

[145] Fagerholm, E. D. *et al.* Cortical Entropy, Mutual Information and Scale-Free Dynamics in Waking Mice. *Cerebral Cortex* **26**, 3945–3952 (2016).

[146] Fekete, T. *et al.* Critical dynamics, anesthesia and information integration: Lessons from multi-scale criticality analysis of voltage imaging data. *NeuroImage* **183**, 919–933 (2018).

[147] Tagliazucchi, E. *et al.* Large-scale signatures of unconsciousness are consistent with a departure from critical dynamics. *Journal of The Royal Society Interface* **13**, 20151027 (2016).

[148] Varley, T. F., Sporns, O., Puce, A. & Beggs, J. Differential effects of propofol and ketamine on critical brain dynamics. *PLoS Computational Biology* **16**, e1008418 (2020).

[149] Aamodt, A. *et al.* EEG Signal Diversity Varies With Sleep Stage and Aspects of Dream Experience. *Frontiers in Psychology* **12**, 655884 (2021).

[150] Aamodt, A. *et al.* EEG Lempel-Ziv complexity varies with sleep stage, but does not seem to track dream experience. *Frontiers in Human Neuroscience* **16**, 987714 (2023).

[151] Abásolo, D., Simons, S., Silva, R. M. d., Tononi, G. & Vyazovskiy, V. V. Lempel-Ziv complexity of cortical activity during sleep and waking in rats. *Journal of Neurophysiology* **113**, 2742–2752 (2015).

[152] Steyn-Ross, D. A. & Steyn-Ross, M. L. Brain and Nonlinear Dynamics: Slow-Wave Sleep Regulates to the Edge of Chaos. In Opris, I. & Casanova, M. F. (eds.) *The Physics of the Mind and Brain Disorders: Integrated Neural Circuits Supporting the Emergence of Mind*, vol. 11 of *Springer Series in Cognitive and Neural Systems*, 213–232 (Springer, Switzerland, 2017).

[153] Toker, D. *et al.* Consciousness is supported by near-critical slow cortical electrodynamics. *Proceedings of the National Academy of Sciences* **119**, e2024455119 (2022).

[154] Farnes, N., Juel, B. E., Nilsen, A. S., Romundstad, L. G. & Storm, J. F. Increased signal diversity/complexity of spontaneous EEG, but not evoked EEG responses, in ketamine-induced psychedelic state in humans. *PLoS ONE* **15**, e0242056 (2020).

[155] Ort, A. *et al.* TMS-EEG and resting-state EEG applied to altered states of consciousness: oscillations, complexity, and phenomenology. *iScience* **26**, 106589 (2023).

[156] Neto, J. P., Spitzner, F. P. & Priesemann, V. Sampling effects and measurement overlap can bias the inference of neuronal avalanches. *PLOS Computational Biology* **18**, e1010678 (2022).

[157] Arviv, O., Goldstein, A. & Shriki, O. Near-Critical Dynamics in Stimulus-Evoked Activity of the Human Brain and Its Relation to Spontaneous Resting-State Activity. *The Journal of Neuroscience* **35**, 13927–13942 (2015).

[158] Meisel, C., Olbrich, E., Shriki, O. & Achermann, P. Fading Signatures of Critical Brain Dynamics during Sustained Wakefulness in Humans. *The Journal of Neuroscience* **33**, 17363–17372 (2013).

[159] Neto, J. P., Spitzner, F. P. & Priesemann, V. A unified picture of neuronal avalanches arises from the understanding of sampling effects. *bioRxiv* (2020).

[160] Priesemann, V. *et al.* Spike avalanches in vivo suggest a driven, slightly subcritical brain state. *Frontiers in Systems Neuroscience* **8**, 108 (2014).

[161] Palva, S. & Palva, J. M. Roles of Brain Criticality and Multiscale Oscillations in Temporal Predictions for Sensorimotor Processing. *Trends in Neurosciences* **41**, 729–743 (2018).

[162] Korchinski, D. J., Orlandi, J. G., Son, S.-W. & Davidsen, J. Criticality in Spreading Processes without Timescale Separation and the Critical Brain Hypothesis. *Physical Review X* **11**, 021059 (2021).

[163] Russo, S. *et al.* TAAC - TMS Adaptable Auditory Control: a universal tool to mask TMS click. *bioRxiv* 2021.09.08.459439 (2021).

[164] Casarotto, S. *et al.* The rt-TEP tool: real-time visualization of TMS-Evoked Potentials to maximize cortical activation and minimize artifacts. *Journal of Neuroscience Methods* **370**, 109486 (2022).

[165] Rosanova, M. *et al.* Sleep-like cortical OFF-periods disrupt causality and complexity in the brain of unresponsive wakefulness syndrome patients. *Nature communications* **9**, 4427 (2018).

[166] Gramfort, A. *et al.* MEG and EEG data analysis with MNE-Python. *Frontiers in Neuroinformatics* **7**, 267 (2013).

[167] Gramfort, A. *et al.* MNE software for processing MEG and EEG data. *NeuroImage* **86**, 446–460 (2014).

[168] Koponen, L. M., Nieminen, J. O. & Ilmoniemi, R. J. Minimum-energy Coils for Transcranial Magnetic Stimulation: Application to Focal Stimulation. *Brain Stimulation* **8**, 124–134 (2015).

[169] Ablin, P., Cardoso, J.-F. & Gramfort, A. Faster Independent Component Analysis by Preconditioning With Hessian Approximations. *IEEE Transactions on Signal Processing* **66**, 4040–4049 (2017).

[170] Pascual-Marqui, R. D. Standardized low-resolution brain electromagnetic tomography (sLORETA): technical details. *Methods and findings in experimental and clinical pharmacology* 5–12 (2002).

[171] Clauset, A., Shalizi, C. R. & Newman, M. E. J. Power-Law Distributions in Empirical Data. *SIAM Review* **51**, 661–703 (2009).

[172] Klaus, A., Yu, S. & Plenz, D. Statistical Analyses Support Power Law Distributions Found in Neuronal Avalanches. *PLoS ONE* **6**, e19779 (2011).

[173] Alstott, J., Bullmore, E. & Plenz, D. Powerlaw: a Python package for analysis of heavy-tailed distributions. *arXiv* (2013).

[174] Dale, A. M. *et al.* Dynamic Statistical Parametric Mapping Combining fMRI and MEG for High-Resolution Imaging of Cortical Activity. *Neuron* **26**, 55–67 (2000).

[175] Bates, D., Mächler, M., Bolker, B. & Walker, S. Fitting linear mixed-effects models using lme4. *Journal of Statistical Software* **67**, 1–48 (2015).

[176] R Core Team. *R: A Language and Environment for Statistical Computing*. R Foundation for Statistical Computing, Vienna, Austria (2023). URL `https://www.R-project.org/`.

[177] Bak, P., Tang, C. & Wiesenfeld, K. Self-organized criticality: An explanation of the 1/f noise. *Physical Review Letters* **59**, 381–384 (1987).

[178] Muñoz, M. A., Dickman, R., Vespignani, A. & Zapperi, S. Avalanche and spreading exponents in systems with absorbing states. *Physical Review E* **59**, 6175–6179 (1999).

[179] Fagerholm, E. D. *et al.* Cascades and Cognitive State: Focused Attention Incurs Subcritical Dynamics. *The Journal of Neuroscience* **35**, 4626–4634 (2015).

[180] Irrmischer, M., Poil, S., Mansvelder, H. D., Intra, F. S. & Linkenkaer-Hansen, K. Strong long-range temporal correlations of beta/gamma oscillations are associated with poor sustained visual attention performance. *European Journal of Neuroscience* **48**, 2674–2683 (2018).

[181] Tomen, N., Rotermund, D. & Ernst, U. Marginally subcritical dynamics explain enhanced stimulus discriminability under attention. *Frontiers in Systems Neuroscience* **8**, 151 (2014).

[182] Ma, Z., Turrigiano, G. G., Wessel, R. & Hengen, K. B. Cortical Circuit Dynamics Are Homeostatically Tuned to Criticality In Vivo. *Neuron* **104**, 655–664.e4 (2019).

[183] Dalla Porta, L. & Copelli, M. Modeling neuronal avalanches and long-range temporal correlations at the emergence of collective oscillations: Continuously varying exponents mimic M/EEG results. *PLOS Computational Biology* **15**, e1006924 (2019).

[184] Achermann, P. & Borbély, A. Coherence analysis of the human sleep electroencephalogram. *Neuroscience* **85**, 1195–1208 (1998).

[185] Dumermuth, G. & Lehmann, D. EEG Power and Coherence during Non-REM and REM Phases in Humans in All-Night Sleep Analyses. *European Neurology* **20**, 429–434 (1981).

[186] Massimini, M., Huber, R., Ferrarelli, F., Hill, S. & Tononi, G. The Sleep Slow Oscillation as a Traveling Wave. *The Journal of Neuroscience* **24**, 6862–6870 (2004).

[187] Mariani, B. *et al.* Neuronal Avalanches Across the Rat Somatosensory Barrel Cortex and the Effect of Single Whisker Stimulation. *Frontiers in Systems Neuroscience* **15**, 709677 (2021).

[188] di Santo, S., Villegas, P., Burioni, R. & Muñoz, M. A. Landau–Ginzburg theory of cortex dynamics: Scale-free avalanches emerge at the edge of synchronization. *Proceedings of the National Academy of Sciences* **115**, 201712989 (2018).

[189] Priesemann, V., Munk, M. H. & Wibral, M. Subsampling effects in neuronal avalanche distributions recorded in vivo. *BMC Neuroscience* **10**, 40 (2009).

[190] Boly, M. *et al.* Hierarchical clustering of brain activity during human nonrapid eye movement sleep. *Proceedings of the National Academy of Sciences* **109**, 5856–5861 (2012).

[191] Spoormaker, V. I. *et al.* Development of a Large-Scale Functional Brain Network during Human Non-Rapid Eye Movement Sleep. *The Journal of Neuroscience* **30**, 11379–11387 (2010).

[192] Tagliazucchi, E. *et al.* Large-scale brain functional modularity is reflected in slow electroencephalographic rhythms across the human non-rapid eye movement sleep cycle. *NeuroImage* **70**, 327–339 (2013).

[193] Gautam, S. H., Hoang, T. T., McClanahan, K., Grady, S. K. & Shew, W. L. Maximizing Sensory Dynamic Range by Tuning the Cortical State to Criticality. *PLOS Computational Biology* **11**, e1004576 (2015).

[194] Tagliazucchi, E., Balenzuela, P., Fraiman, D. & Chialvo, D. R. Criticality in Large-Scale Brain fMRI Dynamics Unveiled by a Novel Point Process Analysis. *Frontiers in Physiology* **3**, 15 (2012).

[195] Cohen, M. X. Midfrontal theta tracks action monitoring over multiple interactive time scales. *NeuroImage* **141**, 262–272 (2016).

[196] Euler, M. J., Wiltshire, T. J., Niermeyer, M. A. & Butner, J. E. Working memory performance inversely predicts spontaneous delta and theta-band scaling relations. *Brain Research* **1637**, 22–33 (2016).

[197] Tinker, J. & Velazquez, J. L. P. Power law scaling in synchronization of brain signals depends on cognitive load. *Frontiers in Systems Neuroscience* **8**, 73 (2014).

[198] Li, M. *et al.* Transitions in information processing dynamics at the whole-brain network level are driven by alterations in neural gain. *PLOS Computational Biology* **15**, e1006957 (2019).

[199] Wilting, J. *et al.* Operating in a Reverberating Regime Enables Rapid Tuning of Network States to Task Requirements. *Frontiers in Systems Neuroscience* **12**, 55 (2018).

[200] Wilting, J. & Priesemann, V. Inferring collective dynamical states from widely unobserved systems. *Nature Communications* **9**, 2325 (2018).

[201] Capouskova, K., Kringelbach, M. L. & Deco, G. Modes of cognition: Evidence from metastable brain dynamics. *NeuroImage* **260**, 119489 (2022).

[202] Gärtner, M. *et al.* Aberrant Long-Range Temporal Correlations in Depression Are Attenuated after Psychological Treatment. *Frontiers in Human Neuroscience* **11**, 340 (2017).

[203] Mumtaz, W., Malik, A. S., Ali, S. S. A., Yasin, M. A. M. & Amin, H. Detrended Fluctuation Analysis for Major Depressive Disorder. *2015 37th Annual International Conference of the IEEE Engineering in Medicine and Biology Society (EMBC)* **2015**, 4162–4165 (2015).

[204] Radulescu, A. R., Rubin, D., Strey, H. H. & Mujica□Parodi, L. R. Power spectrum scale invariance identifies prefrontal dysregulation in paranoid schizophrenia. *Human Brain Mapping* **33**, 1582–1593 (2012).

[205] Slezin, V. *et al.* Multifractal analysis as an aid in the diagnostics of mental disorders. *Nordic Journal of Psychiatry* **61**, 339–342 (2007).

[206] Moran, J. K., Michail, G., Heinz, A., Keil, J. & Senkowski, D. Long-Range Temporal Correlations in Resting State Beta Oscillations are Reduced in Schizophrenia. *Frontiers in Psychiatry* **10**, 517 (2019).

[207] Nikulin, V. V., Jönsson, E. G. & Brismar, T. Attenuation of long-range temporal correlations in the amplitude dynamics of alpha and beta neuronal oscillations in patients with schizophrenia. *NeuroImage* **61**, 162–169 (2012).

[208] Lorenz, E. N. Deterministic Nonperiodic Flow. *Journal of the Atmospheric Sciences* **20**, 130–141 (1963).

[209] Shine, J. M. *et al.* Human cognition involves the dynamic integration of neural activity and neuromodulatory systems. *Nature Neuroscience* **22**, 289–296 (2019).

[210] Woodman, M. M. & Jirsa, V. K. Emergent Dynamics from Spiking Neuron Networks through Symmetry Breaking of Connectivity. *PLoS ONE* **8**, e64339 (2013).

[211] Freyer, F., Aquino, K., Robinson, P. A., Ritter, P. & Breakspear, M. Bistability and Non-Gaussian Fluctuations in Spontaneous Cortical Activity. *Journal of Neuroscience* **29**, 8512–8524 (2009).

[212] Freyer, F. *et al.* Biophysical Mechanisms of Multistability in Resting-State Cortical Rhythms. *Journal of Neuroscience* **31**, 6353–6361 (2011).

[213] Freyer, F., Roberts, J. A., Ritter, P. & Breakspear, M. A Canonical Model of Multistability and Scale-Invariance in Biological Systems. *PLoS Computational Biology* **8**, e1002634 (2012).

[214] Valdes, P. A., Jimenez, J. C., Riera, J., Biscay, R. & Ozaki, T. Nonlinear EEG analysis based on a neural mass model. *Biological Cybernetics* **81**, 415–424 (1999).

[215] Deco, G., Jirsa, V. K., Robinson, P. A., Breakspear, M. & Friston, K. The Dynamic Brain: From Spiking Neurons to Neural Masses and Cortical Fields. *PLoS Computational Biology* **4**, e1000092 (2008).

[216] Roberts, J. A. *et al.* Metastable brain waves. *Nature Communications* **10**, 1056 (2019).

[217] Tognoli, E. & Kelso, J. The Metastable Brain. *Neuron* **81**, 35–48 (2014).

[218] Váša, F. *et al.* Effects of lesions on synchrony and metastability in cortical networks. *NeuroImage* **118**, 456–467 (2015).

[219] Chung, S., Hill, A. T., Rogasch, N. C., Hoy, K. E. & Fitzgerald, P. B. Use of theta-burst stimulation in changing excitability of motor cortex: A systematic review and meta-analysis. *Neuroscience & Biobehavioral Reviews* **63**, 43–64 (2016).

[220] Fitzgerald, P. B., Fountain, S. & Daskalakis, Z. J. A comprehensive review of the effects of rTMS on motor cortical excitability and inhibition. *Clinical Neurophysiology* **117**, 2584–2596 (2006).

[221] Jannati, A., Oberman, L. M., Rotenberg, A. & Pascual-Leone, A. Assessing the mechanisms of brain plasticity by transcranial magnetic stimulation. *Neuropsychopharmacology* **48**, 191–208 (2023).

[222] Daskalakis, Z. J., Levinson, A. J. & Fitzgerald, P. B. Repetitive Transcranial Magnetic Stimulation for Major Depressive Disorder: A Review. *The Canadian Journal of Psychiatry* **53**, 555–566 (2008).

[223] Rachid, F. Safety and Efficacy of Theta-Burst Stimulation in the Treatment of Psychiatric Disorders. *The Journal of Nervous and Mental Disease* **205**, 823–839 (2017).

[224] Abou-Saleh, M. T., Suhaili, A. R. A., Karim, L., Prais, V. & Hamdi, E. Single photon emission tomography with 99m Tc-HMPAO in Arab patients with depression. *Journal of Affective Disorders* **55**, 115–123 (1999).

[225] Baxter, L. R. *et al.* Reduction of Prefrontal Cortex Glucose Metabolism Common to Three Types of Depression. *Archives of General Psychiatry* **46**, 243–250 (1989).

[226] Fitzgerald, P. B. Targeting repetitive transcranial magnetic stimulation in depression: do we really know what we are stimulating and how best to do it? *Brain Stimulation* **14**, 730–736 (2021).

[227] Li, C.-T., Su, T.-P., Wang, S.-J., Tu, P.-C. & Hsieh, J.-C. Prefrontal glucose metabolism in medication-resistant major depression. *British Journal of Psychiatry* **206**, 316–323 (2015).

[228] Fröhlich, F., Sejnowski, T. J. & Bazhenov, M. Network Bistability Mediates Spontaneous Transitions between Normal and Pathological Brain States. *The Journal of Neuroscience* **30**, 10734–10743 (2010).

[229] Hayes, A. M. & Andrews, L. A. A complex systems approach to the study of change in psychotherapy. *BMC Medicine* **18**, 197 (2020).

[230] Lowe, C. J., Manocchio, F., Safati, A. B. & Hall, P. A. The effects of theta burst stimulation (TBS) targeting the prefrontal cortex on executive functioning: A systematic review and meta-analysis. *Neuropsychologia* **111**, 344–359 (2018).

[231] Ngetich, R., Zhou, J., Zhang, J., Jin, Z. & Li, L. Assessing the Effects of Continuous Theta Burst Stimulation Over the Dorsolateral Prefrontal Cortex on Human Cognition: A Systematic Review. *Frontiers in Integrative Neuroscience* **14**, 35 (2020).

[232] Bolton, D. A. & Staines, W. R. Transient inhibition of the dorsolateral prefrontal cortex disrupts attention-based modulation of tactile stimuli at early stages of somatosensory processing. *Neuropsychologia* **49**, 1928–1937 (2011).

[233] Mediano, P. A. *et al.* Fluctuations in Neural Complexity During Wakefulness Relate To Conscious Level and Cognition. *bioRxiv* 2021.09.23.461002 (2021).

[234] Nilsen, A. S., Juel, B. E. & Storm, J. F. Measures of states of consciousness during attentional and cognitive load. *bioRxiv* 586149 (2019).

[235] Arns, M., Cerquera, A., Gutiérrez, R. M., Hasselman, F. & Freund, J. A. Non-linear EEG analyses predict non-response to rTMS treatment in major depressive disorder. *Clinical Neurophysiology* **125**, 1392–1399 (2014).

[236] Chung, S. W. *et al.* Impact of different intensities of intermittent theta burst stimulation on the cortical properties during TMS-EEG and working memory performance. *Human Brain Mapping* **39**, 783–802 (2017).

[237] Chung, S. W. *et al.* Demonstration of short-term plasticity in the dorsolateral prefrontal cortex with theta burst stimulation: A TMS-EEG study. *Clinical Neurophysiology* **128**, 1117–1126 (2017).

[238] Cheng, G. L., Tang, J., Walsh, V., Butterworth, B. & Cappelletti, M. Differential effects of left parietal theta-burst stimulation on order and quantity processing. *Brain Stimulation* **6**, 160–165 (2013).

[239] Caulfield, K. A. *et al.* Assessing the Intra- and Inter-Subject Reliability of the Perturbational Complexity Index (PCI) of Consciousness for Three Brain Regions Using TMS-EEG. *bioRxiv* 2020.01.08.898775 (2020).

[240] Fecchio, M. *et al.* The spectral features of EEG responses to transcranial magnetic stimulation of the primary motor cortex depend on the amplitude of the motor evoked potentials. *PLOS ONE* **12**, e0184910 (2017).

[241] Borckardt, J. J., Nahas, Z., Koola, J. & George, M. S. Estimating Resting Motor Thresholds in Transcranial Magnetic Stimulation Research and Practice. *The Journal of ECT* **22**, 169–175 (2006).

[242] Sen, C. B. A. *et al.* Active and resting motor threshold are efficiently obtained with adaptive threshold hunting. *PLoS ONE* **12**, e0186007 (2017).

[243] Kothe, C. A. E. & Jung, T. P. Artifact Removal Techniques with signal reconstruction.

[244] Lakatos, P., Gross, J. & Thut, G. A New Unifying Account of the Roles of Neuronal Entrainment. *Current Biology* **29**, R890–R905 (2019).

[245] Kähkönen, S., Komssi, S., Wilenius, J. & Ilmoniemi, R. J. Prefrontal TMS produces smaller EEG responses than motor-cortex TMS: implications for rTMS treatment in depression. *Psychopharmacology* **181**, 16–20 (2005).

[246] Rosanova, M. *et al.* Natural Frequencies of Human Corticothalamic Circuits. *The Journal of Neuroscience* **29**, 7679–7685 (2009).

[247] Premoli, I. *et al.* TMS-EEG Signatures of GABAergic Neurotransmission in the Human Cortex. *The Journal of Neuroscience* **34**, 5603–5612 (2014).

[248] Vernet, M. *et al.* Insights on the neural basis of motor plasticity induced by theta burst stimulation from TMS–EEG. *European Journal of Neuroscience* **37**, 598–606 (2013).

[249] Ozdemir, R. A. *et al.* Reproducibility of cortical response modulation induced by intermittent and continuous theta-burst stimulation of the human motor cortex. *Brain Stimulation* **14**, 949–964 (2021).

[250] Gedankien, T., Fried, P. J., Pascual-Leone, A. & Shafi, M. M. Intermittent theta-burst stimulation induces correlated changes in cortical and corticospinal excitability in healthy older subjects. *Clinical Neurophysiology* **128**, 2419–2427 (2017).

[251] Shine, J. M. The thalamus integrates the macrosystems of the brain to facilitate complex, adaptive brain network dynamics. *Progress in Neurobiology* **199**, 101951 (2021).

[252] Afrasiabi, M. *et al.* Consciousness depends on integration between parietal cortex, striatum, and thalamus. *Cell Systems* **12**, 363–373.e11 (2021).

[253] Bastos, A. M. *et al.* Neural effects of propofol-induced unconsciousness and its reversal using thalamic stimulation. *eLife* **10**, e60824 (2021).

[254] Malekmohammadi, M., Price, C. M., Hudson, A. E., DiCesare, J. A. T. A. & Pouratian, N. Propofol-induced loss of consciousness is associated with a decrease in thalamocortical connectivity in humans. *Brain: a journal of neurology* (2019).

[255] Bocaccio, H. *et al.* The avalanche-like behaviour of large-scale haemodynamic activity from wakefulness to deep sleep. *Journal of the Royal Society Interface* **16**, 20190262 (2019).

[256] Eldaief, M. C., Halko, M. A., Buckner, R. L. & Pascual-Leone, A. Transcranial magnetic stimulation modulates the brain's intrinsic activity in a frequency-dependent manner. *Proceedings of the National Academy of Sciences* **108**, 21229–21234 (2011).

[257] Qiu, S., Yi, W., Wang, S., Zhang, C. & He, H. The Lasting Effects of Low-Frequency Repetitive Transcranial Magnetic Stimulation on Resting State EEG in Healthy Subjects. *IEEE Transactions on Neural Systems and Rehabilitation Engineering* **28**, 832–841 (2020).

[258] Tononi, G. The integrated information theory of consciousness: an updated account. *Archives Italiennes de Biologie* (2012).

[259] Tononi, G., Boly, M., Massimini, M. & Koch, C. Integrated information theory: from consciousness to its physical substrate. *Nature Reviews Neuroscience* **17**, 450–461 (2016).

[260] Haldeman, C. & Beggs, J. M. Critical Branching Captures Activity in Living Neural Networks and Maximizes the Number of Metastable States. *Physical Review Letters* **94**, 058101 (2005).

[261] Kuśmierz, L., Ogawa, S. & Toyoizumi, T. Edge of Chaos and Avalanches in Neural Networks with Heavy-Tailed Synaptic Weight Distribution. *Physical Review Letters* **125**, 028101 (2020).

[262] Hochstetter, J. *et al.* Avalanches and edge-of-chaos learning in neuromorphic nanowire networks. *Nature Communications* **12**, 4008 (2021).

[263] Kanders, K., Lorimer, T. & Stoop, R. Avalanche and edge-of-chaos criticality do not necessarily co-occur in neural networks. *Chaos: An Interdisciplinary Journal of Nonlinear Science* **27**, 047408 (2017).

[264] Zare, M. & Grigolini, P. Criticality and avalanches in neural networks. *Chaos, Solitons & Fractals* **55**, 80–94 (2013).